AD-A067 561 NAVAL POSTGRADUATE SCHOOL MONTEREY CALIF F/G 20/4
PRESSURE ON THE INTERFACE BETWEEN A CONVERGING FLUID WEDGE AND --ETC(U)
DEC 78 M KAWAMURA, I IOANNOU

UNCLASSIFIED NL

1 OF 2
AD A067561



AD A067561

DDC FILE COPY

2 NW

NAVAL POSTGRADUATE SCHOOL

Monterey, California

LEVEL II



DDC
RECEIVED
APR 20 1979
A

THESIS

PRESSURE ON THE INTERFACE BETWEEN A CONVERGING FLUID WEDGE AND A FAST FLUID BOTTOM

by

Masami Kawamura

and

Ioannis Ioannou

December 1978

Thesis Advisors: A.B. Coppens; J.V. Sanders

Approved for public release; distribution unlimited.

79 04 19 021

UNCLASSIFIED

SECURITY CLASSIFICATION OF THIS PAGE (When Data Entered)

REPORT DOCUMENTATION PAGE	READ INSTRUCTIONS BEFORE COMPLETING FORM
1. REPORT NUMBER	2. GOVT ACCESSION NO. 3. RECIPIENT'S CATALOG NUMBER
4. TITLE (and Subtitle) (6) Pressure on the Interface Between a Converging Fluid Wedge and a Fast Fluid Bottom,	(9) 5. TYPE OF REPORT & PERIOD COVERED Master's Thesis; December 1978
	6. PERFORMING ORG. REPORT NUMBER
7. AUTHOR(s) (10) Masami Kawamura, Ioannis Ioannou	8. CONTRACT OR GRANT NUMBER(s)
9. PERFORMING ORGANIZATION NAME AND ADDRESS Naval Postgraduate School Monterer, California 93940	10. PROGRAM ELEMENT, PROJECT, TASK AREA & WORK UNIT NUMBERS
11. CONTROLLING OFFICE NAME AND ADDRESS Naval Postgraduate School Monterey, California 93940	(11) 12. REPORT DATE December 1978
	13. NUMBER OF PAGES 102
14. MONITORING AGENCY NAME & ADDRESS(if different from Controlling Office) (12) 103 p.	15. SECURITY CLASS. (of this report)
	15a. DECLASSIFICATION/DOWNGRADING SCHEDULE

16. DISTRIBUTION STATEMENT (of this Report)

Approved for public release; distribution unlimited.

17. DISTRIBUTION STATEMENT (of the abstract entered in Block 20, if different from Report)

18. SUPPLEMENTARY NOTES

19. KEY WORDS (Continue on reverse side if necessary and identify by block number)

Pressure Amplitude
Phase Distribution

20. ABSTRACT (Continue on reverse side if necessary and identify by block number)

The pressure amplitude and phase distribution along the interface between a tapered fluid layer and an underlying fast fluid bottom were investigated both theoretically and experimentally.

Two different theoretical models were compared experimentally: a simple model based on a combination of normal modes and ray theory and an exact solution based on the method

DD FORM 1 JAN 73 1473 (Page 1) EDITION OF 1 NOV 68 IS OBSOLETE S/N 0102-014-6601

251 450

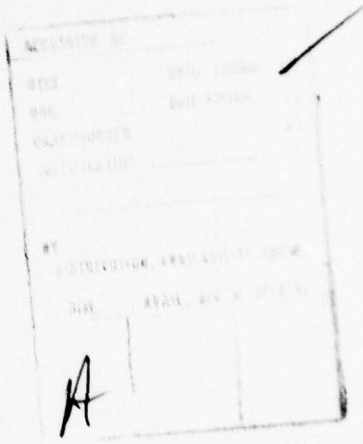
UNCLASSIFIED

SECURITY CLASSIFICATION OF THIS PAGE (When Data Entered)

79 04 19 021

(20. ABSTRACT Cont'd)

of images. The experiment was conducted at 100 kHz with a wedge of silicon oil separated from a large tank of fresh water by a thin Mylar diaphragm. The simple model failed to predict adequately the pressure amplitude and phase along the interface. The method of images gave accurate predictions.



Approved for public release; distribution unlimited.

Pressure on the Interface Between a Converging Fluid Wedge and a Fast Fluid Bottom

by

Masami Kawamura
Lieutenant, Japan Maritime Self Defense Force
B.S., Naval Postgraduate School, 1978

and

Ioannis Ioannou
Lieutenant Commander, Hellenic Navy
B.S., Naval Postgraduate School, 1978

Submitted in partial fulfillment of the
requirements for the degree of

MASTER OF SCIENCE IN ENGINEERING ACOUSTICS

from the

NAVAL POSTGRADUATE SCHOOL
December 1978

Authors Masami Kawamura

Approved by: Alan B. Coppens
Thesis Advisor

James V. Sanders
Thesis Advisor

Chairman, Department of Physics and Chemistry

William M. Tolles
Dean of Science and Engineering

ABSTRACT

The pressure amplitude and phase distribution along the interface between a tapered fluid layer and an underlying fast fluid bottom were investigated both theoretically and experimentally.

Two different theoretical models were compared experimentally: a simple model based on a combination of normal modes and ray theory and an exact solution based on the method of images. The experiment was conducted at 100 KHz with a wedge of silicon oil separated from a large tank of fresh water by a thin mylar diaphragm. The simple model failed to predict adequately the pressure amplitude and phase along the interface. The method of images gave accurate predictions.

TABLE OF CONTENTS

I. INTRODUCTION ---------- 8

II. THEORY ---------- 15

A. PRESSURE DISTRIBUTION PREDICTED BY A SIMPLE MODEL ---------- 15

1. Basic Concept ---------- 15

2. Pressure Distribution along the Bottom - 21

3. Pressure Distribution under the Bottom - 22

B. PRESSURE DISTRIBUTION ALONG THE BOTTOM PREDICTED BY THE METHOD OF IMAGES ---------- 26

III. EXPERIMENT ---------- 40

A. APPARATUS ---------- 40

1. Water Tank ---------- 41

2. Wedge ---------- 41

3. Source Transducer ---------- 42

4. Receiver and Attachment ---------- 44

5. Slope Measurement Assembly ---------- 44

6. Electrical Setup ---------- 45

7. Auxiliary Apparatus ---------- 46

B. PROCEDURE ---------- 46

1. Sound Speed Measurements ---------- 46

2. Density Measurements ---------- 46

3. Measurement of the Slope Angle --------- 47

4. Measurement of Pressure Amplitude along the Bottom ---------- 47

5. Measurement of Pressure Phase along the Bottom ---------- 48

IV. RESULTS AND COMPARISON ---------- 65

A. EXPERIMENT VS. SIMPLE MODEL ---------- 66

1. Pressure ---------- 66

2. Phase ---------- 67

B. EXPERIMENT VS. METHOD OF IMAGES ---------- 68

1. Pressure ---------- 69

2. Phase ---------- 70

C. ATTEMPTED RECONCILIATION ---------- 72

V. CONCLUSION ---------- 89

APPENDIX A: COMPUTER PROGRAM "WEDGE O" ---------- 90

APPENDIX B: INCIDENT ANGLE FOR A DISTANCE SOURCE ----- 98

BIBLIOGRAPHY ---------- 100

INITIAL DISTRIBUTION LIST ---------- 101

ACKNOWLEDGMENTS

The authors wish to thank Jack Brennan for his technical assistance in the experiments.

I. INTRODUCTION

As sound from the open ocean propagates up onto the continental shelf, lower frequencies become lost to the water column; energy is transmitted into the bottom. If the bottom has a speed of sound in excess of that of the water, then it is predicted [Ref. 1,2] that a highly collimated beam will form in the bottom.

For a channel of constant depth overlying fast bottom, normal-mode theory shows that if the frequency of the sound is less than the cutoff frequency of the mode energy can be transferred into the bottom. This can be seen if the normal mode is represented by upward-going and downward-going rays in the layer. As the frequency of the signal is decreased, the incidence (grazing) angle between the ray and the bottom increase. Energy continues to be perfectly reflected and remains trapped in the layer with no transfer into the bottom, until the incidence angle becomes equal to the critical angle. At that frequency the mode stops propagating in the layer and energy is transferred into the bottom. This concept can qualitatively be applied to a tapered layer over a fast bottom. As a propagating mode travels up the wedge, the incidence angle of the equivalent ray increases with each bounce until it reaches the critical angle, at which point energy will be transmitted into the bottom.

Theoretical and experimental studies of this phenomenon have been carried out at the NPS for three years encompassing three generations of experimental setups.

Lt. Edwards [Ref. 1] with his thesis adviser, Professor A.B. Coppens carried out initial investigations in a large tank filled with brine solution over which a thin layer of olive oil was carefully added. Since the interface between the two fluids was horizontal, a wedge-shaped upper layer was created by inserting a board of pressure-release material at an angle to the horizontal. The sound field was observed in the bottom fluid at various distances and depths. When plotted on properly chosen coordinates, the data were observed to cluster about a single curve consistent with the existence of narrow beam of sound enetering the bottom at a relatively shallow inclination.

In the meantime, Professor Coppens developed a simple theoretical model that predicted the shape of the beam pattern.

In an attempt to obtain more precise data, Lt. Netzorg [Ref. 2], with his thesis adviser, Professor J.V. Sanders, redesigned the apparatus to consist of a wedge of water separated from a small tank of brine by a 1-mil Mylar diaphragm stretched tightly within a frame. The bottom and sides of the tank were lined with absorbing material to reduce reflections. The results showed that the entry point of the beam was close to where it was predicted by the

simple model. Agreement between experiment and theory was fair but not good enough to verify the model.

Subsequent to these first experiments a more refined model has been constructed, with silicon oil in the wedge and a large water tank for the bottom. But the results obtained in this apparatus by Professor Sanders were still significantly disturbed by what appeared to be some sort of interference.

Experimental results from the three generations are compared to the predictions of the simple model in Table I-1 and Fig. I-1. Significant differences between theory and experiment were observed on the lower side of the beam pattern. In one extreme example, two peaks of beam were observed in a third generation of experiments. Generally, the observed angle of depression of the beam is shallower and the beam width narrower than predicted by the simple model.

At this point, the research effort was redirected to go back to examining the amplitude and phase distribution along the bottom; these quantities provide the link between the acoustic field in the layer and the formation of the beam in the bottom.

The objective of this research reported herein are to:

1) Develop a simple, closed form expression for the pressure distribution along the bottom that can be used to reliably predict the beam pattern to the bottom.

2) Calculate the pressure (including phase) along the bottom predicted by application of the method of images and compare with experimental results.

In this report, two different coordinate systems are used. The first is a special coordinate system applicable to the simple model; the origin is located at a point on the bottom where the lowest mode reaches cutoff. The second is a general coordinate system more suitable for the image calculations and experiment; the origin is located at the apex. These two coordinate systems are shown in Fig. I-2a,b.

GENERATION	EXPERIMENT	F [kHz]	BETA [rad]	C1/C2	ρ_2/ρ_1	BEAM DEPRESION ANGLE [deg]		BEAM WIDTH (-6 dB) [deg]	
						EXPERIMENT	SIMPLE MODEL	EXPERIMENT	SIMPLE MODEL
I	E1-1	76	0.040	0.82	1.29	12.5	22.5	18.0	29.5
	E1-2	76	0.052	0.82	1.29	17.5	26.0	19.0	27.5
II	E2-1	150	0.027	0.88	1.15	13.5~15.5	20.0	15.0	20.75
	E2-2	150	0.044	0.88	1.15	13.3~14.0	24.0	14.4~15.5	22.38
	E2-3	150	0.046	0.92	1.08	12.7~14.7	20.0	12.9~13.5	17.63
	E2-4	150	0.077	0.88	1.15	16.4~20.0	30.0	21.0~22.5	29.5
III	E3-1*	100	0.020	0.78	0.98	5.5 10.2	18.5	10.0 ——	20.0
	E3-2	100	0.029	0.78	0.98	24.4	23.0	——	——
	E3-3	100	0.020	0.78	0.98	20.5	18.5	17.0	20.0
	E3-4	100	0.038	0.78	0.98	13.0	24.5	22.5	27.5

* 2 peaks were observed.

Table I. Comparison of the experiments with the simple model

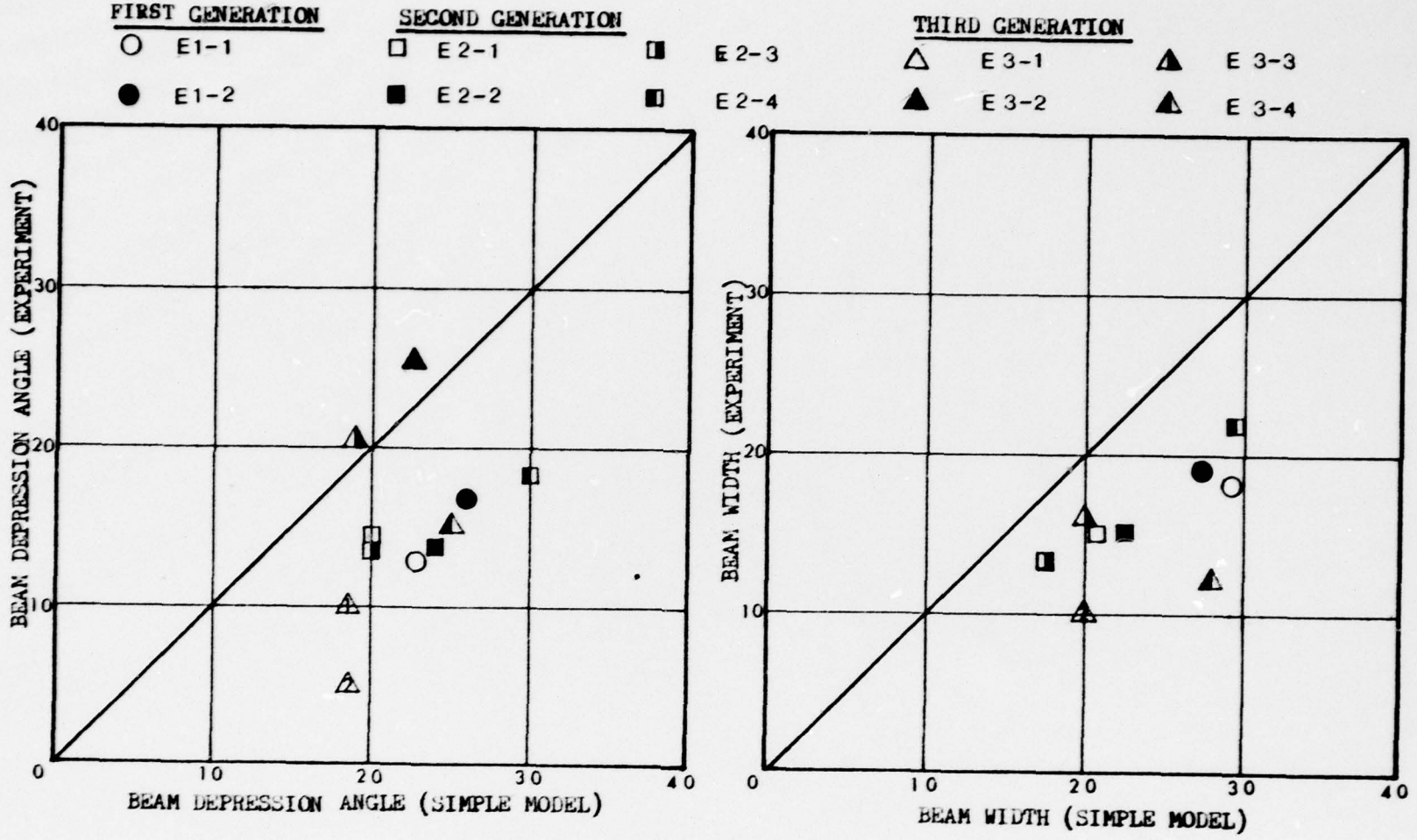


Fig.1-1 Comparison of the experiments with the simple model

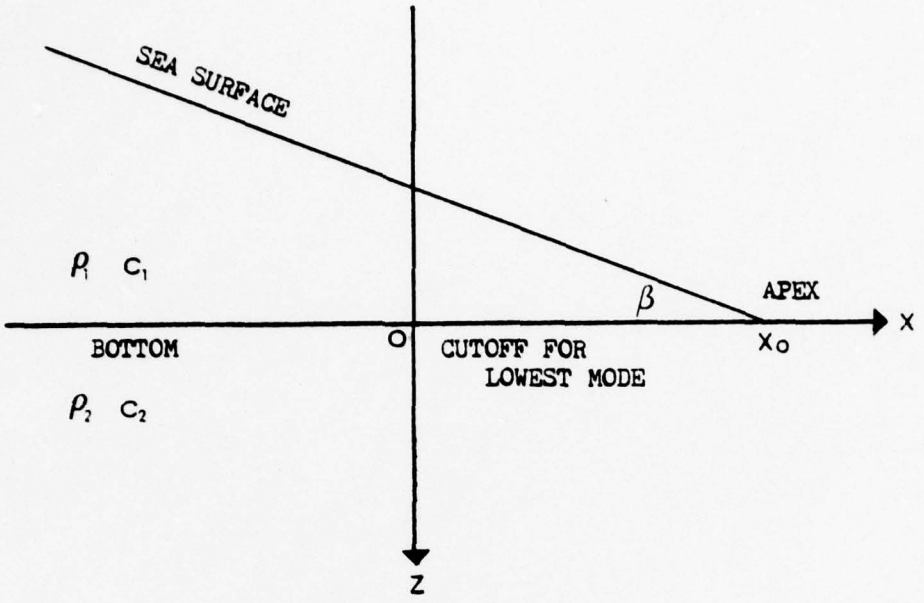


Fig.1-2a Coordinate system for the simple model

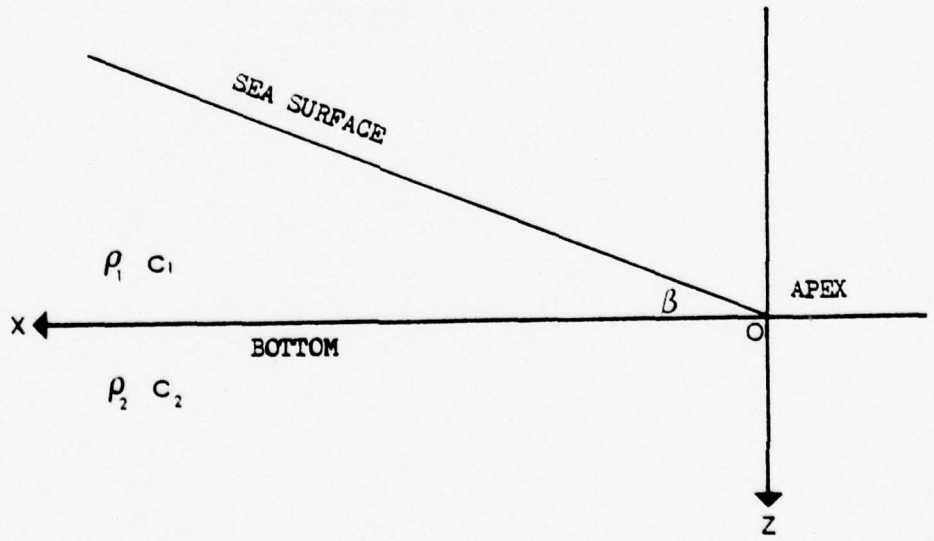


Fig.1-2b General coordinate system

II. THEORY

A. PRESSURE DISTRIBUTION PREDICTED BY A SIMPLE MODEL

1. Basic Concept

The purpose of this part is to summarize the theoretical background necessary to conceptualize the propagation of sound in a tapered fluid layer above a fast bottom, using a combination of normal modes and ray theory.

a. Layer of Uniform Depth

One-dimensional propagation in a fluid layer of uniform depth H with speed of sound c_1 and density ρ_1, overlying a second layer with a faster speed of sound c_2, and density ρ_2 can be exactly represented by an equation of the form

$$P = \sum_n A_n \sin(K_{z',n} z') e^{i(\omega t - K_{x',n} x')} \qquad \text{(II-1)}$$

where z' is the depth, x' is the horizontal distance, $K_{z',n}$ and $K_{x',n}$ are the components of the propagation vector $\vec{k}$ for the n^{th} mode in the z' and x' direction respectively. A_n is the magnitude of the n^{th} mode. For propagating modes, the propagation vector $\vec{k}$ can be represented as in Fig. II-1. The angle between $\vec{k}$ and the horizontal is θ. Snell's law gives the relationship between the speeds of sound in the layer and the critical angle θ_c.

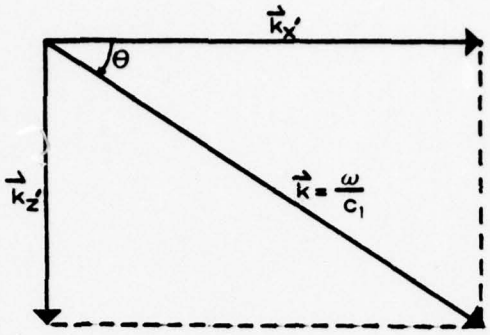


Fig. II-1. The propagation vector $\vec{k}$ and its components

$$\theta_c = \text{arc cos} \frac{c_1}{c_2} \tag{II-2}$$

As long as $\theta < \theta_c$ the energy is totally reflected. However, when $\theta > \theta_c$ energy is transmitted through the previously totally-reflecting surface.

To satisfy the requirements of propagation, $k_{z'_n}$ must be a constant, real number for each mode and from Ref. 3,

$$\tan k_{z'_n} H = -\left(\frac{\rho_2}{\rho_1}\right)\left(\frac{k_{z'_n}}{\gamma_n}\right) \tag{II-3}$$

where

$$\gamma_n = \sqrt{k_{x'}^2 - \left(\frac{\omega}{c_2}\right)^2} \tag{II-4}$$

At cutoff $\theta = \theta_c$ and then the geometry of Fig. II-1 implies $k_{x'} = \frac{\omega}{c_2}$ so that

$$k_{z',n} H = (n - \tfrac{1}{2})\pi \qquad \text{(II-5)}$$

and for a mode with frequency just above its cutoff frequency f_c there is a pressure antinode at the bottom.

Now by writing Eq. II-1 in the form

$$\underset{\sim}{P} = \sum_n \frac{A_n}{2i} \left(e^{ik_{z',n} z'} - e^{-ik_{z',n} z'}\right) e^{i(\omega t - kx')}$$

$$= -\frac{1}{2} \sum_n i A_n \{ e^{i(\omega t - k_{x',n} x' + k_{z',n} z')} - e^{i(\omega t - k_{x',n} x' - k_{z',n} z')} \} \qquad \text{(II-6)}$$

we have two plane waves that propagate with wave number $\vec{k} = k_{x_n'}\hat{x} \pm k_{x_n'}\hat{z}'$. If we assume that the frequency is slowly lowered, higher modes are cutoff as the frequency decreases with $k_{z',n}$ approaching $(n - \frac{1}{2})\frac{\pi}{H}$

b. A Tapered Layer

Let us now consider a wedge with angle δ as indicated in Fig. II-2 and II-3, where X_o' is the distance from $\theta = \theta_c$ to the apex, and x_s' is the distance of closest approach (Turnaround distance) of the indicated ray. In this case each bounce off the bottom increases θ by 2δ. At the point where $\theta = \theta_c$ energy begins to penetrate into the lower layer. The resulting attenuated ray bounces off the

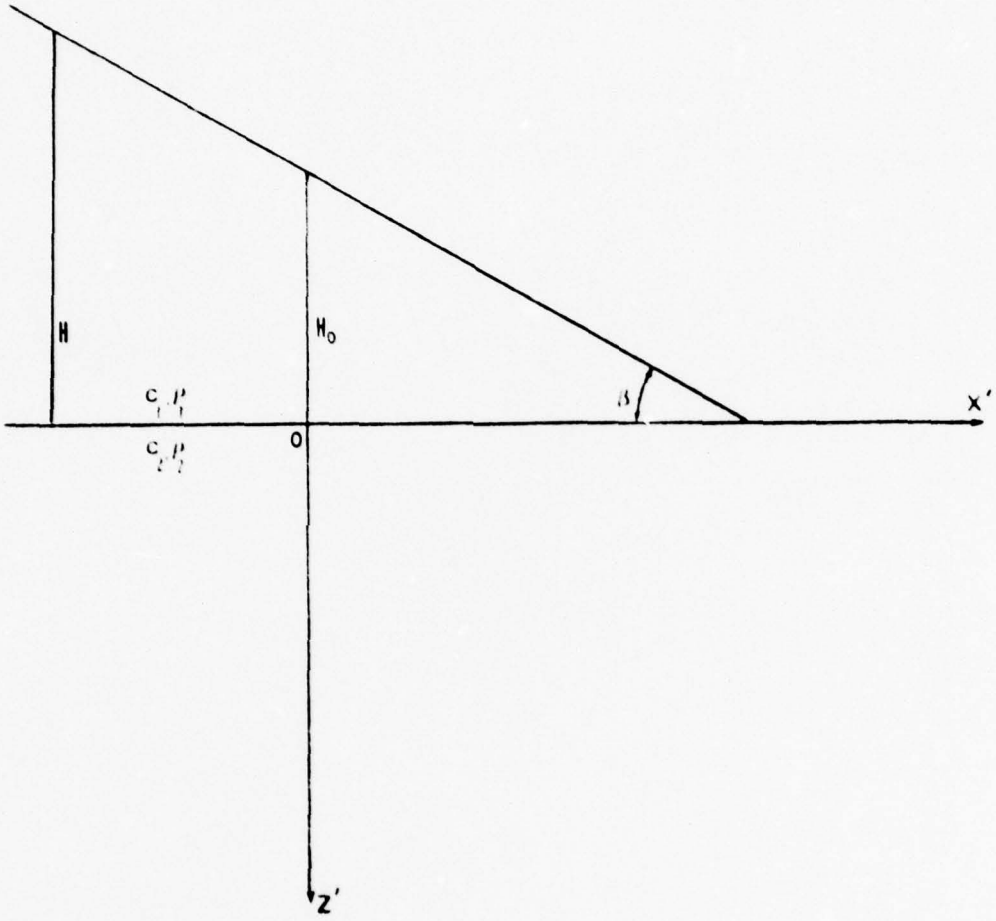


Fig. II-2. The geometry of a wedge

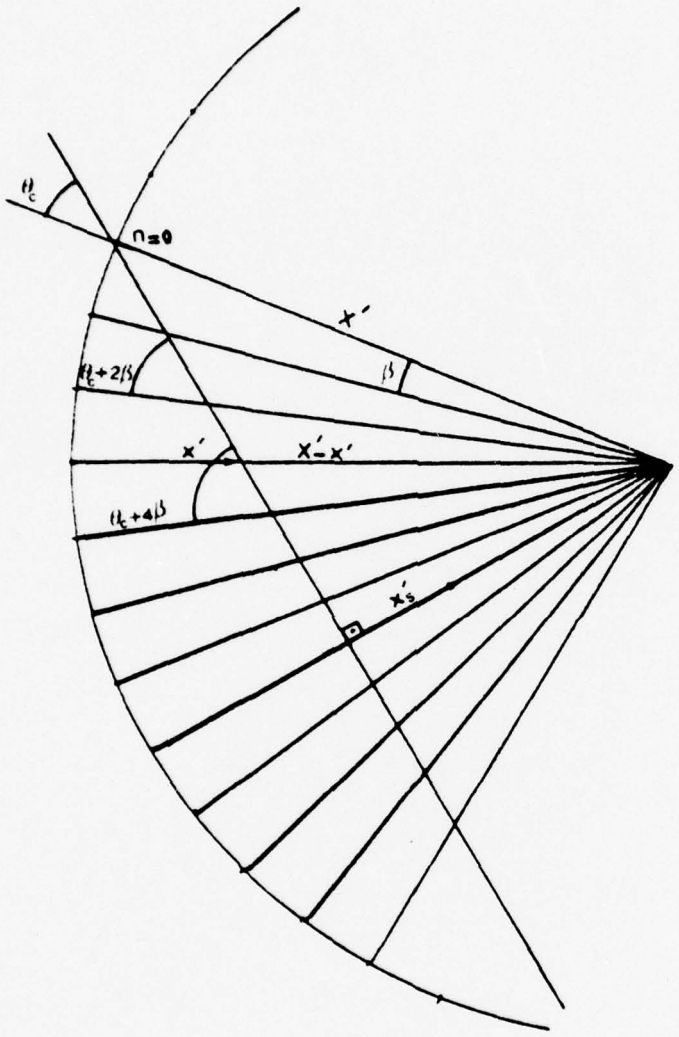


Fig. II-3. Bounces off the bottom of a wedge

top and makes another collision with the bottom, losing still more energy. This process continues until the wave reaches the "Turnaround distance" x'_s defined by:

$$x'_s = X'_o(1 - \sin \theta_c) \qquad \text{(II-7)}$$

For the wedge then, the frequency remains constant while θ increases with each bounce off the bottom until that depth H_o is reached for which $\theta = \theta_c$ where

$$H_o = \frac{(n - \frac{1}{2})\pi}{k_{z'_n}} \qquad \text{(II-8)}$$

From Fig. II-1 we obtain at cutoff

$$k_{z'_n} = k \sin \theta_c \qquad \text{(II-9)}$$

where

$$k = \frac{2\pi}{\lambda} \qquad \text{(II-10)}$$

and substituting Eq. (II-9) into Eq. (II-8) yields

$$H_o = \frac{(n - \frac{1}{2})\lambda}{2 \sin \theta_c} \qquad \text{(II-11)}$$

Knowing H_o allows calculation of the value of $x' = X'_o$ where energy will begin to be transmitted into the bottom.

2. Pressure Distribution along the Bottom

A.B. Coppens [Ref. 4] formulated an approximate model to predict the characteristics of the transmitted beam in the bottom. The expressions for the pressure amplitude and $k_{x'}$ are:

$$A = A_o e^{-\Lambda} \tag{II-12}$$

$$k_{x'} = \sqrt{\frac{\omega}{c_1} - k_{z'}^2} = \frac{\omega}{c_1}\sqrt{1 - \left(\frac{\sin \theta_c}{1 - \frac{x'}{X'_o}}\right)^2} \tag{II-13}$$

where x', X'_o, are defined from the geometry of Fig. II-1, θ_c from Eq. II-2, A_o is the pressure amplitude at $x' = 0$, and Λ defined as

$$\Lambda = \frac{\tan \theta_c}{s}\left\{\frac{b^2}{b^2-1}\frac{c}{\sqrt{b^2-1}}\left[\arcsin \frac{c^2+bz}{c(b+z)} - \arcsin \frac{c}{|b|}\right]\right.$$

$$- \frac{1}{2}\frac{b}{b-1}\frac{c}{\sqrt{1-c^2}}\left[\arcsin \frac{c^2+bz}{c(1+z)} - \arcsin c\right]$$

$$\left. + \frac{1}{2}\frac{1}{b+1}\frac{c}{\sqrt{1-c^2}}\left[\arcsin \frac{c^2-z}{c(1-z)} - \arcsin c\right]\right\} \tag{II-14}$$

where

$$b = \frac{\rho_2}{\rho_1} \tag{II-15}$$

$$c = \cos \theta_c = \frac{c_1}{c_2} \tag{II-16}$$

$$z = \sqrt{1 - (1 - \frac{x'}{X'_o})^2} \tag{II-17}$$

In the case where $\frac{x'}{X'_o} << \frac{1}{2} \cos^2\theta_c$ this model may be simplified further

$$A = A_o \, e^{-\frac{\rho_1}{\rho_2} \frac{\tan\theta_c}{\beta} \frac{2\sqrt{2}}{3} (\frac{x'}{X'_o})^{3/2}} \tag{II-18}$$

and

$$\alpha = -k_{x'} x' = -x' \frac{\omega}{c_1} \sqrt{1 - (\frac{\sin \theta_c}{1 - \frac{x'}{X'_o}})^2} \tag{II-19}$$

$$\theta = \text{arc sin } (\frac{\sin \theta_c}{1 - \frac{x'}{X'_o}}) \tag{II-20}$$

3. Pressure Distribution under the Bottom

In this part we present without detailed derivation A.B. Coppens [Ref. 2] work concerning the pressure distribution under the bottom based on the simple model and obtained through the use of the Green's function and the method of stationary phase. Two basic assumptions were considered for this development.

a. The plane wave has wavefronts that are parallel to the shore line.

b. The pressure distribution on the bottom can be viewed as an acoustical source which generates the beam of sound projected into the bottom. The geometry is indicated in Fig. II-4.

The Green's function formulation for this case can be developed through the geometry of Fig. II-4 as follows: At the point (x',z') the instantaneous pressure is given by

$$\underset{\sim}{P} = \underset{\sim}{P}(r',t) = \underset{\sim}{P}(r')\, e^{i\omega t} \qquad \text{(II-21)}$$

where

$$\underset{\sim}{P}(r') = \frac{1}{4\pi} \int_{-\infty}^{\infty} \underset{\sim}{P}_s(x'') \frac{\partial G}{\partial z'}\Big|_{z'=0} dx'' \qquad \text{(II-22)}$$

The integrand of Eq. (II-22) is formed from the pressure distribution at the bottom

$$\underset{\sim}{P}_s(x'') = \frac{1}{\sqrt{1 - \frac{x''}{X'_o}}} A(x'')\, e^{-i \frac{\omega}{c_1} \sqrt{1-\left(\frac{\sin\theta_c}{1 - \frac{x''}{X'_o}}\right)^2}\, x''} \qquad \text{(II-23)}$$

and the Green's function for a line source is

$$\underset{\sim}{G}(r',r'') = i\pi H_o^{(2)}(|r'-r''|) \qquad \text{(II-24)}$$

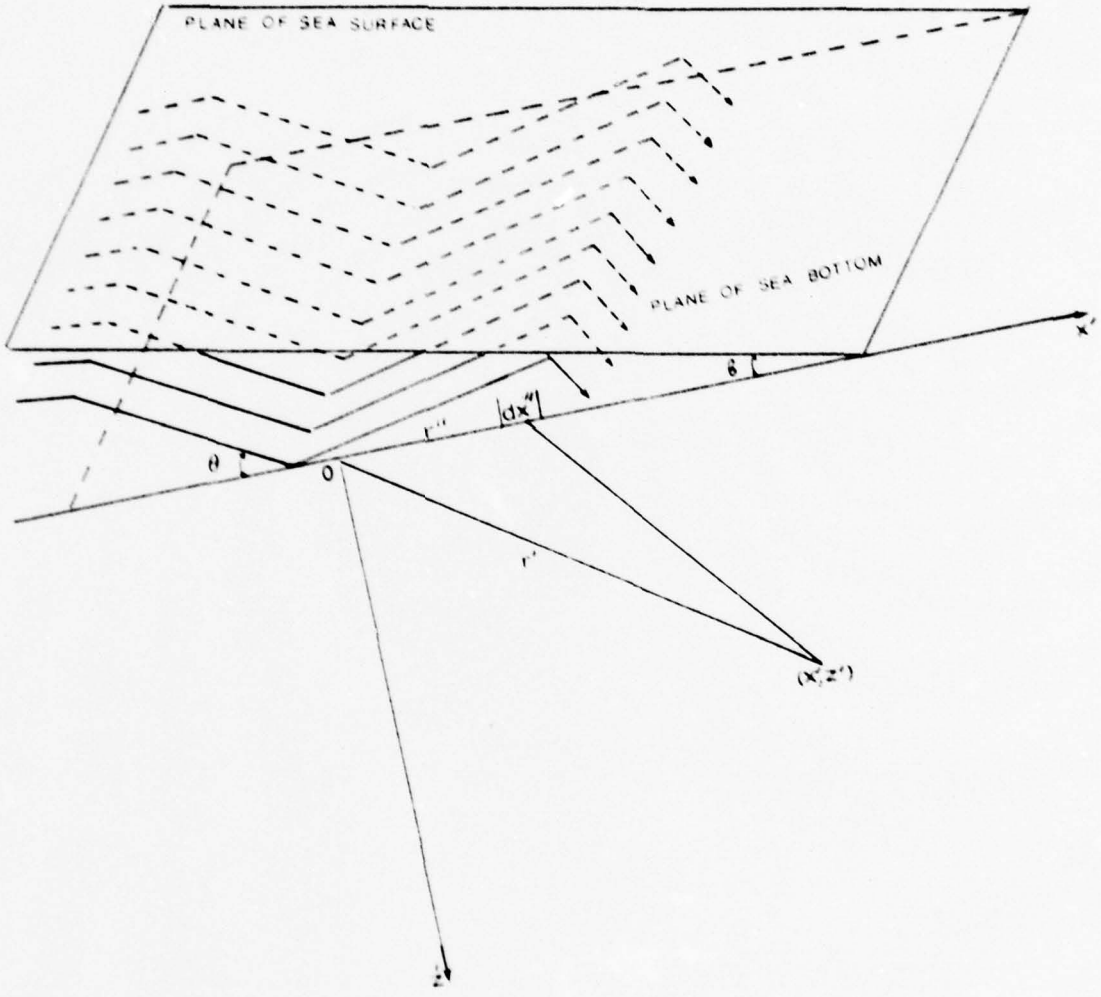


Fig. II-4. Plane wave propagation in the wedge

In Eq. (II-23) the term $\frac{1}{\sqrt{1 - \frac{x''}{X'_o}}}$ is an a <u>postiori</u> correction for the cylindrical convergence of sound. In the absence of losses into the bottom and if there is no energy loss within for the wedge, the pressure amplitude would behave as

$$\frac{P_H}{P_{H_o}} = \sqrt{\frac{H_o}{H}} \qquad \text{(II-25)}$$

also from the geometry of Fig. II-2 we have

$$\frac{H_o}{H} = \frac{1}{1 - \frac{x''}{X'_o}} \qquad \text{(II-26)}$$

so that

$$\frac{P_H}{P_{H_o}} = \frac{1}{\sqrt{1 - \frac{x''}{X'_o}}} \qquad \text{(II-27)}$$

The term A(x") is the pressure amplitude on the bottom and the exponential term is the corresponding phase.

This pressure distribution is an integral of the general form

$$I = \int_{-\infty}^{\infty} F(x)\, e^{G(x)}\, dx \qquad \text{(II-28)}$$

where F(x) varies slowly compared with the exponential factor. The value of the integral can be well approached with the method of stationary phase.

Using the above method and assuming the simple model for $\frac{x''}{X'_o} << \frac{1}{2}\cos^2\theta_c$, and for small β the following expression for the pressure distribution was developed:

$$|\underset{\sim}{P}| = \frac{A}{2\sqrt{2}}\sqrt{\frac{r}{X'_o}}\, v\, e^{-\frac{\rho_1}{\rho_2}\frac{\tan\theta_c}{\beta}\frac{1}{6\sqrt{2}}v^3} \qquad \text{(II-29)}$$

where

$$v = \frac{\sqrt{2(1-\cos\theta)}}{\tan\theta_c} \simeq \frac{\sin\theta}{\tan\theta_c} \qquad \text{(II-30)}$$

2. Pressure Distribution along the Bottom Predicted by the Method of Images

Since the simple model did not yield results agreeing with the experimental measurements, it was decided to use the exact but more cumbersome method of images to attempt to predict the pressure distribution on the bottom.

Let the source be a distance X from the apex of the wedge and a depth H below the sea surface as indicated in Fig. II-5.

Define

$$\phi_d \triangleq \text{arc sin}\,\frac{H}{X} \qquad \text{(II-31)}$$

and

$$\phi_o \triangleq \beta - \phi_d \qquad \text{(II-32)}$$

where β is the angle between the sea surface and bottom, ϕ_d is the angle formed at the apex between the source and the sea surface, and ϕ_o is the analogous angle for the source and the bottom.

If ϕ_n is the angle formed at the apex between the n^{th} image and the bottom then Fig. II-5 reveals

$$\begin{aligned}
\phi_1 &= \beta + \phi_d = 2\beta - \phi_o \\
\phi_2 &= 3\phi_o + 2(\beta-\phi_o) = 2\beta+\phi_o \\
&\vdots \\
\phi_3 &= 3\phi_o + 4(\beta-\phi_o) = 4\beta-\phi_o
\end{aligned} \qquad \text{(II-33)}$$

or more generally

$$\begin{aligned}
\phi_n &= (n+1)\phi_o + n(\beta-\phi_o) = n\beta + \phi_o \quad \text{for n even} \\
\phi_n &= n\phi_o + (n+1)(\beta-\phi_o) = (n+1)\beta - \phi_o \quad \text{for n odd}
\end{aligned} \qquad \text{(II-34)}$$

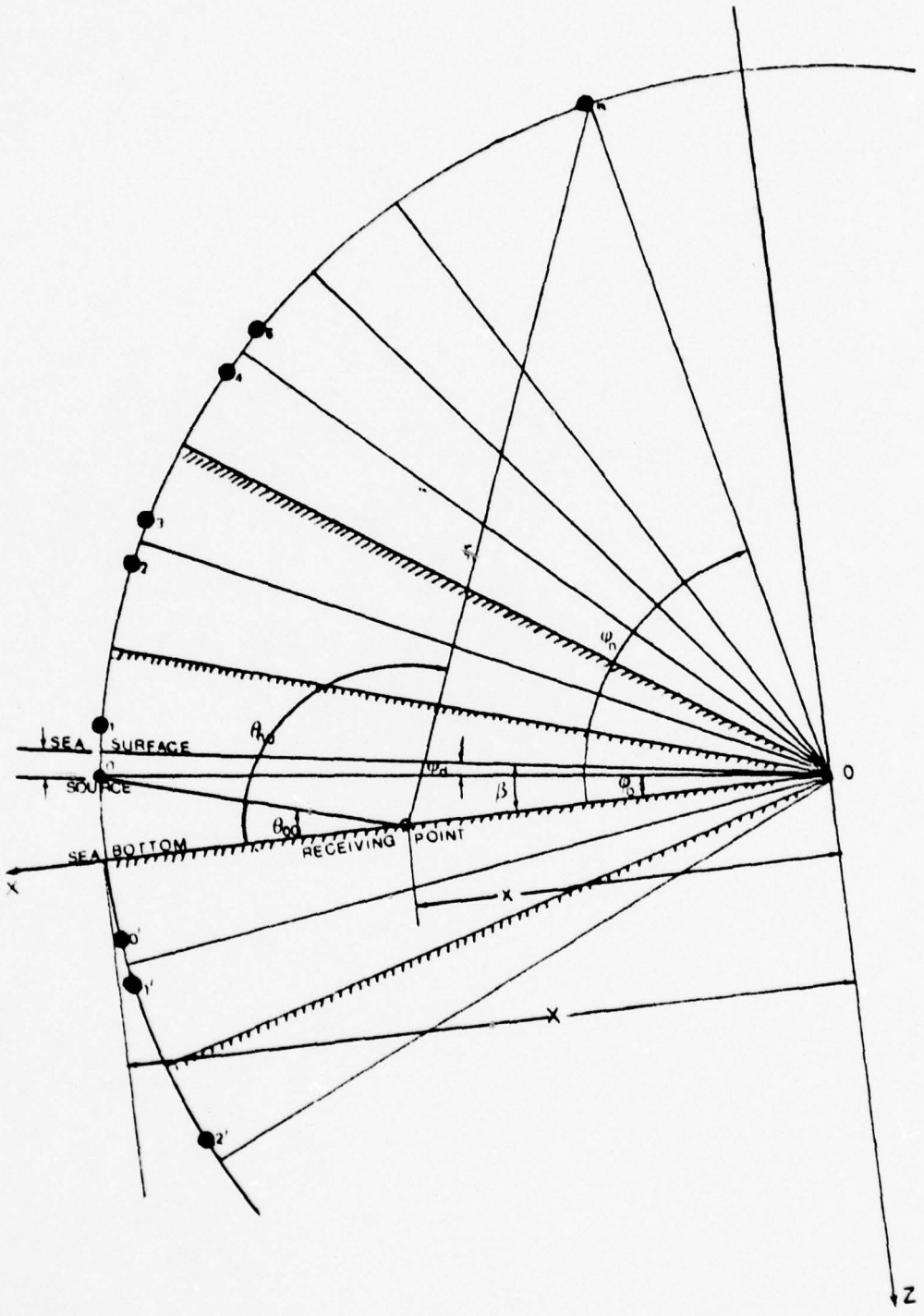


Fig. II-5. Geometry of a wedge by the method of images

This set of equations can be reduced further to one expression:

$$\phi_n = \{n + \tfrac{1}{2}[1-(-1)^n]\}\beta + (-1)^n\phi_o = 2\ \mathrm{INT}[\tfrac{n+1}{2}]\beta + (-1)^n\phi_o \qquad \text{(II-35a)}$$

Also for the symmetric member n' of the paired images we obtain

$$\phi_{n'} = \{n' + \tfrac{1}{2}[1-(-1)^{n'}]\}\beta - (-1)^{n'}\phi_o = 2\ \mathrm{INT}[\tfrac{n'+1}{2}]\beta + (-1)^{n'}\phi_o \qquad \text{(II-35b)}$$

where INT[ ] denotes the largest integer which is equal to, or smaller than the argument.

Considering the geometry of Fig. II-5 and II-6 we can derive expressions for the distances r_n and $r_{n'}$, which represents the distance between a receiving point on the bottom at distance x from the apex and the n^{th} and n'^{th} image respectively. Also we can derive expressions for the angles θ_{no} and $\theta_{n'o}$ which formed at the receiving point between the bottom and the images n and n' respectively.

These expressions are:

$$r_n = \sqrt{X^2 + x^2 - 2Xx\cos\phi_n} \qquad \text{(II-36a)}$$

$$r_{n'} = \sqrt{X^2 + x^2 - 2Xx\cos\phi_{n'}} \qquad \text{(II-36b)}$$

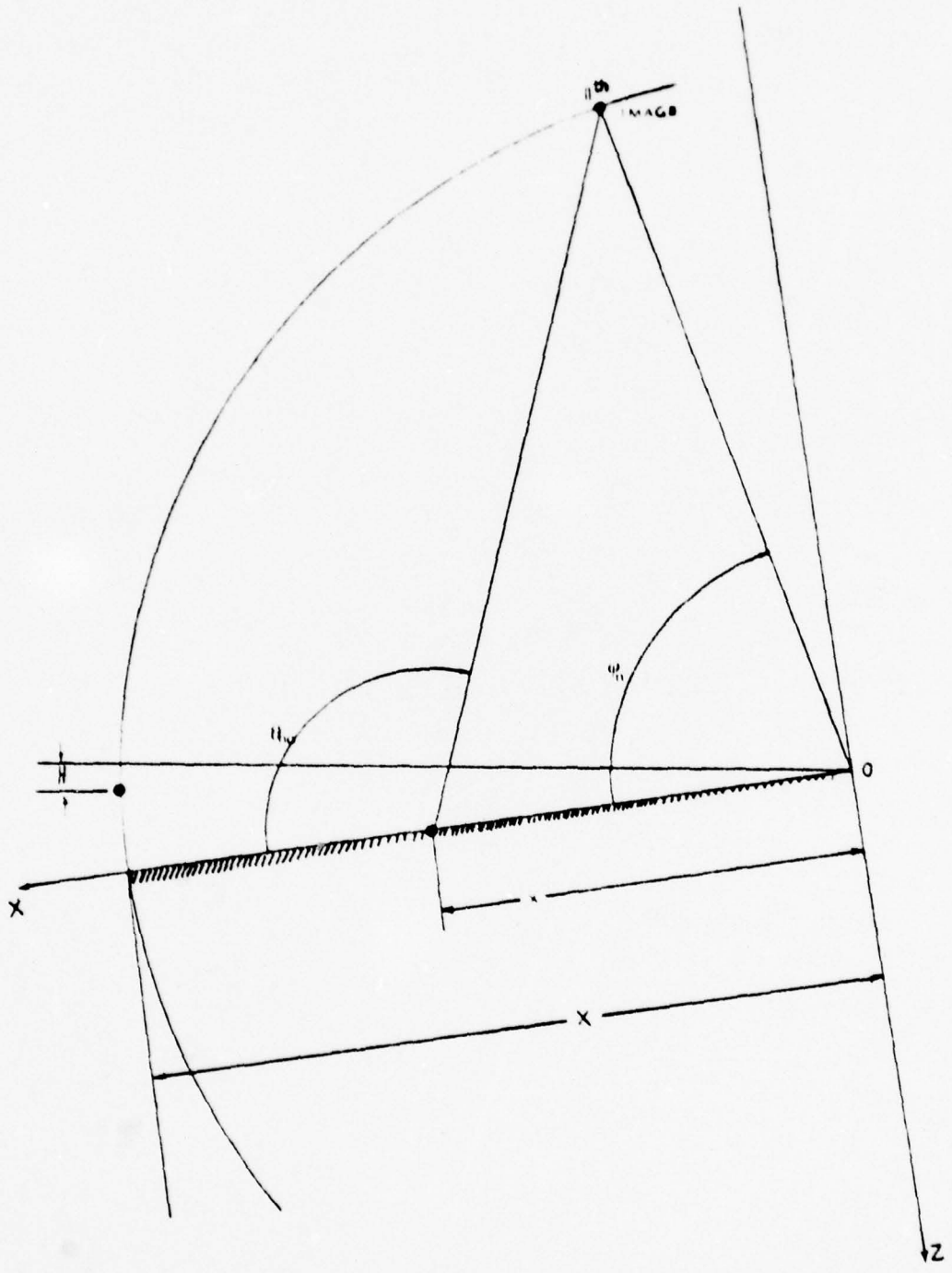


Fig. II-6. Geometric development of the image's position with respect to the receiving point

$$\theta_{no} = \arctan\left[\frac{\sin \phi_n}{\cos \phi_n - \frac{x}{X}}\right] \qquad \text{(II-37a)}$$

$$\theta_{n'o} = \arctan\left[\frac{\sin \phi_{n'}}{\cos \phi_{n'} - \frac{x}{X}}\right] \qquad \text{(II-37b)}$$

Let us now define θ_{nm} and $\theta_{n'm}$ as the angles of incidence for the m^{th} bounce from the bottom for the n and n' image respectively, m = 1,2,3, ... (The o^{th} bounce is the last-one before reaching the receiver.) From the geometry of Fig. II-5 and Fig. II-7 we obtain expressions for θ_{nm} as follows:

$$\begin{aligned}
\theta_{21} &= \theta_{20} - 2\beta \\
\theta_{31} &= \theta_{30} - 2\beta \\
\theta_{41} &= \theta_{40} - 2\beta \qquad \text{(II-38)} \\
\theta_{42} &= \theta_{40} - 4\beta \\
\theta_{51} &= \theta_{50} - 2\beta \\
&\vdots
\end{aligned}$$

The general expression is

$$\theta_{nm} = \theta_{no} - 2m\beta \qquad \text{(II-39a)}$$

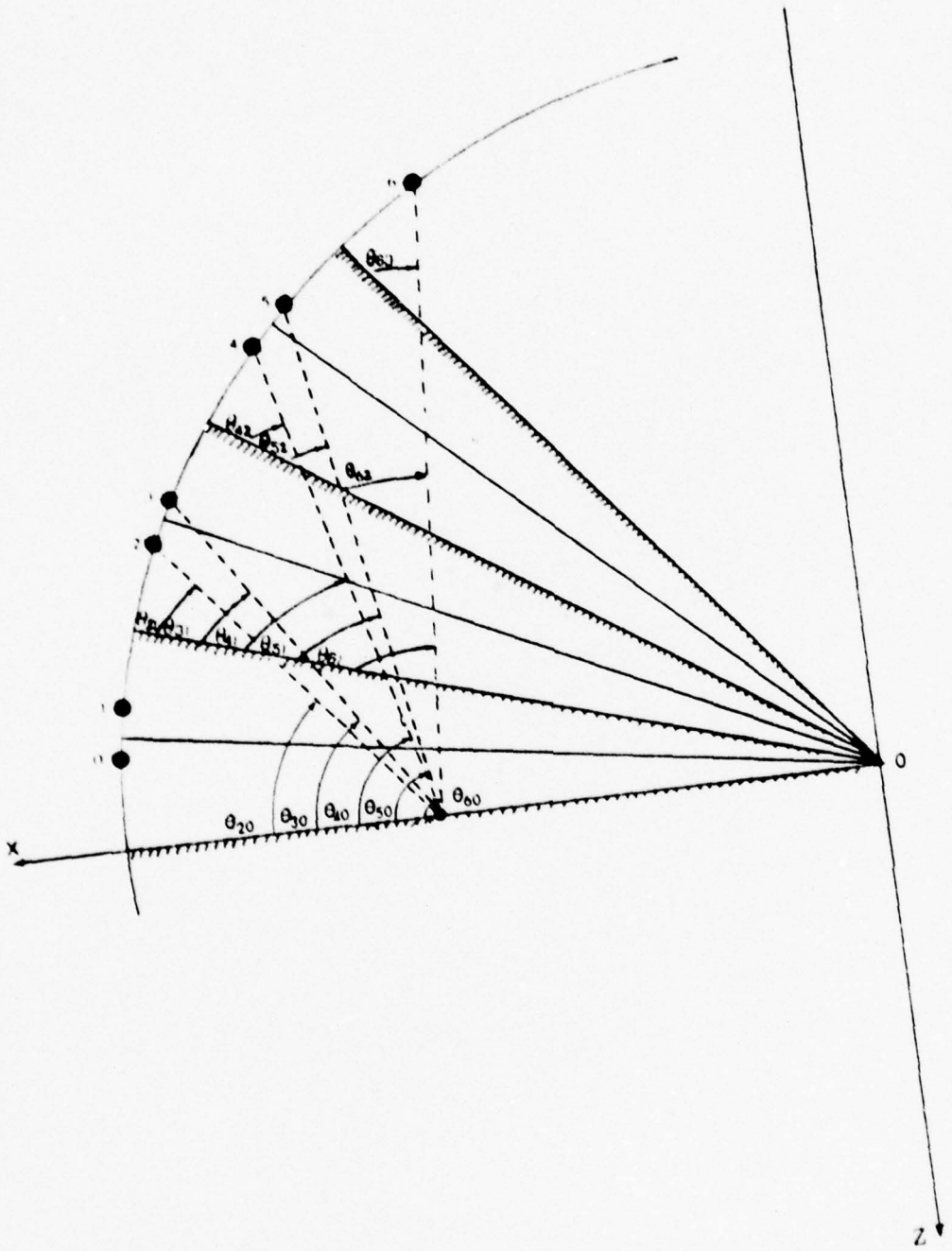


Fig. II-7. Geometric development of reflection angles

Also for the symmetric member n' of the n^{th} pair we obtain

$$\theta_{n'm} = \theta_{n'o} - 2m\delta \qquad \text{(II-39b)}$$

and the maximum number of bounces of the n^{th} and n'^{th} image is

$$m_{max} \triangleq M = \frac{1}{2}(n-1) + \frac{1}{4}\{1 - (-1)^{n+1}\}$$

$$= \frac{1}{2}(n'-1) + \frac{1}{4}\,1 - \{(-1)^{n'+1}\}$$

$$= \text{INT}\left[\frac{\phi_n}{2\delta}\right] = \text{INT}\left[\frac{\phi_{n'}}{2\delta}\right] \qquad \text{(II-40)}$$

If the receiving point is on the bottom, then from Fig. II-8 we obtain:

1. The distance from each member of a pair of images (n,n') to the receiving point is the same, i.e., $r_n = r_{n'}$.
2. The number of reflections (from the bottom) from the n'^{th} image to the receiving point is one more than the n^{th} image.
3. The grazing angle to the bottom is the same for each corresponding bottom bounce so that the reflection coefficients for corresponding bounces are equal, except the last bounce for the n'^{th} image .

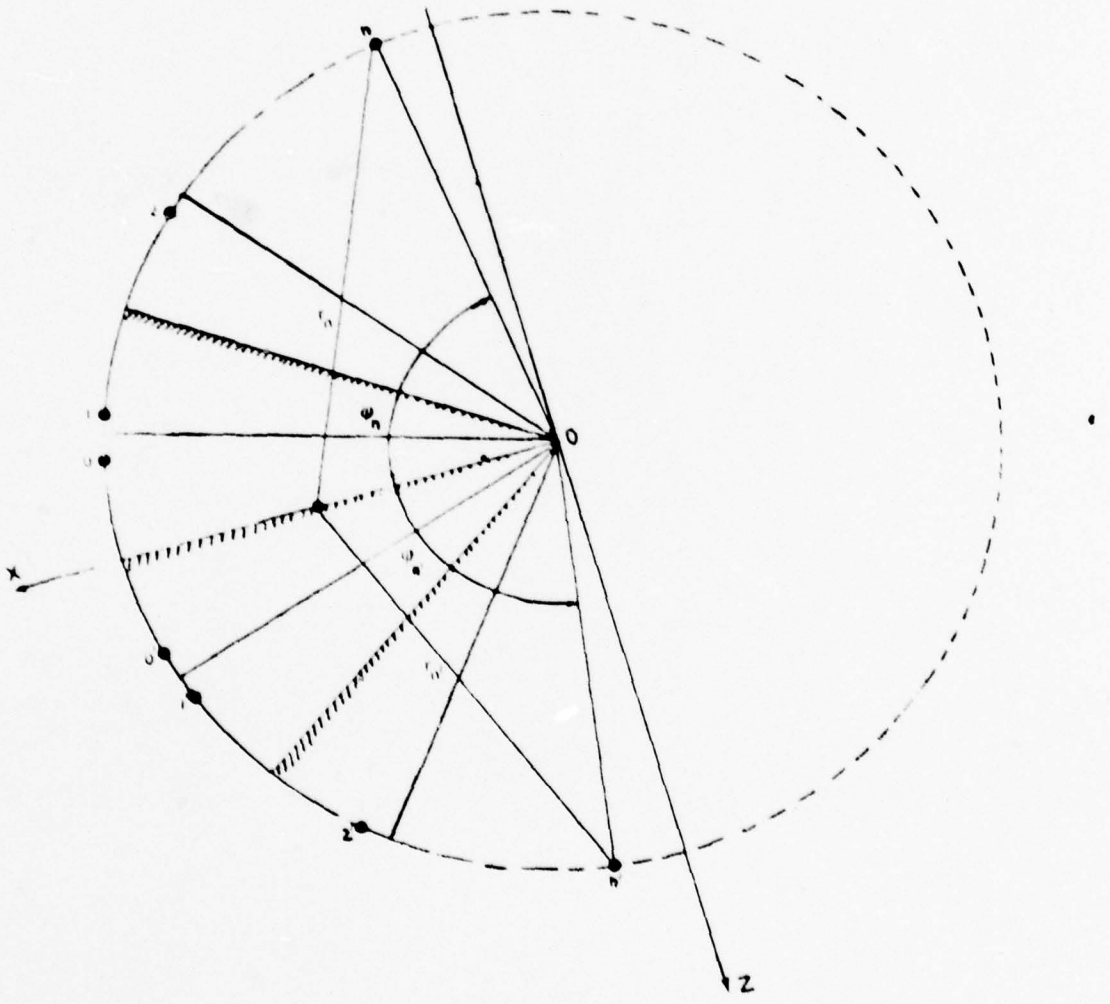


Fig. II-8. Geometry of symmetric images

Consequently $\underset{\sim}{R}_{nm} = \underset{\sim}{R}_{n'm}$ where $\underset{\sim}{R}_{nm}$ and $\underset{\sim}{R}_{n'm}$ are the reflections coefficients for the m^{th} bounce of the n^{th} and n'^{th} image respectively.

The reflection coefficients for the n^{th} image are given by

$$\underset{\sim}{R}_{nm} = \frac{\frac{\rho_2 c_2}{\rho_1 c_1} - \underset{\sim}{\psi}_{nm}}{\frac{\rho_2 c_2}{\rho_1 c_1} + \underset{\sim}{\psi}_{nm}} \qquad \text{(II-41)}$$

where

$$\underset{\sim}{\psi}_{nm} = \frac{\sqrt{1 - (\frac{c_2}{c_1})^2 \cos^2\theta_{nm}}}{\sin \theta_{nm}} \quad \text{for } \theta_{nm} \geq \theta_c \qquad \text{(II-42)}$$

and

$$\underset{\sim}{\psi}_{nm} = -i \frac{\sqrt{(\frac{c_2}{c_1})^2 \cos^2\theta_{nm} - 1}}{\sin \theta_{nm}} \quad \text{for } \theta_{nm} < \theta_c \qquad \text{(II-43)}$$

with

$$\theta_c = \arccos (\frac{c_1}{c_2}) \qquad \text{(II-44)}$$

Let us now consider the pressure $\underset{\sim}{P}(x)$ at a point x on the bottom. The contributions from the paired images are

$$\sum_{n=0}^{N} \{\frac{1}{r_n} e^{-ikr_n} \prod_{m=1}^{M} \underset{\sim}{R}_{nm} (-1)^{INT[\frac{n+1}{2}]} \} \qquad \text{(II-45)}$$

and

$$\sum_{n=0}^{N} \{\frac{1}{r_{n'}} e^{-ikr_{n'}} \prod_{m=0}^{M} \underset{\sim}{R}_{n'm} (-1)^{INT[\frac{n'+1}{2}]} \} \qquad \text{(II-46)}$$

(The n^{th} and n'^{th} images differ only in that n^{th} image has no $\underset{\sim}{R}_{no}$ reflection.)

The complex pressure is

$$\underset{\sim}{P}(x) = \sum_{n=0}^{N} \{\frac{1}{r_n} e^{-ikr_n} (-1)^{INT[\frac{n+1}{2}]} (1+\frac{1}{\underset{\sim}{R}_{no}}) \prod_{m=0}^{M} \underset{\sim}{R}_{nm}\} \qquad \text{(II-47)}$$

A computer program was constructed to calculate this complex pressure (amplitude and phase). This program, with the corresponding flow chart, is presented in Appendix A.

In case of a source so distant that it can be assumed to be at $r \to \infty$ then the geometry of Fig. II-9 yields the approximation

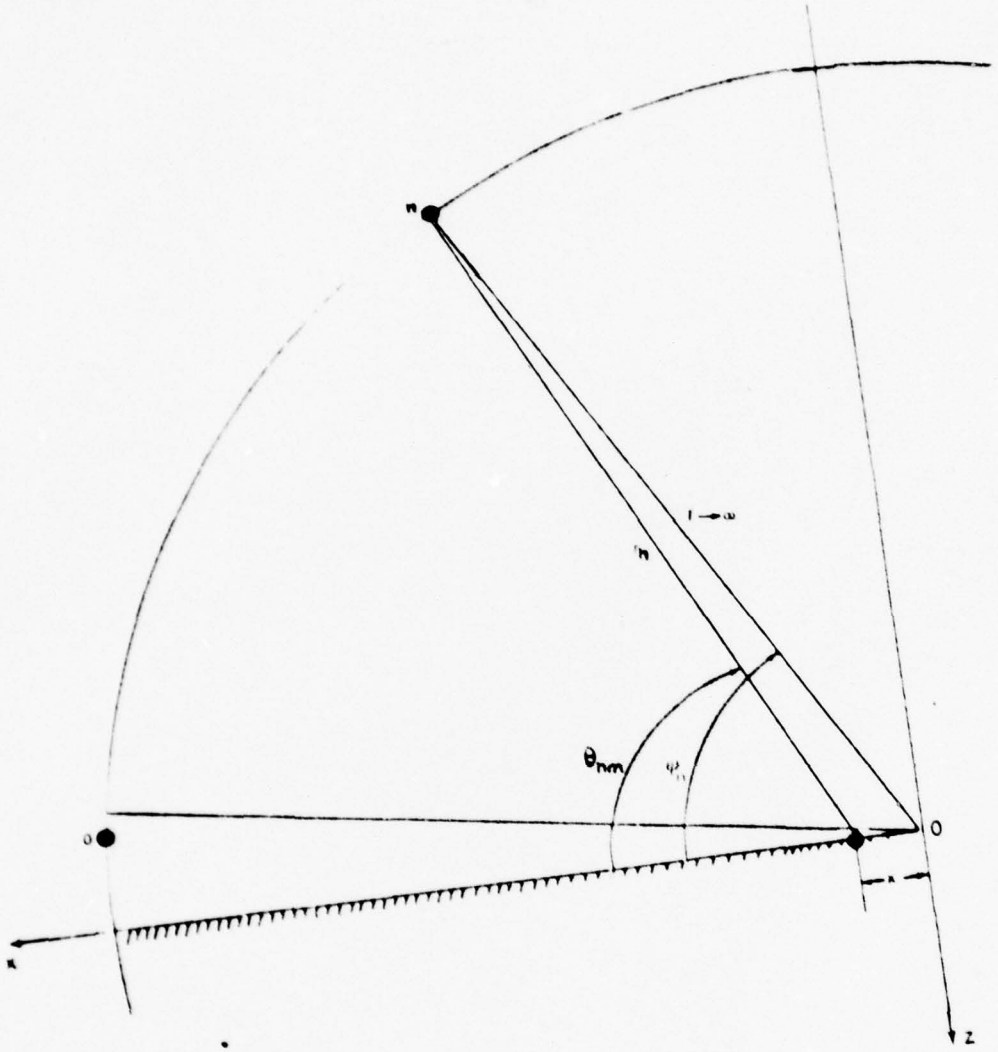


Fig. II-9. The geometry of distance source approximation

$$\theta_{no} \simeq \phi_n \tag{II-48}$$

which simplify the mathematics significantly. Here

$$\underset{\sim}{R}_{no} = \underset{\sim}{R}(\theta_{no}) \simeq \underset{\sim}{R}(\phi_n) \tag{II-49}$$

In this case, the expression for reflection coefficients are (see Appendix B)

$$\begin{aligned}
&\prod_{m=0}^{M} \underset{\sim}{R}_{om} = \underset{\sim}{R}_o = \underset{\sim}{R}(\phi_o) \\
&\prod_{m=0}^{M} \underset{\sim}{R}_{1m} = \underset{\sim}{R}_1 = \underset{\sim}{R}(\phi_1) \\
&\prod_{m=0}^{M} \underset{\sim}{R}_{2m} = \underset{\sim}{R}_o \underset{\sim}{R}_1 = \underset{\sim}{R}(\phi_o)\underset{\sim}{R}(\phi_1) \\
&\prod_{m=0}^{M} \underset{\sim}{R}_{3m} = \underset{\sim}{R}_1 \underset{\sim}{R}_3 = \underset{\sim}{R}(\phi_1)\underset{\sim}{R}(\phi_3) \\
&\quad \vdots \\
&\prod_{m=0}^{M} \underset{\sim}{R}_{nm} = \prod_{m=0}^{M} \underset{\sim}{R}_{n-2,m} \cdot \underset{\sim}{R}_n = \prod_{m=0}^{M} \underset{\sim}{R}_{n-2,m} \cdot \underset{\sim}{R}(\phi_n)
\end{aligned} \tag{II-50}$$

for $n \geq 2$

where the right hand sides of Eqs. (II-50) depend only on n, then define

$$\underset{\sim}{\Gamma}(n) \triangleq \begin{cases} \underset{\sim}{R}_o & \text{for } n = 0 \\ \underset{\sim}{R}_1 & \text{for } n = 1 \\ \underset{\sim}{\Gamma}(n-2)\underset{\sim}{R}_n & \text{for } n \geq 2 \end{cases} \qquad \text{(II-51)}$$

Also, the geometry of Fig. II-9 gives

$$r_n = r - x \cos \phi_n \qquad \text{(II-52)}$$

Substitution of Eq. ((II-50), (II-51), (II-52) into Eq. (II-47) yields

$$\underset{\sim}{P}(x) = \frac{1}{r} e^{-ikr} \sum_{n=0}^{N} e^{ikx\cos\phi_n} (-1)^{INT[\frac{n+1}{2}]} \{1 + \frac{1}{\underset{\sim}{R}(n)}\} \underset{\sim}{\Gamma}(n) \qquad \text{(II-53)}$$

The last expression for pressure is the approximation for a distant source, which is described in detail elsewhere [Ref. 4].

The advantage of Eq. (II-53) with respect to Eq. (II-47) is that because the elimination of product term, the calculations are greatly simplified.

III. EXPERIMENT

Initially it was intended that the beam pattern in the bottom would be exhaustively investigated, and a larger experimental system with silicon oil in the wedge and a large water tank for the bottom was designed. But, even in the new system, it was observed that the beam pattern was being significantly disturbed by unknown interferences that caused the apparent angle of the beam to move to shallower angles than predicted by the simple theory described in II-A and made the beam seem narrower than predicted. This interference was definitely not from the walls or bottom of the water tank. It might have been associated with the wedge, but whether it was an inherent property of wedge propagation omitted from the theory II-A or merely an artifact of the experimental setup was the question.

In an attempt to study this question more thoroughly, the experiment was redirected to investigate the amplitude and phase of pressure on the bottom of the wedge.

A. APPARATUS

The experimental facility consisted of a wedge of silicon oil overlying a large tank of fresh water; the two fluids being kept apart by a thin Mylar membrane. A photograph of the apparatus is shown in Fig. III-1. The sound source, positioned at the end of the silicon-oil wedge, sent a pulsed signal toward the apex of the wedge. It was

possible to position the receiver anywhere within the fresh water region, but in this experiment the receiver was mainly placed close to the bottom of the wedge. The geometry is shown in Fig. III-2.

1. Water Tank (Fig. III-3a,b,c)

The water tank, constructed of 3/4 in. thick plywood, had the inside surfaces painted with Varathane but were otherwise uncoated. It was filled with tap water at room temperature.

2. Wedge (Fig. III-4)

The silicon oil was contained in a frame whose sides were made of 1/2 in. x 2 in. aluminum and whose bottom consisted of a thin Mylar sheet. Half-mil thick, aluminum-coated Mylar was fastened to the bottom of the frame by first taping a sheet of Mylar, metalized side up to a flat surface. Then the aluminum frame was placed on the Mylar, and the edges outlined by a sign pen. A bead of "Royal bond GRIP" contact cement was applied to the bottom of the frame and to the marked areas of Mylar. After the cement was completely dry (about 15 minutes), the frame was placed on the Mylar and about 50 pounds of weight placed on top of the frame. After the contact cement had cured for 12 hours, a coat of "Silver print conductive paint" was applied to the outside joint between the Mylar and the frame. This provides electrical contact between the Mylar and the frame. (This was necessary to allow measurement of the slope of the wedge as will be explained in a later

section.) The excess Mylar was trimmed flush with the outside edge of the frame by a razor blade. As a final step, a thin coat of the "Silicone rubber sealant" was applied to both the outside and inside of the Mylar-frame interface to prevent leaks. Because the tension in the Mylar tended to bend the walls of the frame inward, a 3/8 in. diameter aluminum rod was used as a "frame spreader" to spread the frame and keep Mylar flat. The length of the frame spreader was adjustable. It was placed across the shorter dimension of the frame and adjusted until the Mylar film was mirror flat. Aluminum arms at each end were used to suspend the wedge from the top of the water tank. The longer arm was connected to the apex side of the wedge and extended in the propagated direction. The slope of the wedge was set by raising the end of this arm with wooden blocks. The other arm, perpendicular to the propagation direction, was connected to the source side of the wedge. The horizontal level of the wedge was adjusted by means of screws at the ends of this arm.

3. Source Transducer

The source transducer was made by Lt. Netzorg. Construction details are discussed in his thesis [Ref. 2]. The design of the transducer was quite well done: it has sufficient horizontal directivity so that sound is not reflected from the side of the frame, there is negligible sound propagation in the backward direction, and its active

face, 2 cm high by 8 cm wide, is the largest size allowable in the wedge. The experimentally measured directivity is very close to the directivity predicted for a rectangular source (Fig. III-5a,b,c). The theoretical directivity is described as follows:

$$H(\theta,\phi) = \frac{\sin(\frac{1}{2}kL_1\sin\theta)}{\frac{1}{2}kL_1\sin\theta} \cdot \frac{\sin(\frac{1}{2}kL_2\sin\phi)}{\frac{1}{2}kL_2\sin\phi} \quad \text{[Ref. 3,5]} \qquad \text{(III-1)}$$

where

L_1 = Horizontal dimension of an active face of a rectangular source.

L_2 = Vertical dimension of an active face of a rectangular source.

$K = \frac{\omega}{c} = \frac{2\pi}{\lambda}$ Wave number

θ = Horizontal angle measured from a major radiation axis.

ϕ = Vertical angle measured from a major radiation axis.

As a matter of convenience, the directivity measurements were done in the water instead of silicon oil. The frequency used in these measurements was adjusted to give the same wavelength as produced when the source operates at its prescribed frequency in silicon oil. A frequency of 127.8 kHz in fresh water (c_2 = 1503.8 m/sec) produces the same wavelength as 100 kHz in a silicon oil (c_1 = 1176.5 m/sec).

For more accurate comparison between the experimental results and the method of images, the vertical directivity was employed in the computer model "WEDGE O" (APPENDIX-A).

The source transducer was mounted on a support that allowed it to be located anywhere in the upper fluid layer. Vertical adjustments were made by means of a micrometer with 1/2 in. of travel.

4. Receiver and Attachment (Fig. III-6a,b)

A LC-10 hydrophone, manufactured by Celesco Industries, was used as the receiver. It was possible to locate the receiver anywhere in the fresh water. Since the main purpose of the experiment was to investigate the sound pressure distribution on the bottom, the hydrophone was usually located as close to the bottom as possible. The attachment mounted on the frame of the wedge as shown in Fig. III-6a.

At the beginning of this thesis, some measurements were made of the beam pattern in the lower fluid. Then a different attachment was used (Fig. III-6b) which was mounted on the large arm.

In both cases, the depth of they hydrophone was adjustable. In all cases, measurements were made in the vertical plane that contained the acoustic axis of the source transducer.

5. Slope-measurement Assembly (Fig. III-7a,b,c)

The slope measurement assembly consisted of a pin, micrometer, and attachment. Fine vertical adjustments of

the pin were made by means of the micrometer with 1/2-in. of travel. The attachment was mounted on the wedge frame and could be located anywhere in the wedge. The pin was electrically insulated from the frame, so that when an Ohmmeter was attached between the frame and the pin, the precise depth at which the pin contacted the metalized Mylar could be determined.

6. Electrical Setup

Figure III-8 is a block diagram of the electrical setup which consists of a driving system, a receiving system, and a measuring system. The transducer was driven by a General Radio Oscillator (Type 1310) and Tone Burst Generator (Type 1396-A), polarized by a 300 Volts D.C. biasing-voltage [Ref. 2]. The driving frequency (100 kHz) was measured with a Hewlett Packard electronic frequency counter (Type 5233L) and the driving waveform displayed on one channel of a Tektronic Dual-Beam Oscilloscope (Type 565). The received signal was amplified (40 dB) by a Hewlett Packard Amplifier (Type 465-A), and band passed (40 kHz ~ 200 kHz) through a Spencer-Kennedy Laboratories Band Pass Filter (Serial 1683 Model 302). The received signal was displayed on the other channel of the Tektronix Dual-Beam Oscilloscope (Type 565) and the amplitude was measured on this display. The received signal also went to a Hewlett Packard Oscilloscope (Model 120B) where its phase was compared to that of the driving signal.

7. Auxiliary Apparatus

To measure the speeds of sound and densities of fluids, other pieces of equipment were used.

Transducer

Two Hydrophones LC5-2

Analytical Balance

ASTM Vessel

B. PROCEDURE

Before beginning the experiments, the speeds of sound and densities of the fluids (a silicon oil for the upper layer, fresh water for the bottom) and the slope of the bottom was measured with high accuracy.

1. Sound Speed Measurements (Fig. III-9)

The speeds of sound were measured in a pan which had dimensions 10 3/4 in. x 7.0 in. x 1 3/8 in. About 1500 cc of a test fluid was carefully poured into a pan to prevent the entrapment of air bubbles. Two LC5-2 receivers and a transducer were used to measure the speeds of sound. The distance between two receivers was set at exactly 20.0 cm. And the transducer was driven by a 150 kHz pulsed signal. The time of transit for one receiver to the other was measured using the time-delay feature of the dual-beam oscilloscope. The speed of sound was then calculated by dividing the distance by the transit time.

2. Density Measurments

The densities of the two fluids were found by first weighing a 100 ml, ASTM vessel on an analytical balance

readable to one-tenth mg. The vessel was then filled to the 100 ml mark and weighed again. By subtracting the first weight from the second weight, the weight of 100 ml of the test fluid was determined. The weight of the test fluid in grams divided by the 100 ml volume and, the quotient times 1000, gave the density of the test fluid in kg/m^3.

3. Measurement of the Slope Angle

The approximate slope was set by raising the end of the long arm a precalculated height with the use of wooden blocks. Then 3500 cc of silicon oil were slowly poured into the wedge, and the frame-spreader was adjusted to keep the bottom flat. The water level in the tank was then adjusted to keep the apex line (shore line) straight. The source transducer was set at about middle depth on the wedge centerline. The slope angle was accurately measured with the slope-measurement assembly described in the apparatus section. Because the top and bottom of the frame of the wedge are parallel, if the Mylar sheet is flat the distance from a reference level to the bottom should be the same at all points. The distance from a reference level to the surface and to the bottom were measured at several points on the wedge centerline, and the data were plotted. The slope was calculated from the plot as shown in the example illustration in Fig. III-10.

4. Measurement of Pressure Amplitude along the Bottom

The electrical setup of the measurements was shown in Fig. III-8. The oscillator output, set at 100 kHz, was

fed into the tone burst generator. A pulsed signal of 36 cycles of the 100 kHz input with a closed-gate duration time of 10 msec (repetition rate was about 100 Hz) went through the transducer biasing network and then to the source transducer. The driving signal was displayed on one channel of the dual-beam oscilloscope and adjusted for a peak-to-peak voltage of 10 Volts. The receiving signal was displayed on the other channel of the same dual-beam oscilloscope. This was very convenient because the receiving signal was always compared with the driving signal on the same oscilloscope. Reflections of the receiving signal were not observed.

5. Measurement of Pressure Phase along the Bottom

The phase of the receiving pressure was compared to that of the driving signal on an oscilloscope. Fig. III-8 also shows the electrical setup for these measurements. The signal from the oscillator was directly fed into the x-axis of the oscilloscope. The receiving signal was amplified and filtered, then fed into the y-axis of the same oscilloscope. The signal on the x-axis was continuous with a constant amplitude (adjusted to 10 Volts peak-to-peak voltage). On the other hand, the signal applied to the y-axis was pulsed and had an amplitude that depended on the receiver position. The pattern observed on the oscilloscope was an ellipse crossed by a line on the x-axis (like "θ" of the Greek alphabet). The line occurred during the time the received pressure was zero, i.e., between pulses. When the

signal, generated by the oscillator, was sent directly to the transducer, bypassing the tone burst generator, the pattern on the oscilloscope was the same ellipse but without the line on the x-axis. This indicates that the pulse is sufficiently long to allow accurate phase determinations. (It also showed that reflections in the tank were negligible.) But measurements were still difficult, because the amplitude of the receiving signal was not constant and the phase changed very quickly with changes in the receiver position. The phase measurements were done independent of the amplitude measurements. The position of the receiver was recorded when the phase was 0°, 90°, 180° and 270°. (Corresponding to a straight line with positive slope, a symmetric ellipse and a straight line of negative slope.)

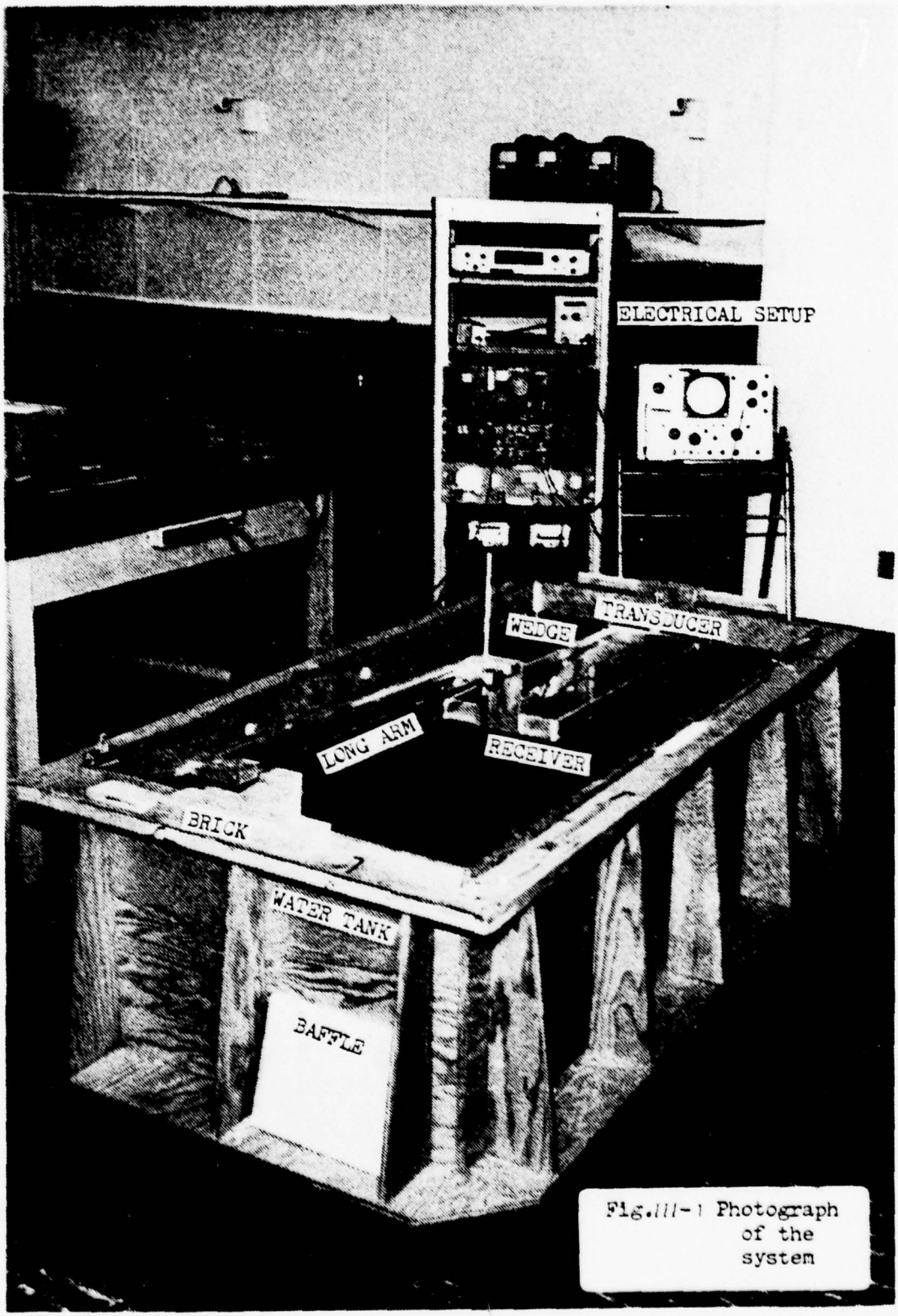


Fig.III-1 Photograph of the system

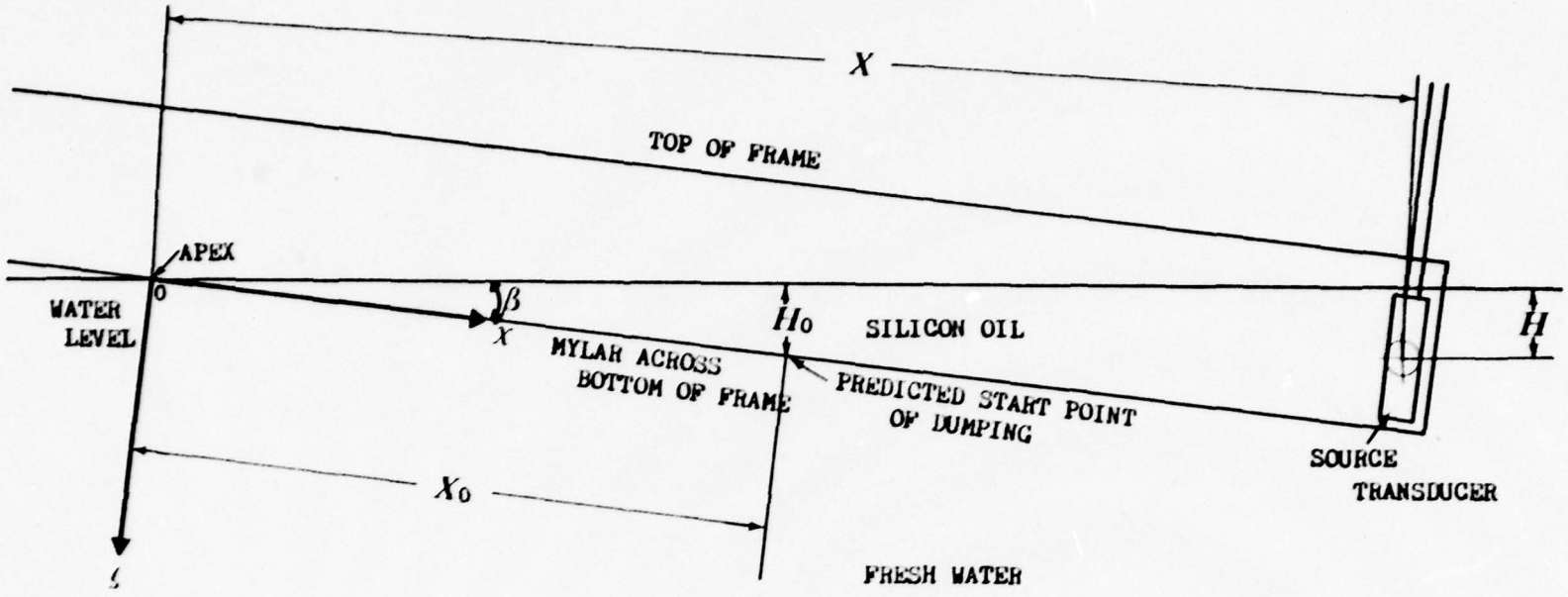


Fig.III-2 Geometry of the system

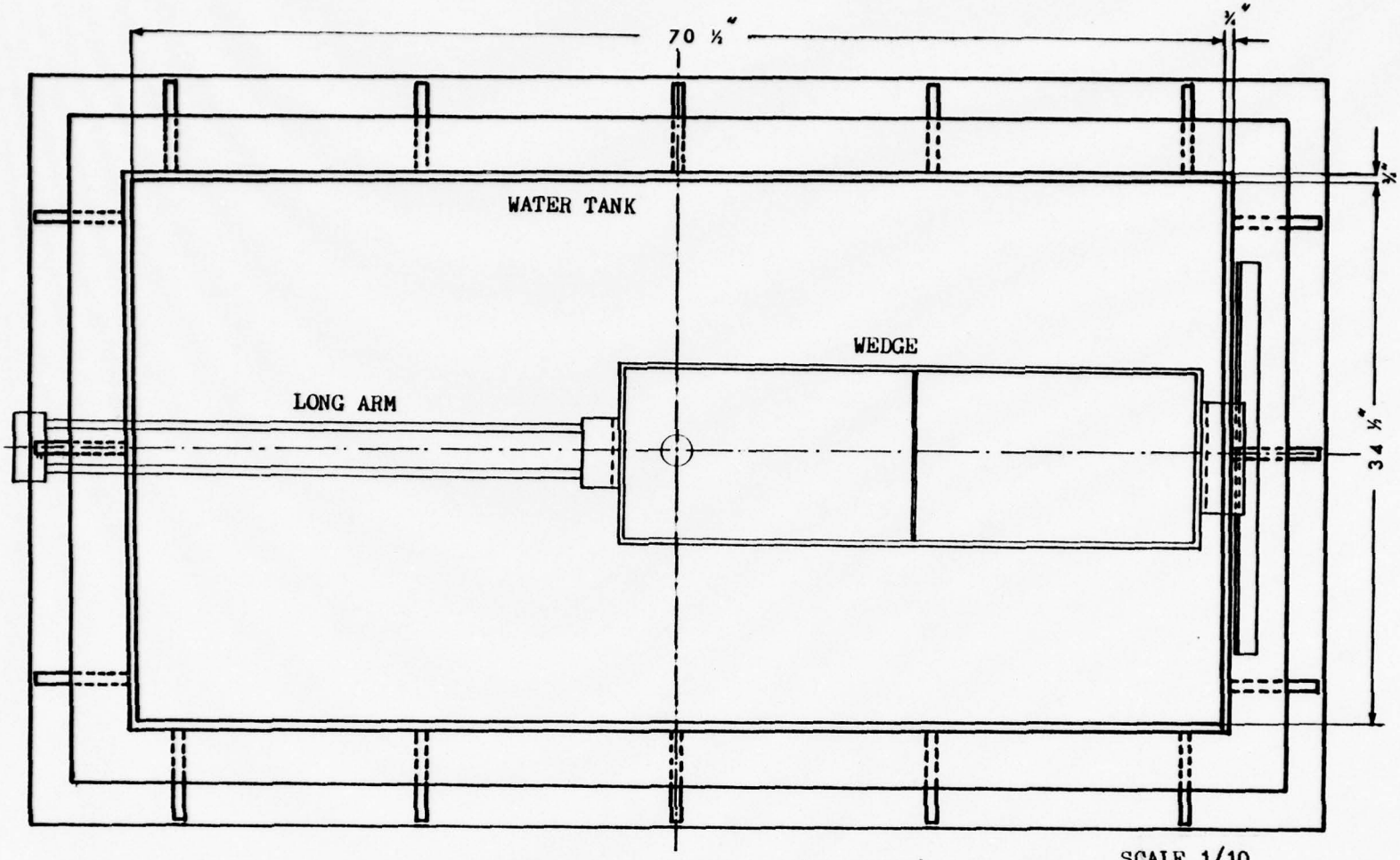


Fig.III-3a Water tank and wedge (Top view)

SCALE 1/10

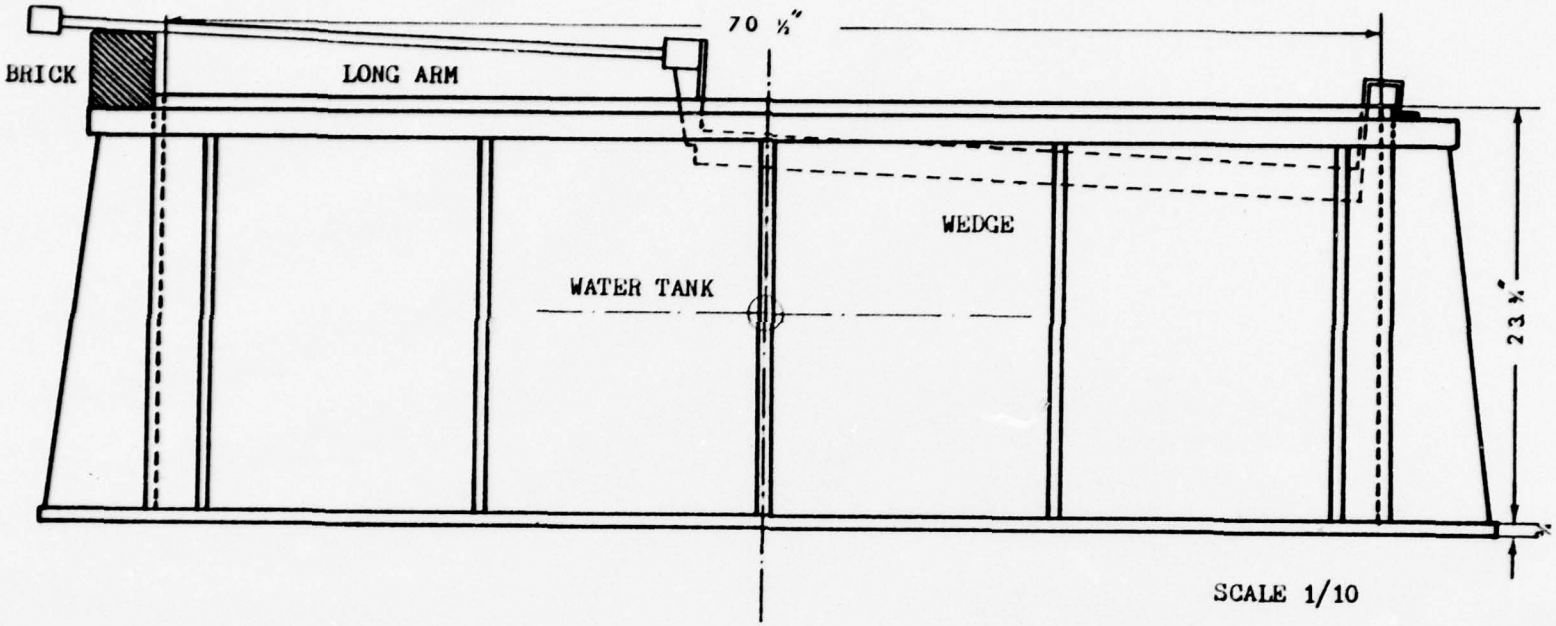


Fig.III-3b Water tank and wedge (Side view 1)

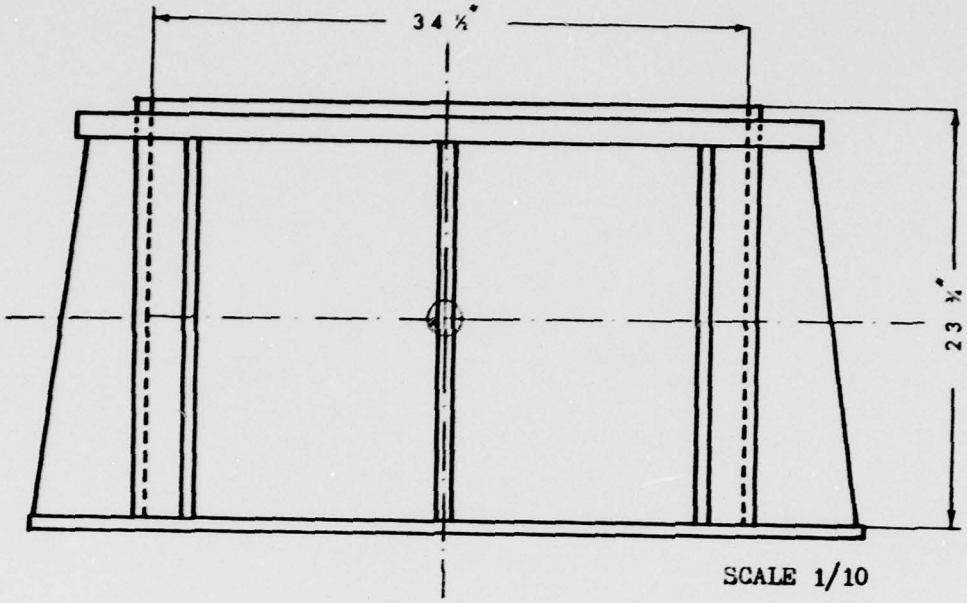


Fig.III-3c Water tank (Side view 2)

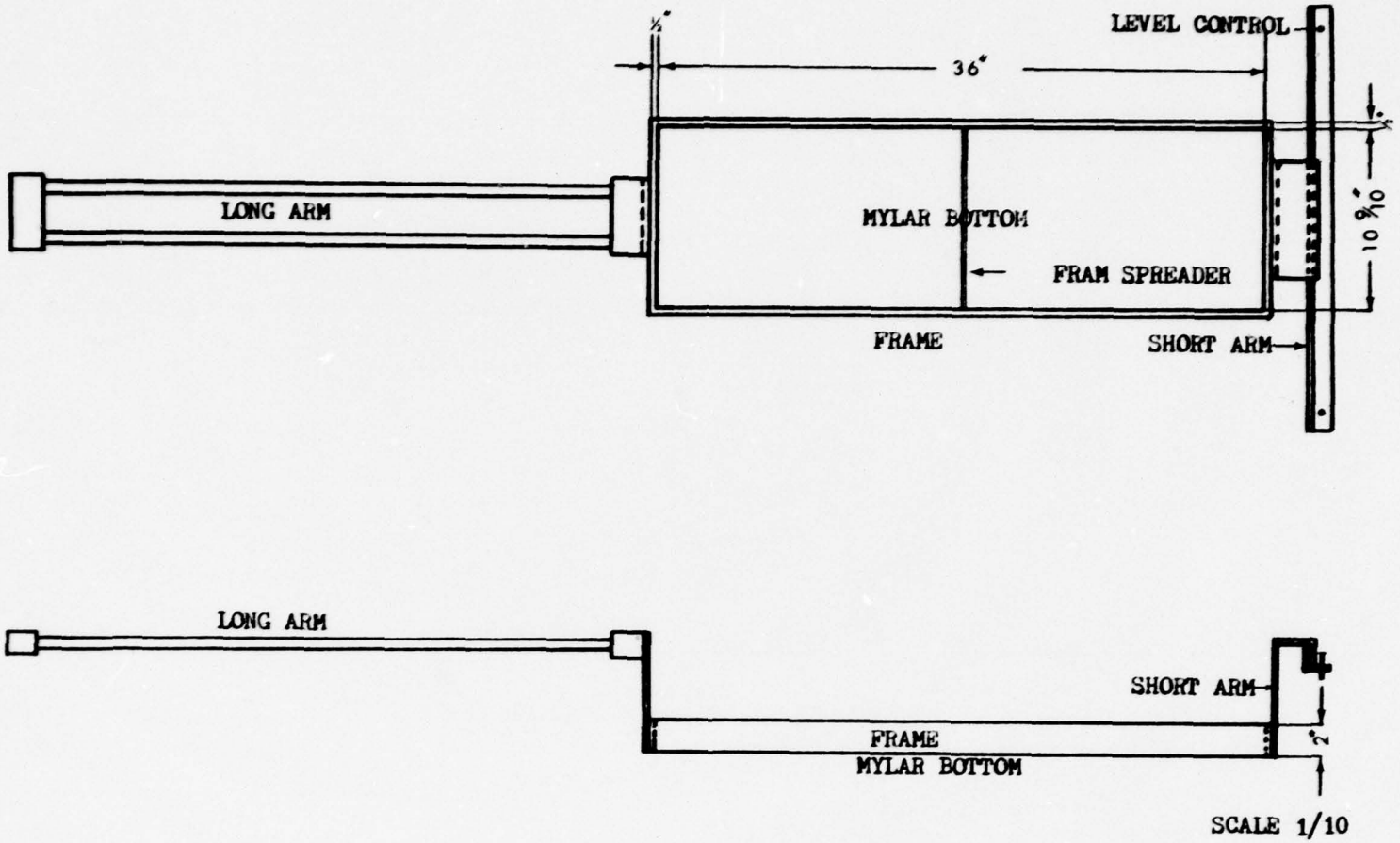


Fig.III-4 Wedge

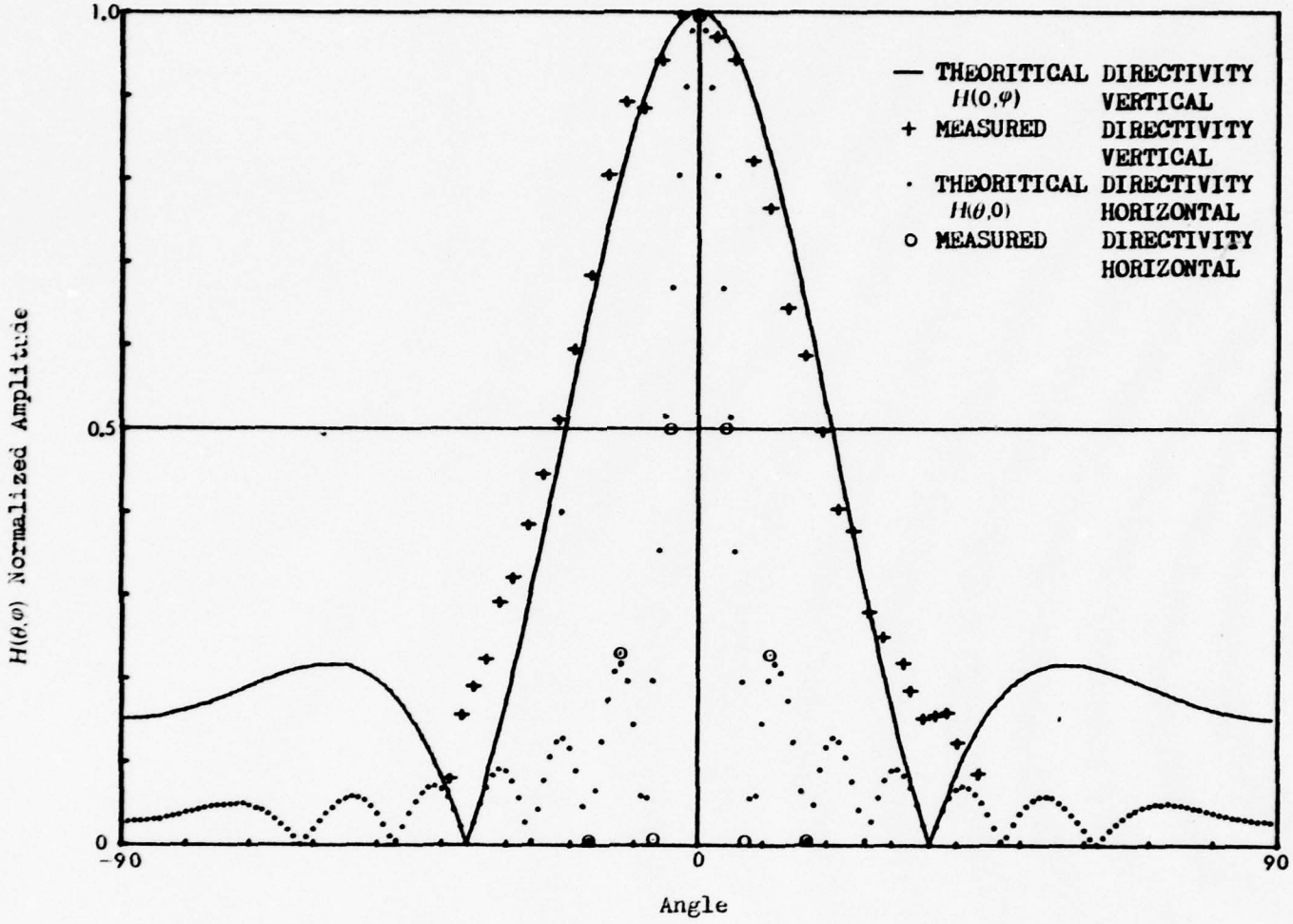


Fig.III-5a Directivity of the source transducer

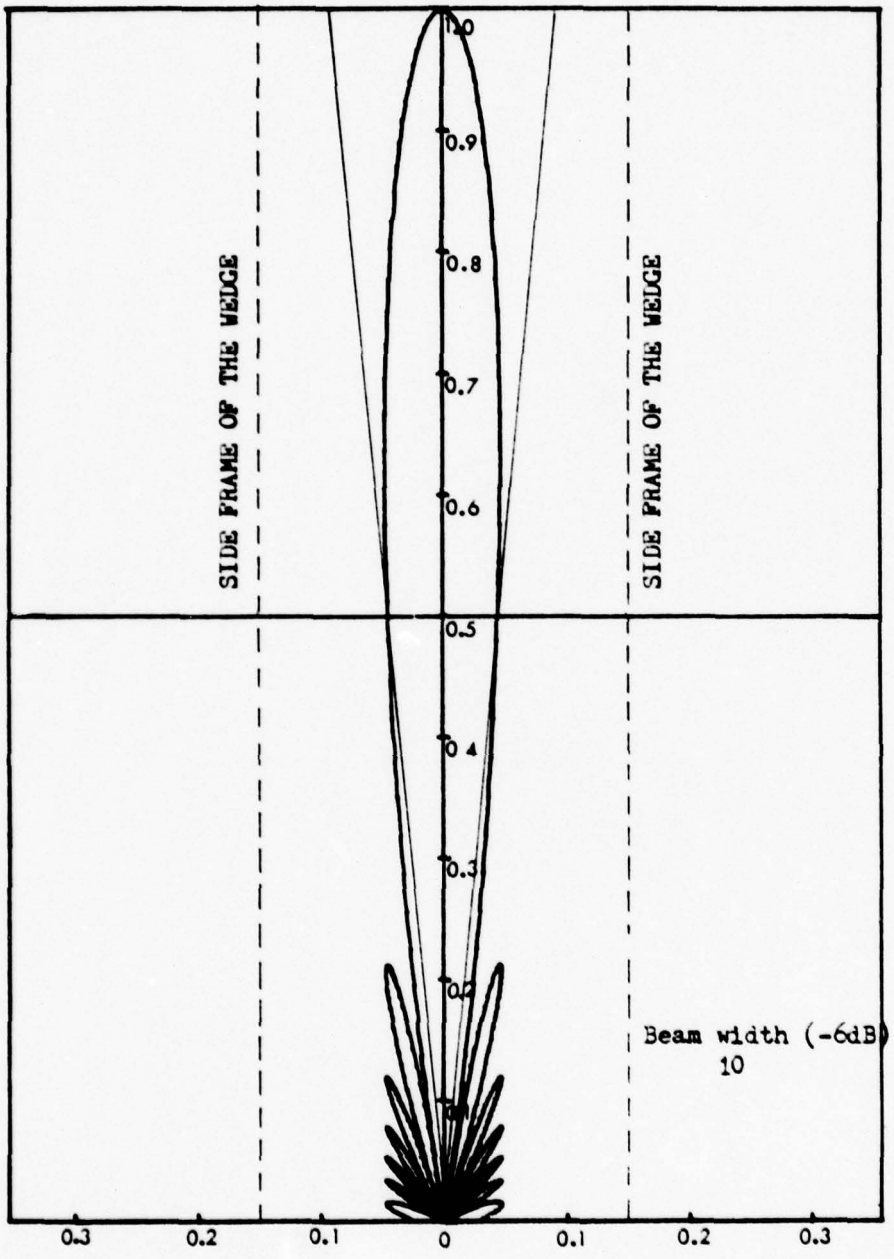


Fig.III-5b Horizontal directivity pattern $H(\theta,0)$ and boundary of the wedge

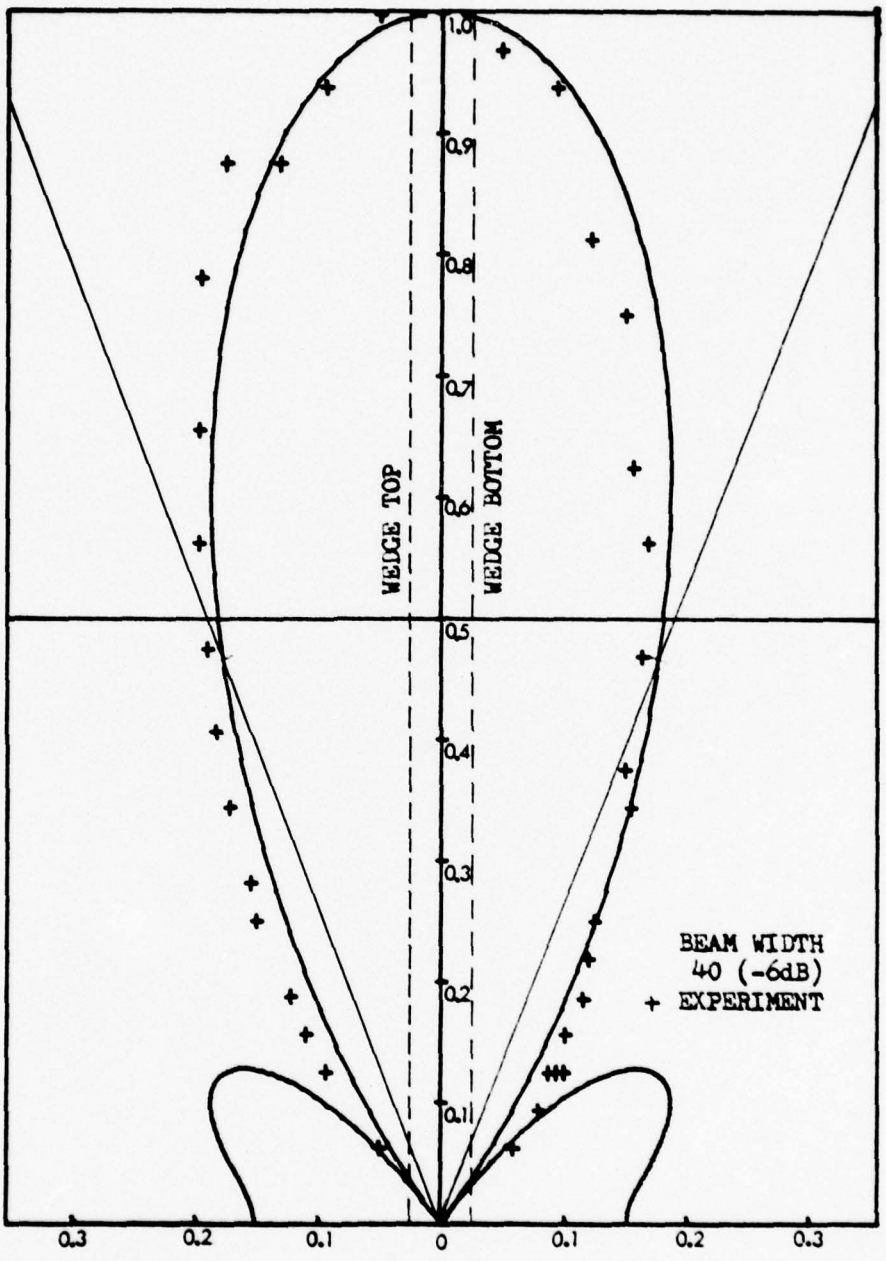


Fig.III-5c Vertical directivity pattern $H(0,\varphi)$
and boundary of the wedge

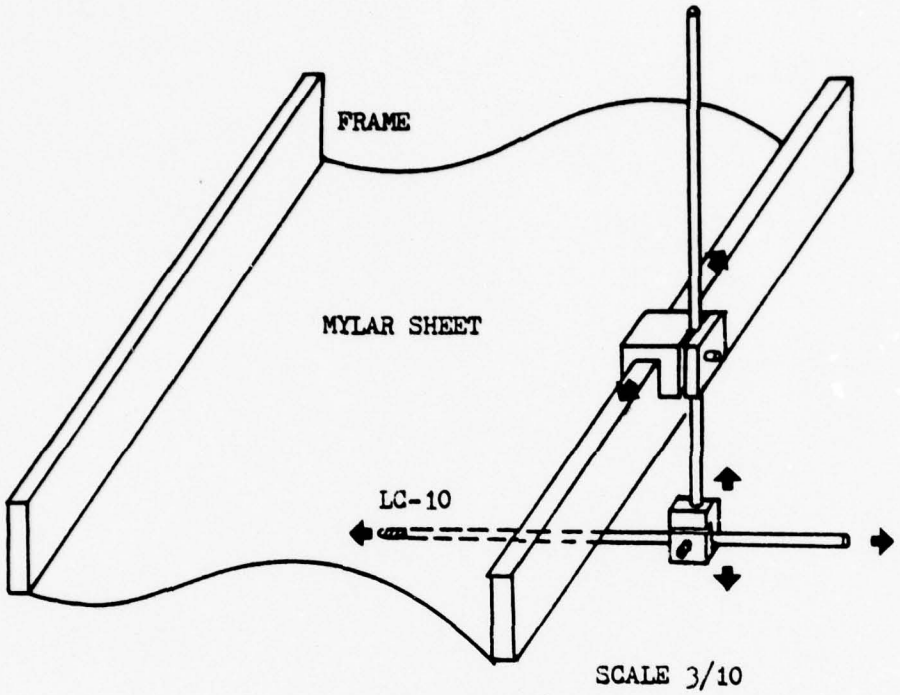


Fig.III-6a Receiver and attachment (1)

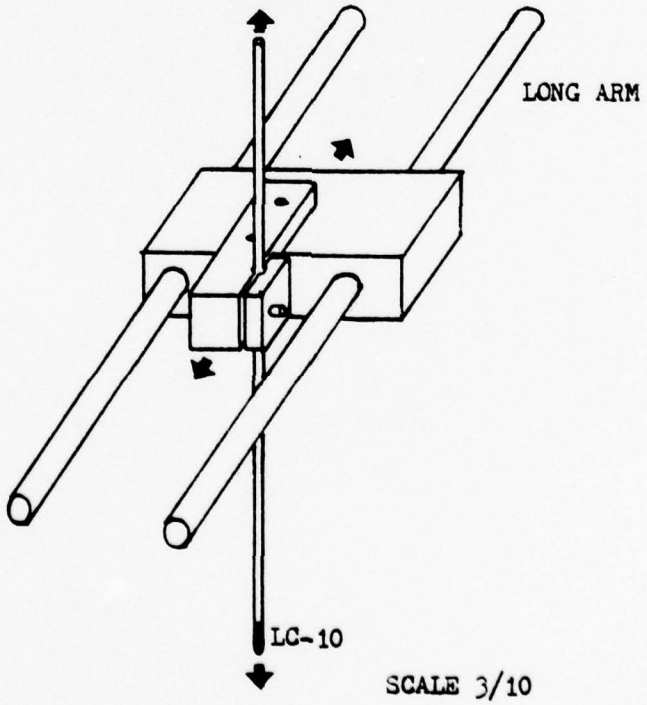


Fig.III-6b Receiver and attachment (2)

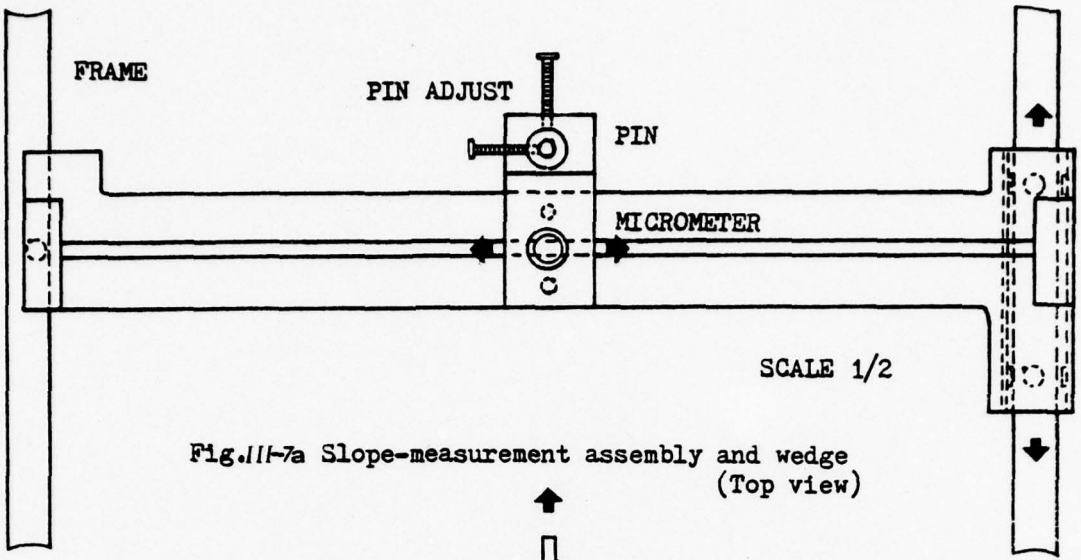


Fig.III-7a Slope-measurement assembly and wedge
(Top view)

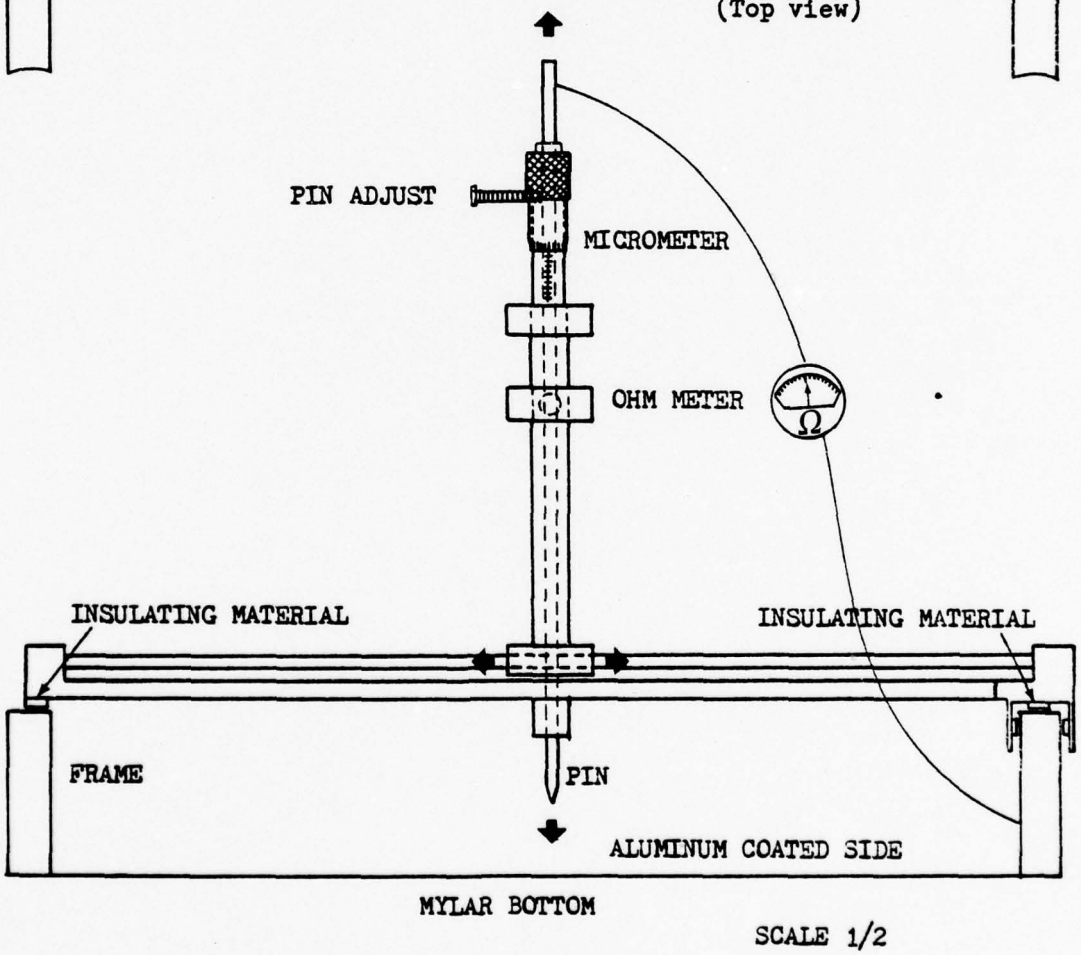


Fig.III-7b Slope-measurement assembly and wedge
(Side view)

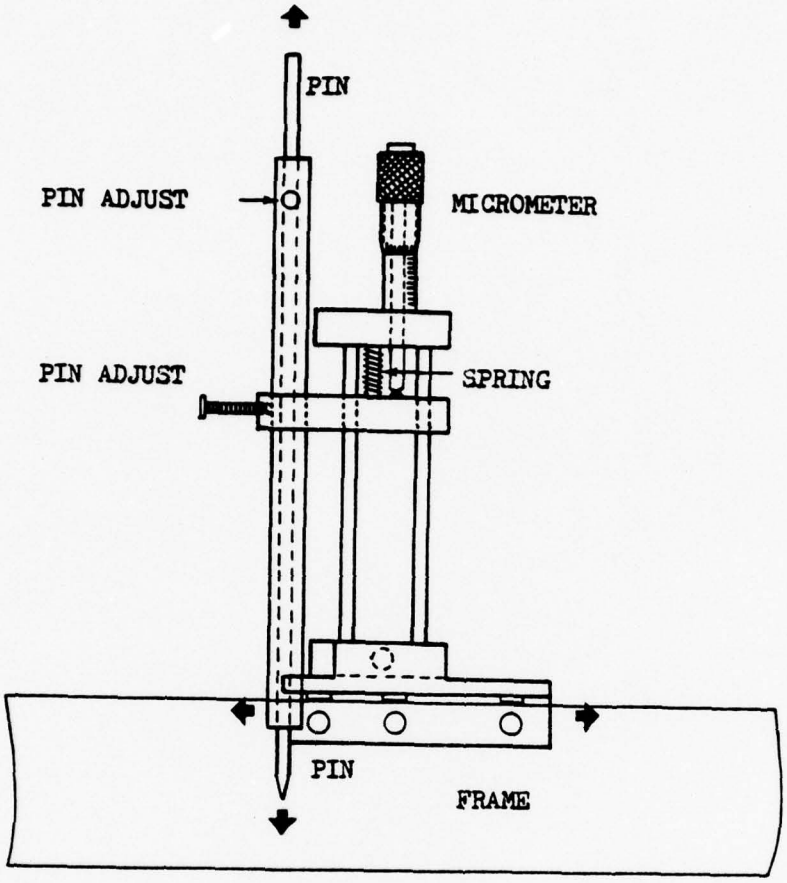


Fig. III-7c Slope-measurement assembly and wedge
(Side view)

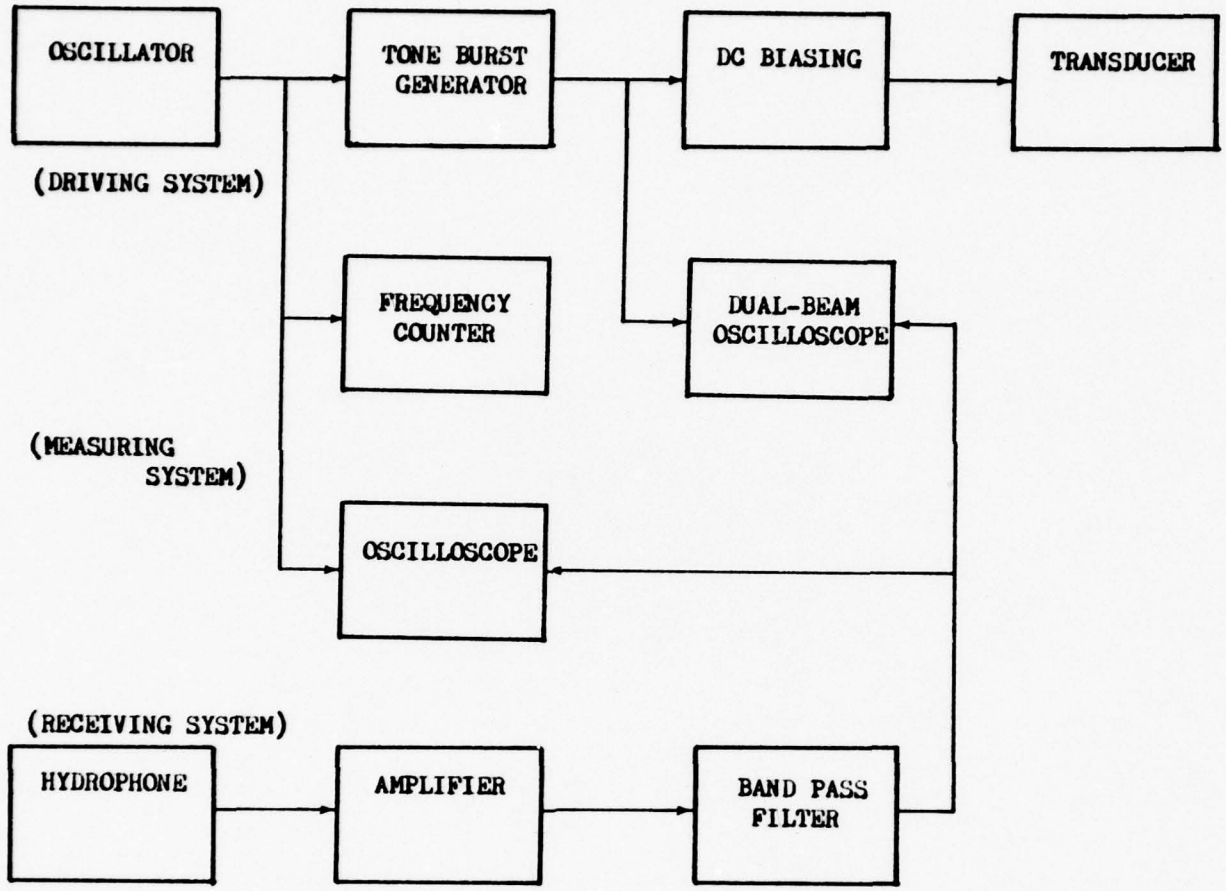


Fig.III-8 Electrical Setup

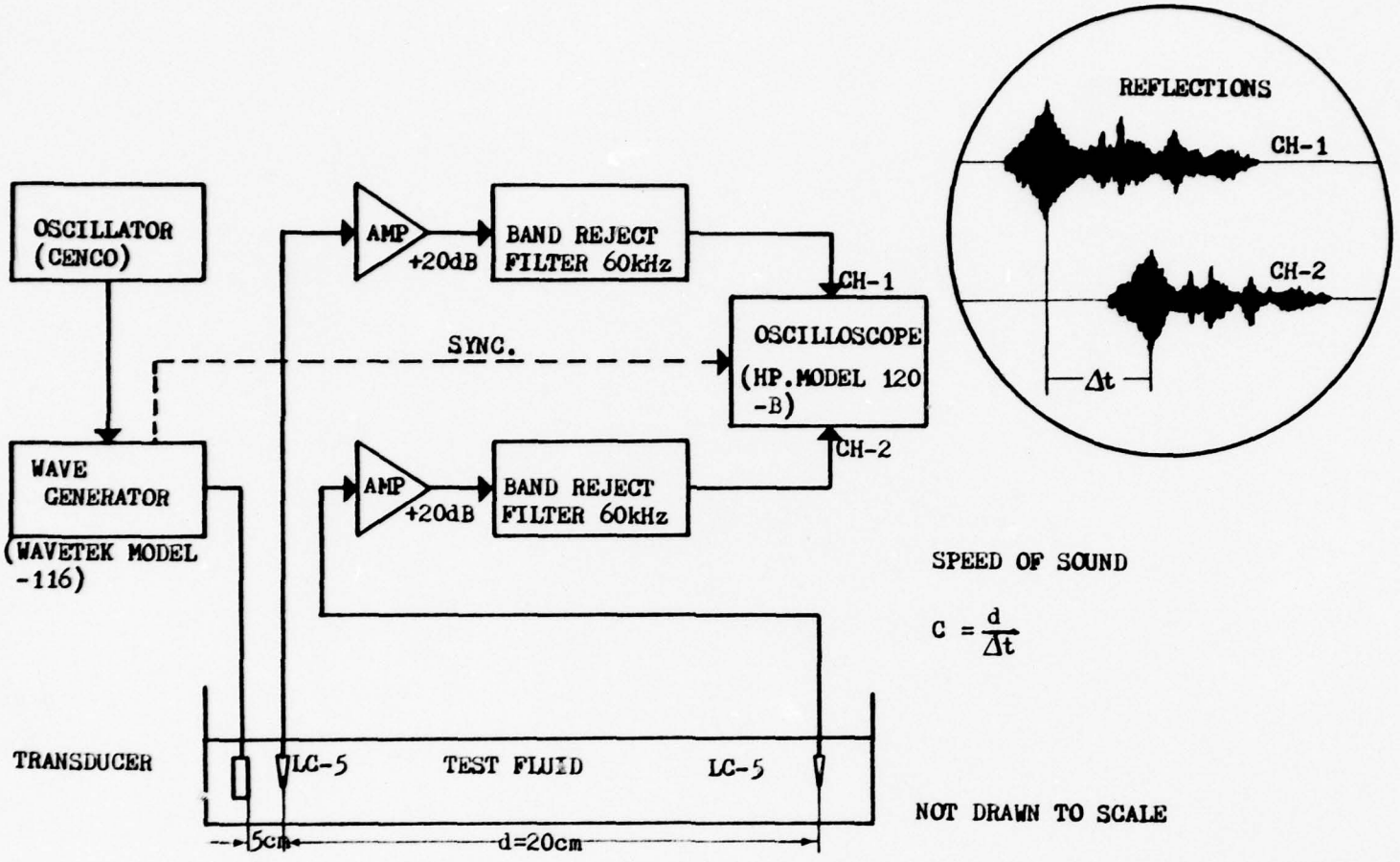


Fig.III-9 Sound speed measurements

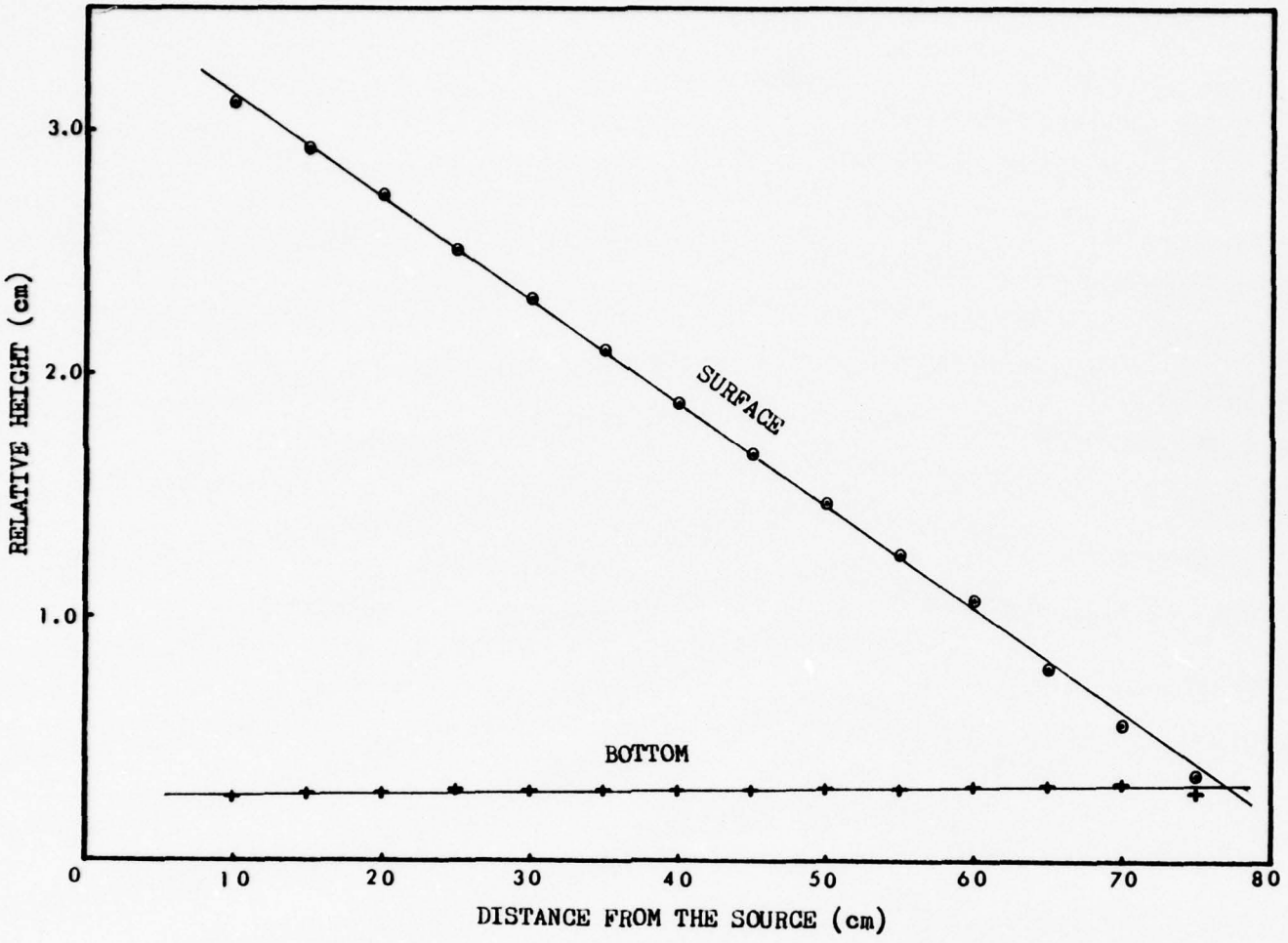


Fig.III-10 Measurement of the slope (CASE 2)

IV. RESULTS AND COMPARISON

Measurements were conducted under two different conditions:

Common Parameters

Speed of sound in the wedge (silicon)	c_1 = 1176.5 m/sec
Speed of sound under the bottom (fresh water)	c_2 = 1503.8 m/sec
Density of a silicon oil	ρ_1 = 1015.0 kg/m^3
Density of a fresh water	ρ_2 = 995.0 kg/m^3
Frequency	f = 100 kHz
Pulse length	L_p = 36 wavelengths
Closed gate duration	t_c = 10 msec
Pulse repetition rate	f_p = 100 Hz

CASE 1

Slope angle	β = 0.047 rad
Source distance from the apex	X = 70.0 cm
Source depth	H = 1.64 cm

CASE 2

Slope angle	β = 0.042 rad
Source distance from the apex	X = 75.5 cm
Source depth	H = 1.57 cm

The speeds of sound and the densities of the fluids were measured at 18.5°C. The two cases differed mainly in the

slope angle: for the first case $\beta = 2.7°$ and for the second $\beta = 2.4°$. These are fairly realistic values: according to Sverdrup-Johnson's - Fleming [Ref. 6], continental slopes off mountainous coasts have, on the average, a slope of about 3.5°, whereas off coasts with wide, well-drained coastal plains, the slope is about 2°. However, there are many different estimates based on different measurements at different locations. For extreme examples, estimates of the average continental slopes range from about 5° to about 0.1° [Ref. 7].

The distance from the apex to the source was limited to less than about 6 times the lowest possible cutoff distance x_o (x_o = 9.92 cm for CASE 1, x_o = 11.34 for CASE 2).

A. EXPERIMENT VS. SIMPLE MODEL

1. Pressure

Figures IV-1a,b show the experimentally-obtained pressure distribution along the bottom. In both cases there was a dominant pressure peak near the lowest cutoff point but shifted slightly in the direction away from the apex. To compare the simple model with the experiment, data and the theoretical curve were plotted on the same graph for the interval $0 \leq x \leq 2x_o$ (Fig. IV-2a,b). There are significant differences between the experimental results and the simple model. The theoretical curves decay quickly, and the model predicts that there should be no energy transmitted into the bottom, outside the region $x_s \leq x \leq X_o$

(the small amount observed in the simple model results from the approximations). On the other hand, the experimental curves have a long tail with energy transmitted continuously into the bottom all the way to the apex, and a pressure peak shifted significantly, so that energy is leaked into the bottom before the cutoff depth, $x > x_o$.

2. Phase

The phase distribution was measured in the region $0 \leq x \leq 6x_o$ for CASE 2. The rate of change in the measured phase was almost constant but with small irregular fluctuations. Figure IV-3 compares the experimental results within the region $0 \leq x \leq 2x_o$ with the results of the simple model calculated from Eq. (II-13)

$$kx' = \frac{\omega}{c_1}\sqrt{1 - \frac{\sin^2\theta_c}{(1 - \frac{x'}{X'_o})^2}}$$

$$\text{Phase} = -k_{x'}x' = -X_o \frac{\omega}{c_1}(1 - \frac{x}{X_o})\sqrt{1 - \frac{\sin^2\theta_c}{(\frac{x}{X_o})^2}} \quad \text{(IV-1)}$$

For comparison with the experiment, the phase was restricted to the interval $-\pi$ to $+\pi$.

Figure IV-4 shows the apparent angle of incidence

$$\theta = \arcsin\left(\frac{\sin\theta_c}{1 - \frac{x'}{X'_o}}\right) = \arcsin\left(\frac{\sin\theta_c}{\frac{x}{X_o}}\right) \quad \text{(IV-20)}$$

which is calculated from the phase $(-k_x, x')$ as discussed in Section II-A2. The graph shows that comparison between the simple model and the experiment is better accomplished by studying θ. The rate of change in the phase is almost constant when $x \geq x_o$, but the incident angle θ changes significantly in this region. The incident angle θ increases with decreasing distance x. At $x = x_o$ the incident angle θ becomes the critical angle θ_c and Eq. (IV-1) shows that $-k_x, x' = 0$. Subsequently the incident angle increases more rapidly as x decreases from x_o to x_s. At the turnaround point $x = x_c$ the angle θ becomes 90° and again $-k_x, x' = 0$. Thus, energy can be transmitted into the bottom only for $x_s \leq x \leq x_o$ according to the model. Precise experimental investigation of the incident angle was difficult because the rate of change in the phase was very small. Significant differences between experiment and the simple model were observed. From the experiment, there is no turnaround point. The experimental pressure distribution has a long tail which means energy can transmit into the bottom all the way to the apex. And the slopes of the phase curves (Fig. IV-3) show significant differences between experiment and the simple model.

B. EXPERIMENT VS. METHOD OF IMAGES

The computer program "WEDGE O" was designed for a comparison between experiment and the method of images. The program has the flexibility of an adjustable source distance and inclusion of the vertical directivity of the source.

1. Pressure

Before beginning the comparisons, the computed pressure distributions were observed with several combinations of distance (x = 100 m) or near source (x = 1 m) and with directional or omni-directional source. In all cases the major pressure peaks and tails were similar; the distance-source case showed slightly smoother pressure distributions and was little effected by source directivity. On the other hand, directivity becomes important if the source was near. As a result, computations were done with the actual source distance (x = 70.0 cm for CASE 1, x = 75.5 cm for CASE 2) and source directivity described in Section III-A3, and these results were compared with the experiment.

Figures IV-5a,b show the comparison between experiment and calculation. Both pressure amplitudes were normalized at the maximum pressure peak. In both cases, there are some quantitative differences, but good qualitative agreement; most of the local maxima and minima occur at the proper positions and with the approximately correct amplitudes.

Figures IV-6a,b are enlarged graphs of Fig. IV-5a,b for the region $0 \leq x \leq 2x_o$. From these graphs, it is obvious that the tails of major peaks of the experiment and theory agreed very well.

2. Phase

Theoretical calculations were also done with the computer program "WEDGEO" for a distant source. The results were compared with experimental data (Fig. IV-7, CASE 2 only) with both phases normalized at $x = X_o$. In the region $X_o \leq x \leq 2X_o$, these phases were almost identical, but some differences were observed for $x < X_o$; the experimentally observed phase changed somewhat more rapidly than that of the theoretical prediction, the difference increasing as the apex was approached. There are some possible explanations for this. The depth of the wedge at $x = X_o$ was 4.7 mm, and most differences were observed where the depth was 3.0 mm or less ($0 \leq x \leq 6$ cm). In this region, the pressure amplitude was very small (Fig. IV-2a), so that measurement of the phase was quite difficult. Also, very close to the apex the surface of the silicon oil might be affected by surface tension and not remain ideally flat.

The incident angles θ in the upper layer were approximated as follows; from Fig. II-1, the angle of incidence is,

$$\theta = \text{arc cos } (\frac{k_{x'}}{k})$$

where

$$k = \frac{\omega}{c_1} = \frac{2\pi f}{c_1} .$$

Two adjacent points x_1', x_2' for which $k_{x'}X'$ have the same values in the interval $-\pi$ to $+\pi$ yield a change in phase of 2π,

$$-k_{x_2'}X_2' + k_{x_1'}X_1' = 2\pi$$

$$k_{x'} = \frac{2\pi}{x_1' - x_2'} = \frac{2\pi}{\Delta x}$$

and

$$\theta = \text{arc cos } (\frac{c_1}{f\Delta x}) \qquad \text{(IV-2)}$$

Figures IV-8a,b show the results for the experiment compared to the results obtained from the method of images and from the simple model. There is no turnaround point (for which we would have $\theta = 90°$). In both cases the incident angle equals the critical angle a little further away from the apex than $x/X_o = 1$, which is consistent with the measured behavior of the amplitude. For $x > X_o$, most of these incident angles were less than the critical angle θ_c, (This does not imply that there is no energy transmitted into the bottom: these incident angles result from the phase-coherent interferences of a large number of images, the fields of which have angles of incidence on the bottom encompassing a range of values, some of which exceed θ_c. This shows a significant difference between the method of images and the simple model for

which energy can not be transmitted into the bottom when the incident angle is less than the critical angle.)

The phase as predicted by the method of images and the experimental phase is nearly linear in x. The amplitude varies more slowly, but perhaps not slowly enough for the method of stationary phase to be applicable.

C. ATTEMPTED RECONCILIATION

The predictions of the simple model do not agree well with the experimental measurements. However, investigations of the pressure field in the bottom would be facilitated if a simple analytical expression for the pressure distribution along the wedge-bottom interface could be formulated.

Consequently, the purpose of this section is to compare the simple model with the method of images for those cases where the source is very distant. The amplitude of the pressure distribution predicted by the simple model has the form

$$A = A_o \, e^{-\left(\frac{\rho_1}{\rho_2}\right)^{k_1} \left(\frac{\tan\theta_c}{\beta}\right)^{k_2} \cdot k_3 \left(\frac{x'}{X_T}\right)^{k_4}} \qquad \text{(IV-3)}$$

where the predicted values are $k_1 = k_2 = 1$, $k_3 = \frac{2\sqrt{2}}{3}$ and $k_4 = \frac{3}{2}$. Changing ρ_1, ρ_2, c_1, c_2 and b it was found that the pressure amplitude depended only on the ratios $\frac{\rho_1}{\rho_2}$, $\frac{\tan\theta_c}{\beta}$.

Next comparing the predictions of the method of images with the simple model also showed that the value $k_4 = \frac{3}{2}$

gave the proper spatial behavior, to reasonable accuracy. This was accomplished by taking ln of both sides of Eq. (IV-3) and plotting then $\ln \frac{A_o}{A}$ vs $\frac{x}{X'_o}$ on log-log paper.

Obviously the slope of the equation

$$\ln\{\ln(\frac{A_o}{A})\} = \ln\{(\frac{\rho_1}{\rho_2})^{k_1} \cdot (\frac{\tan\theta_c}{\beta})^{k_2} \cdot k_3\} + k_4 \ln(\frac{x'}{X'_o}) \qquad \text{(IV-4)}$$

gives k_4.

By the same technique the exponents k_1 and k_2 of $\frac{\rho_1}{\rho_2}$ and $\frac{\tan\theta_c}{\beta}$ and the factor k_3 were examined but in these cases the results for k_1, k_2, k_3 were not constants; but functions apparently dependent on $\frac{\rho_1}{\rho_2}$, $\frac{c_1}{c_2}$, β, $\frac{x'}{X'_o}$.

We can therefore conclude that the simple model is not generally valid for arbitrary values of ρ_1, ρ_2, c_1, c_2, β and $\frac{x'}{X'_o}$. However, it is useful to note that by assuming $k_3 = \frac{1}{4}$ the simple model predictions are brought into good agreement with the experimental measurements for the values

$$\rho_1 = 1.015 \text{ gr/cm}^3$$

$$\rho_2 = 0.995 \text{ gr/cm}^3$$

$$c_1 = 1173.5 \text{ m/sec}$$

$$c_2 = 1503.8 \text{ m/sec}$$

$$\theta_c = 38.706°$$

$$\beta = 0.0476 \text{ rad}$$

After the discovery of this agreement an effort was made to specify the ranges of variables in which the amplitude prediction of the simple model is valid with $k_3 = \frac{1}{4}$.

The simple model requires

$$\frac{x'}{X'_o} << \frac{1}{2} \cos^2\theta_c \qquad \text{(IV-5)}$$

Assuming that the amplitude distribution is unimportant for those values $\frac{x'}{X'_o}$ such that $\frac{A}{A_o} << \frac{1}{e}$, this inequality must be achieved within the restriction (IV-5).

$$\frac{A}{A_o} = e^{-\frac{\rho_1}{\rho_2} \frac{\tan\theta_c}{\beta} \frac{1}{8\sqrt{2}} \cos^2\theta_c} << e^{-1} \qquad \text{(IV-6)}$$

or

$$\beta << \frac{1}{8\sqrt{2}} \sin\theta_c (1 - \sin^2\theta_c) \frac{\rho_1}{\rho_2} \qquad \text{(IV-7)}$$

This inequality was tested on the interval $0.002 \leq \beta \leq 0.005$ for $\theta_c = 60°$ and $\frac{\rho_1}{\rho_2}$ 0.5 or 1.0 there was uniformly good agreement between the simple model and the method of images for $\frac{\rho_1}{\rho_2} = 0.5$, but for $\frac{\rho_1}{\rho_2} = 1.0$ there was strong disagreement between the two models.

Therefore the range of validity of the simple model with $k_3 = \frac{1}{4}$ appears badly limited. Further, since the phase of the simple model does not agree with the experimental measurements and the predictions of the method of images (as already has been mentioned in part IV-A2), we can conclude finally that this model is very weak and its application very restricted.

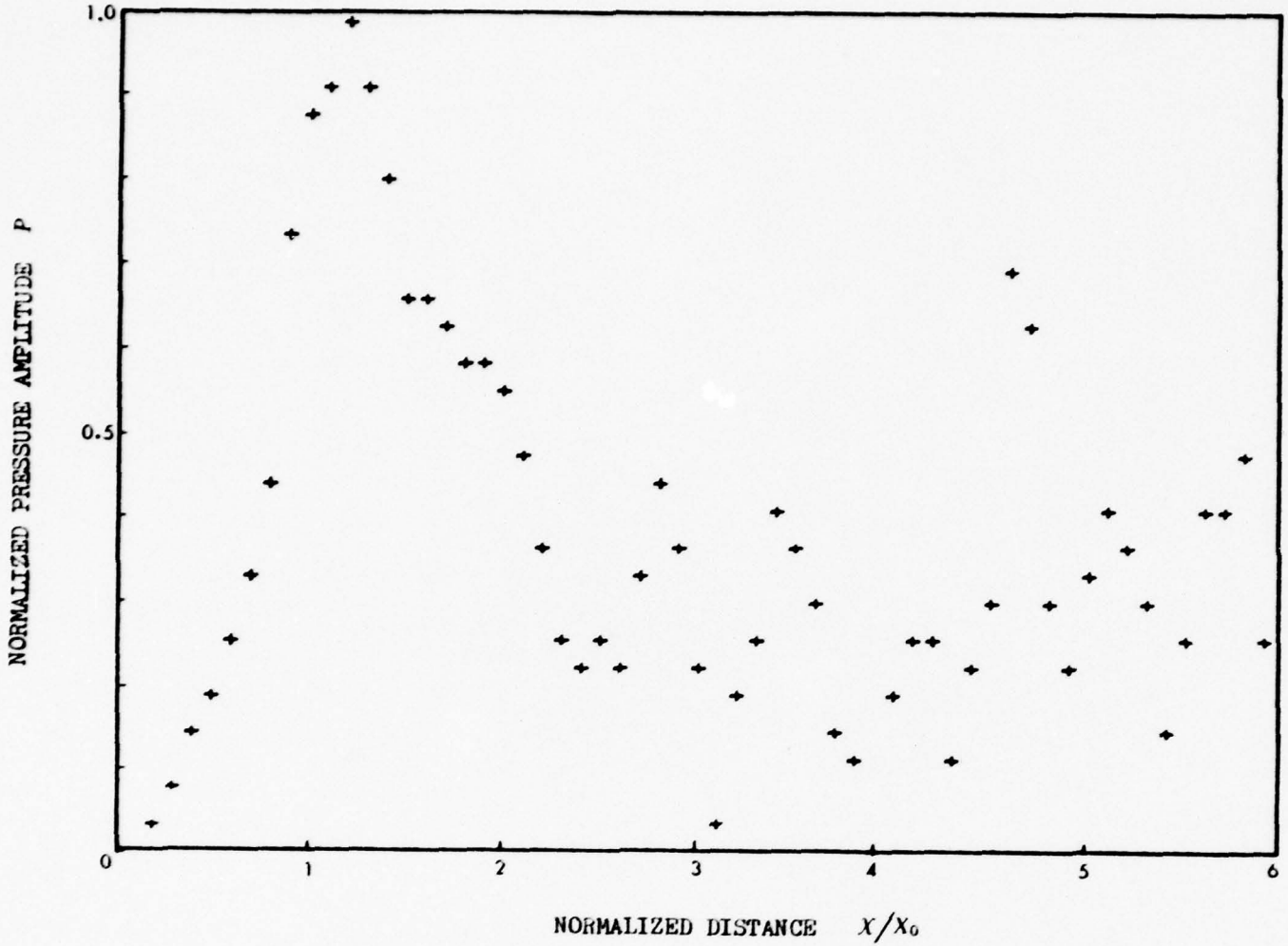


Fig.IV-1a Experimental pressure distribution CASE 1

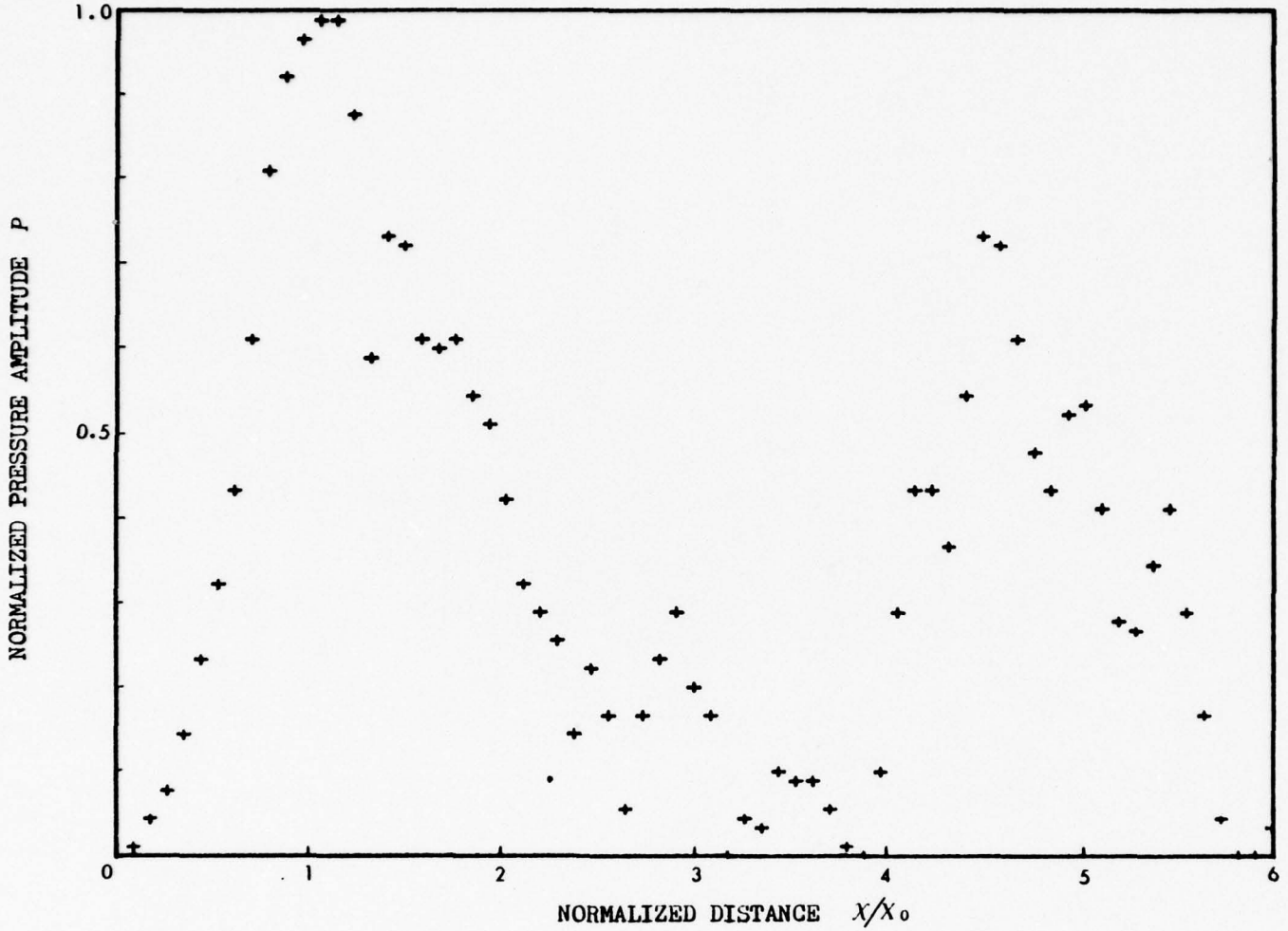


Fig.IV-1b Experimental pressure distribution CASE 2

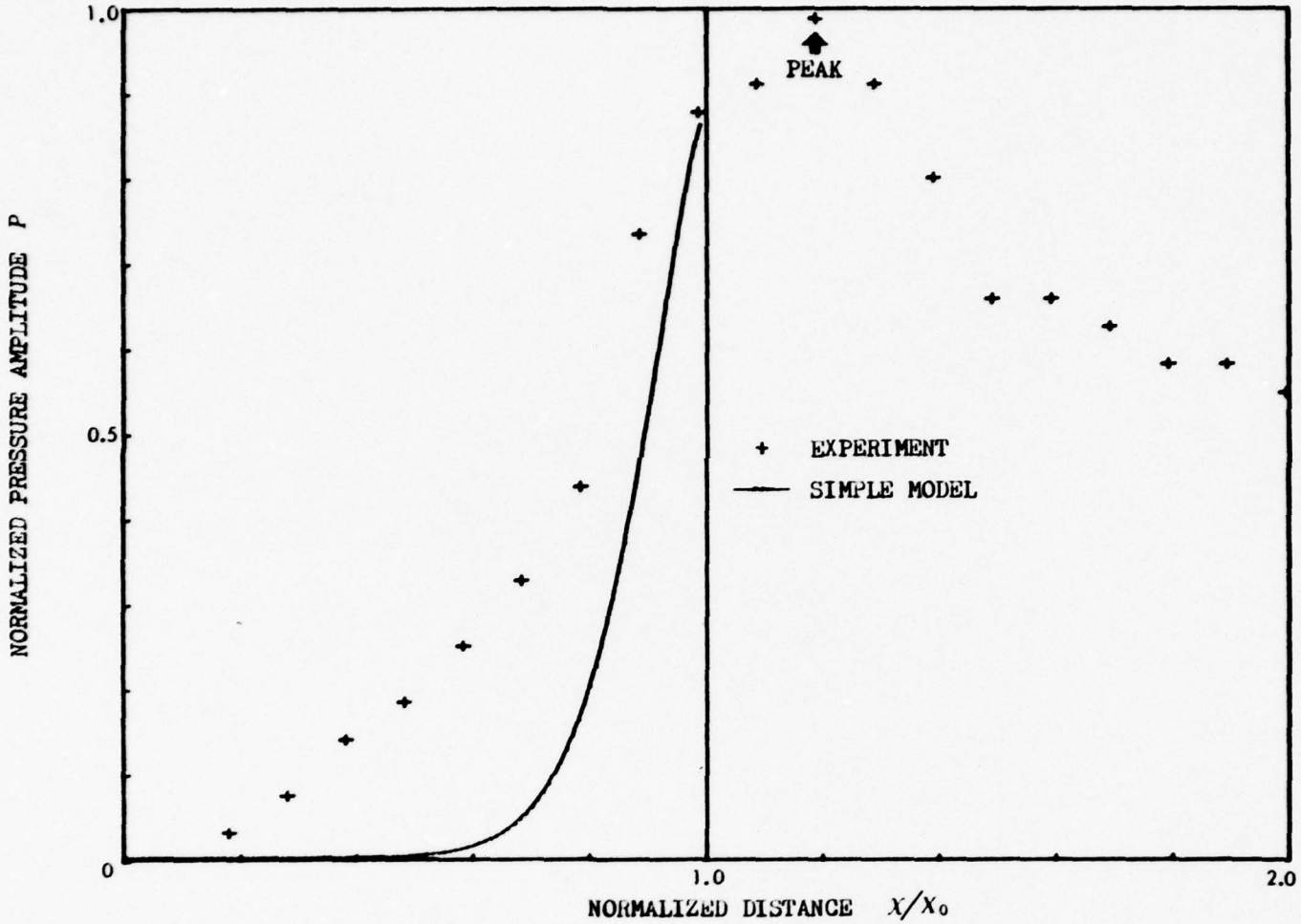


Fig.IV-2a Comparison of pressure amplitude CASE 1
(Experiment VS. simple model)

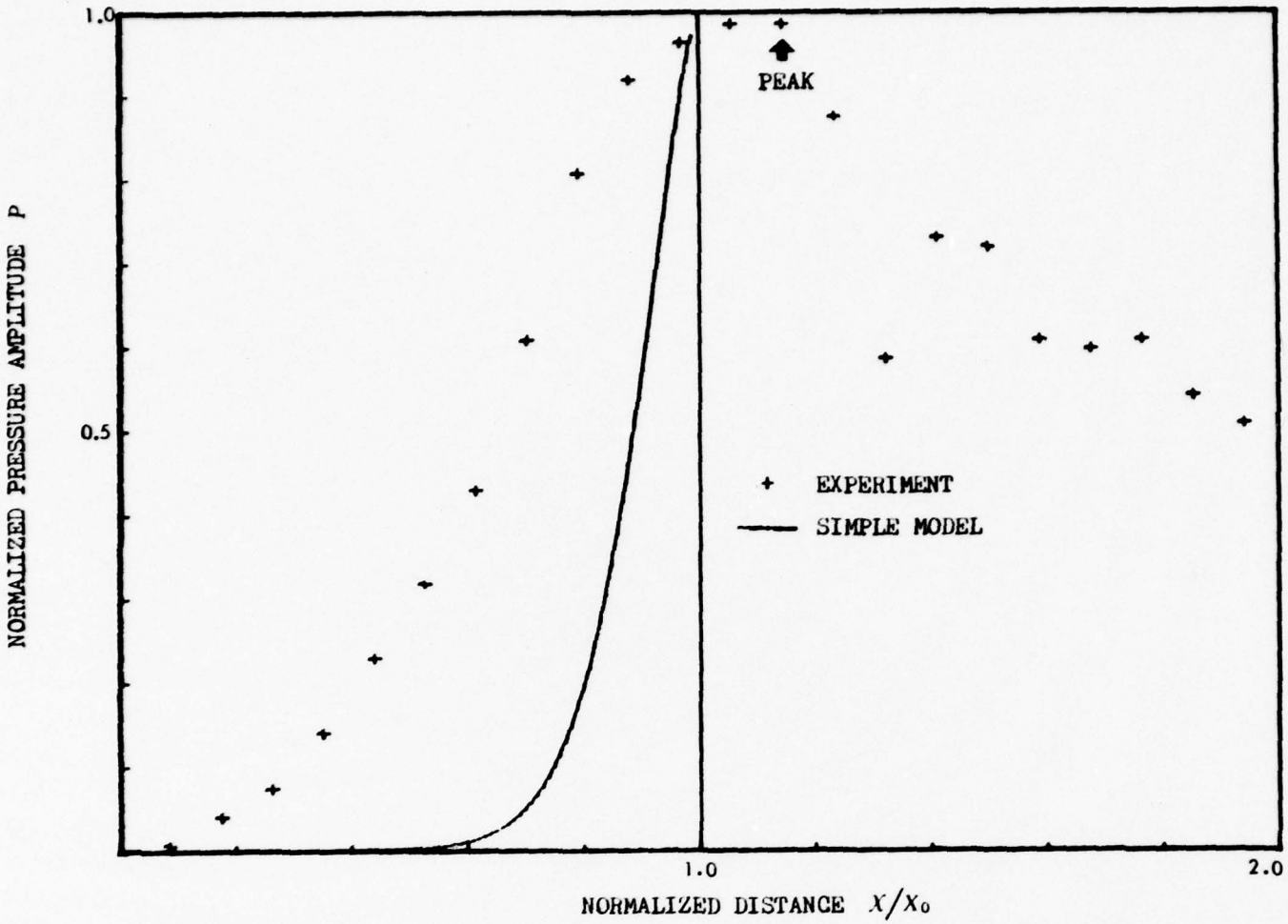


Fig.IV-2b Comparison of pressure amplitude CASE 2
(Experiment VS. simple model)

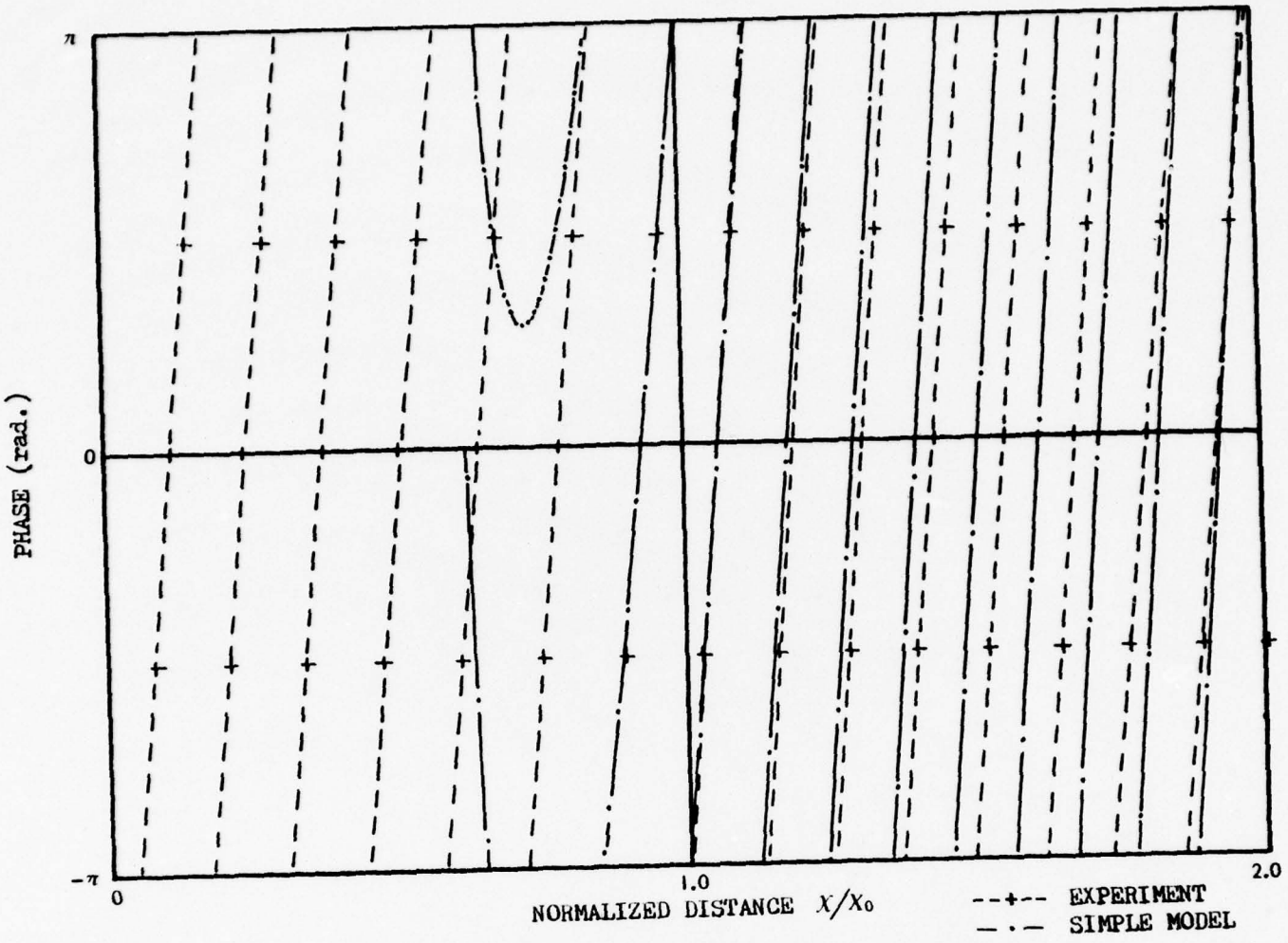


Fig.IV-3 Comparison of phase CASE 2
(Experiment VS. simple model)

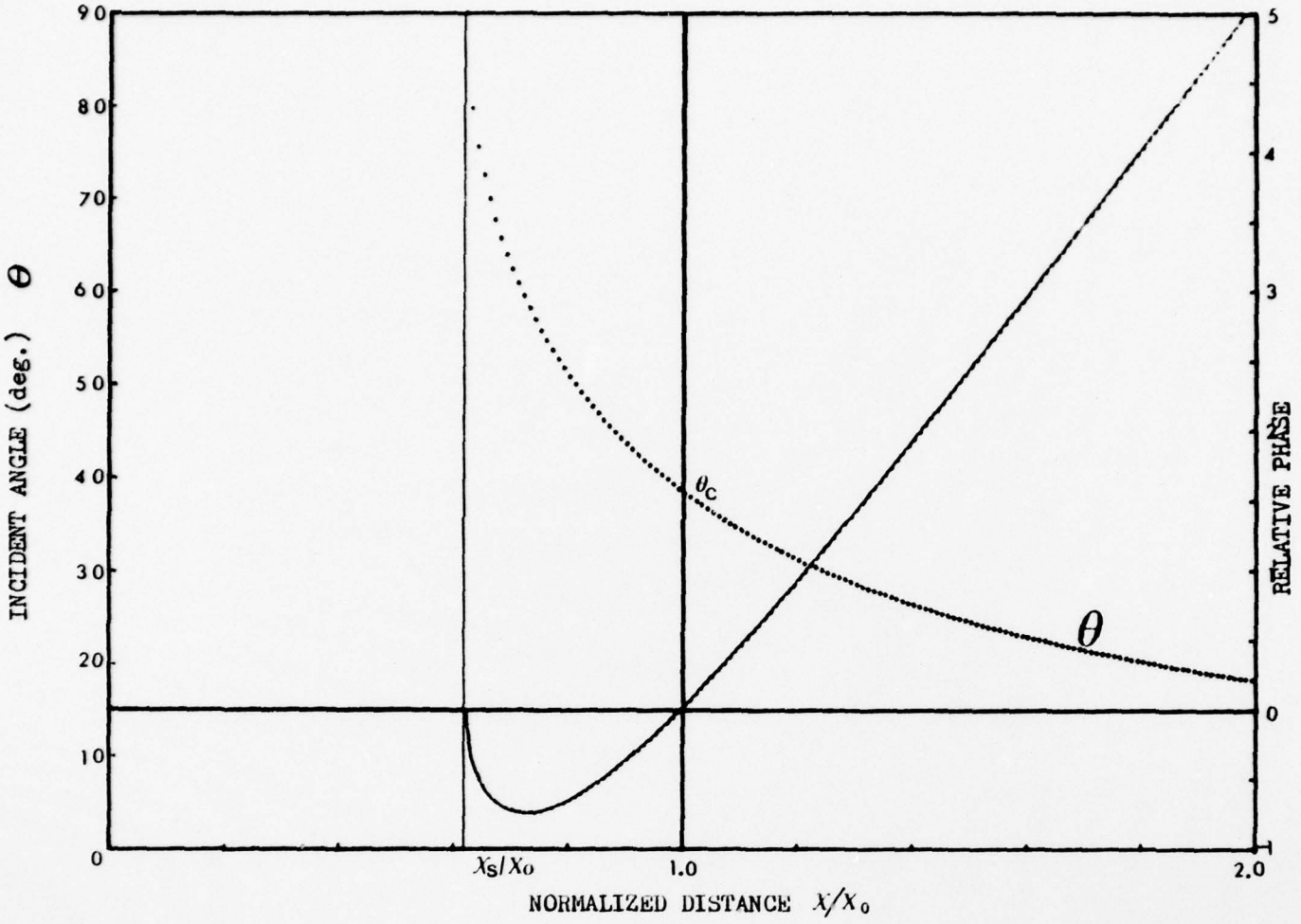


Fig.IV-4 Theoretical phase and incident angle (Simple model)

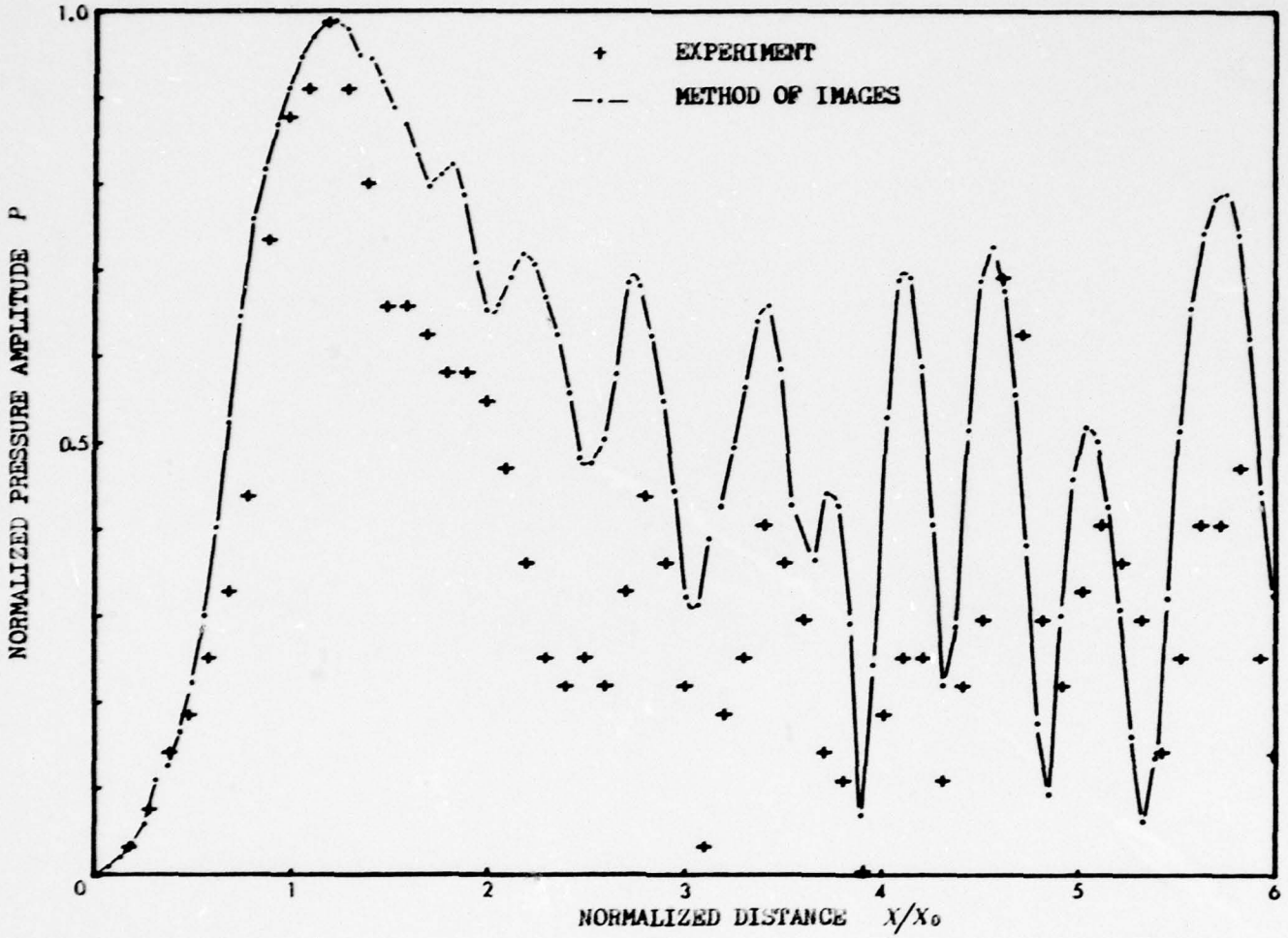


Fig.IV-5a Comparison of pressure amplitude CASE 1
(Experiment VS. method of images)

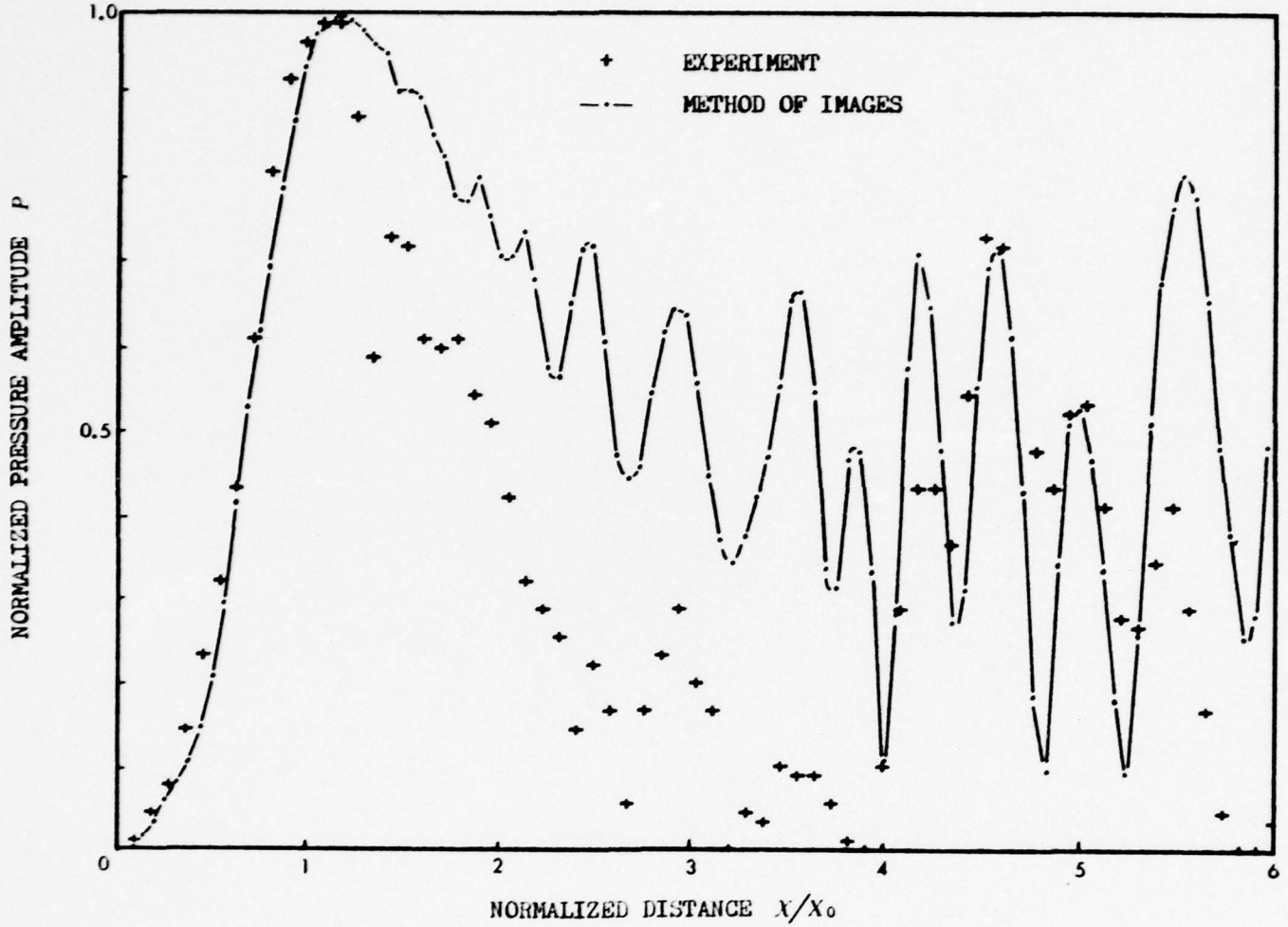


Fig.IV-5b Comparison of pressure amplitude CASE 2
(Experiment VS. method of imafes)

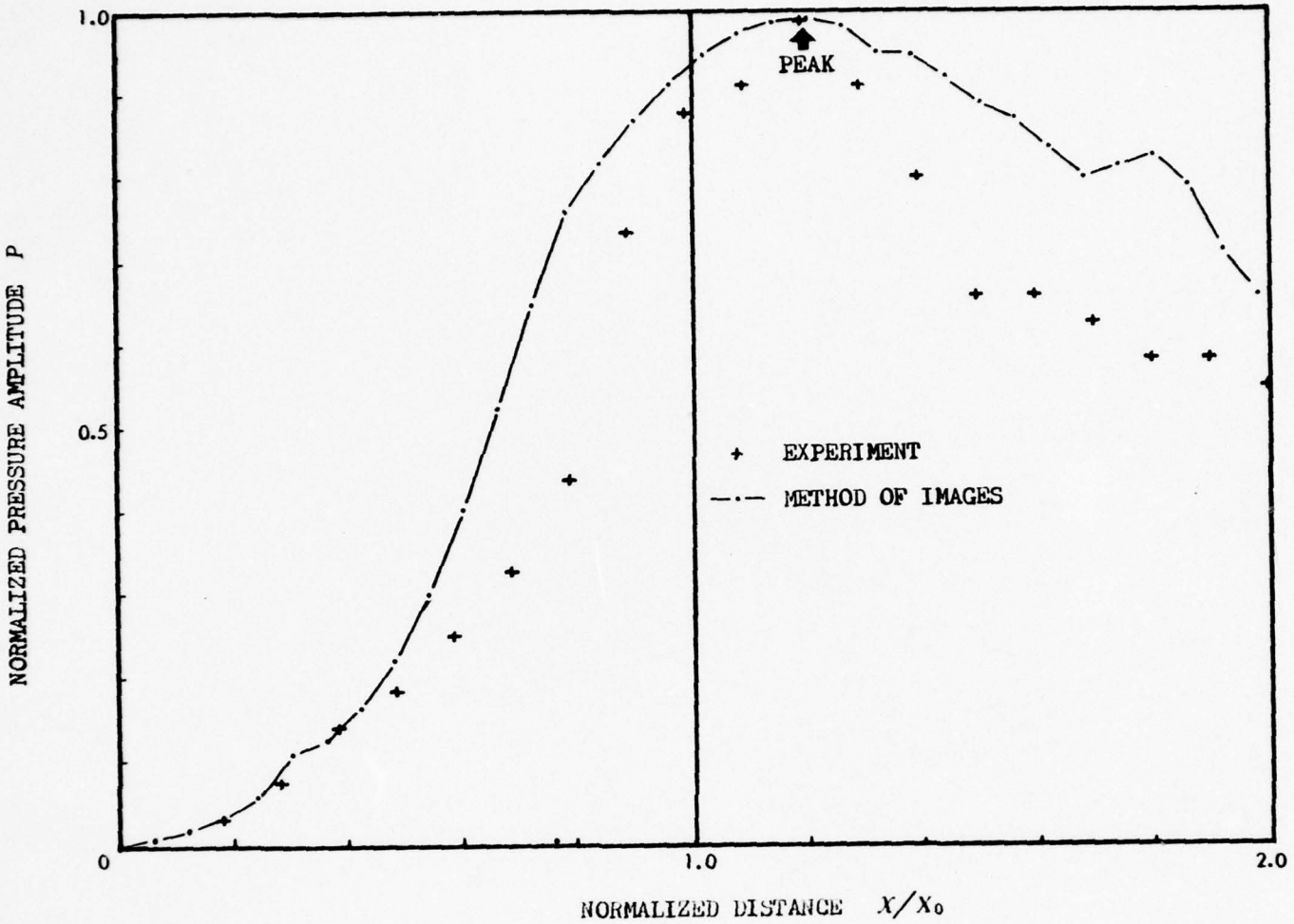


Fig.IV-6a Comparison of pressure amplitude CASE 1
(Experiment VS.method of images)

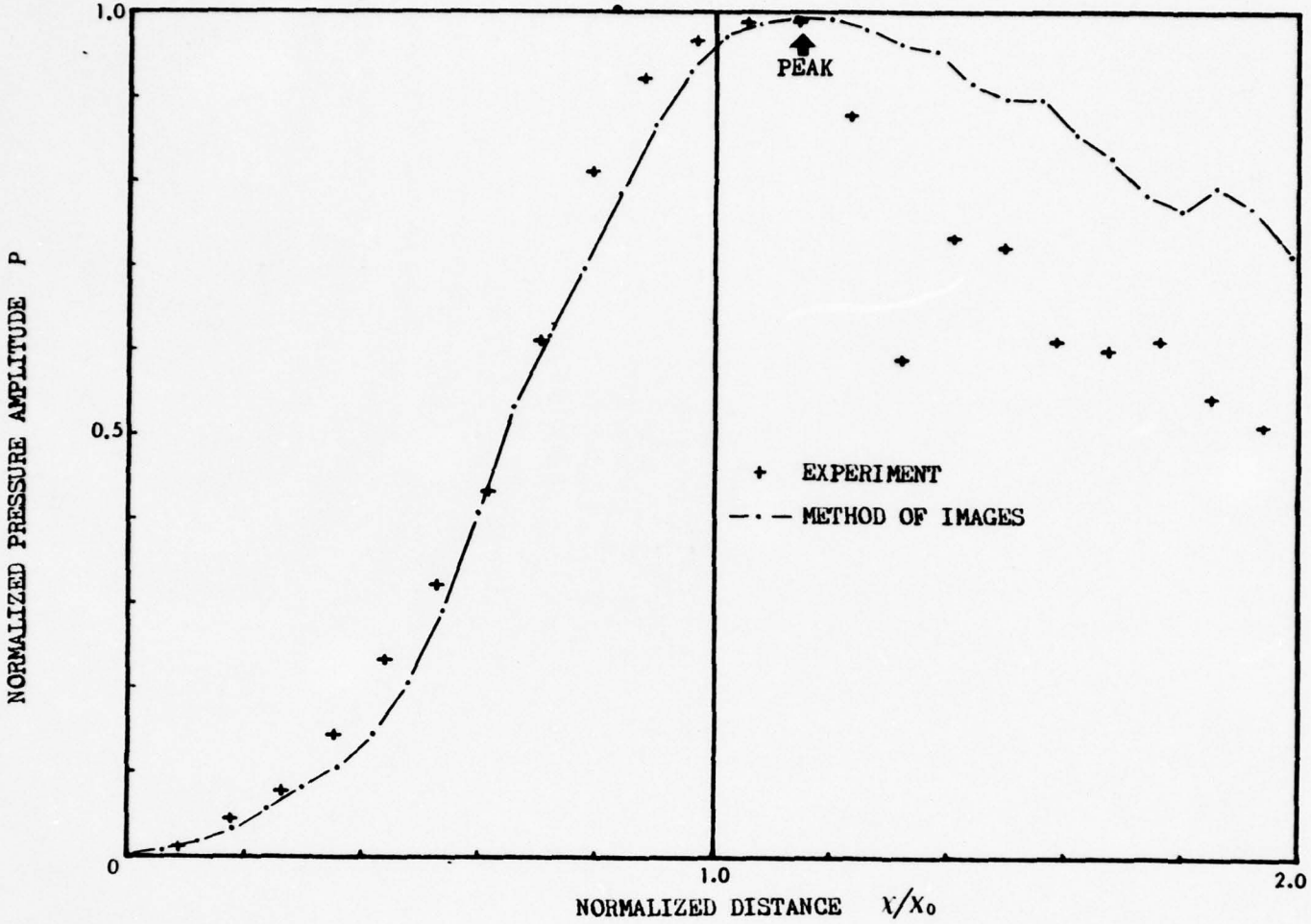


Fig.IV-6b Comparison of pressure amplitude CASE 2
(Experiment VS. method of images)

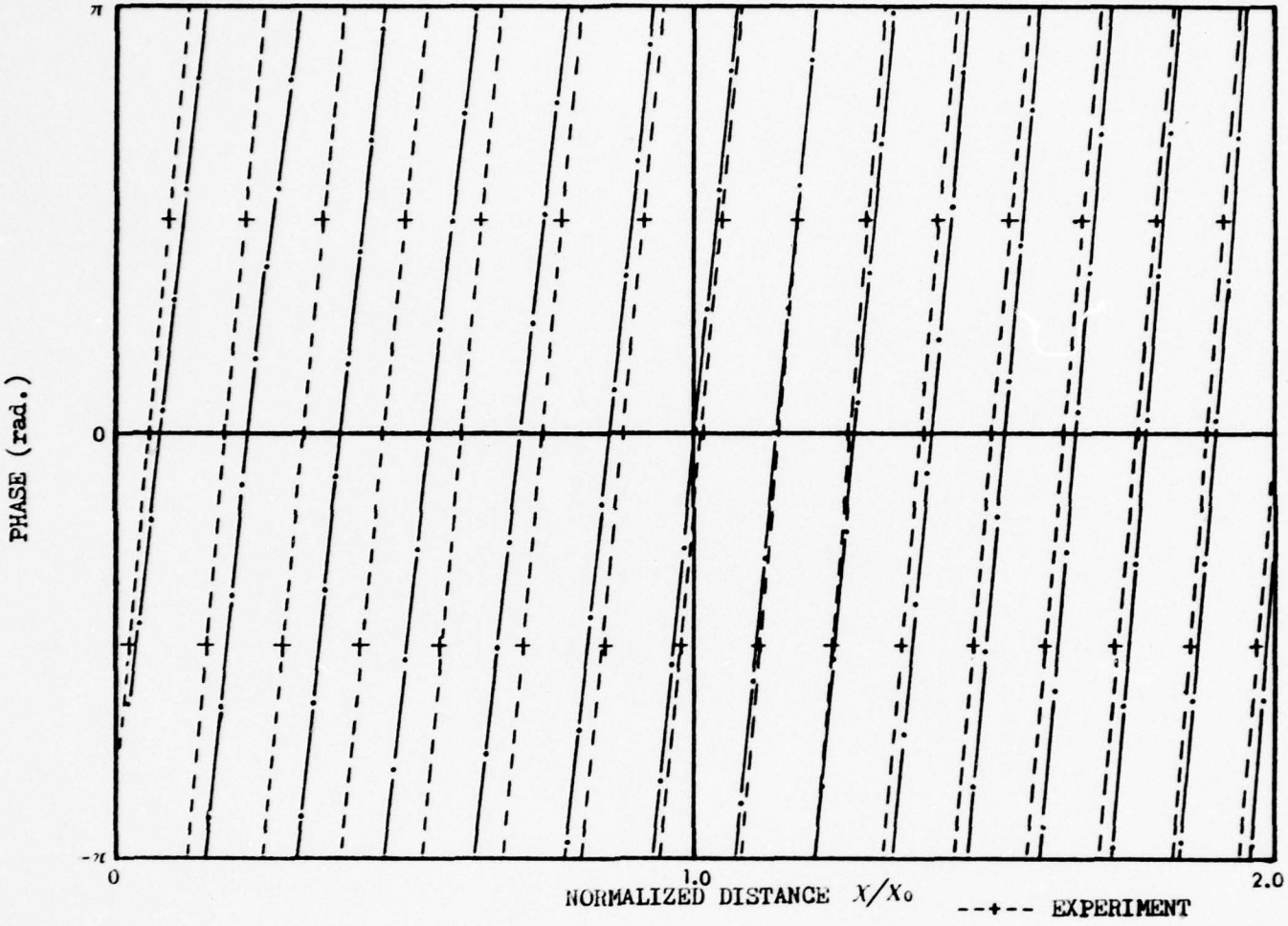


Fig.IV-7 Comparison of phase CASE 2
(Experiment VS. method of images)

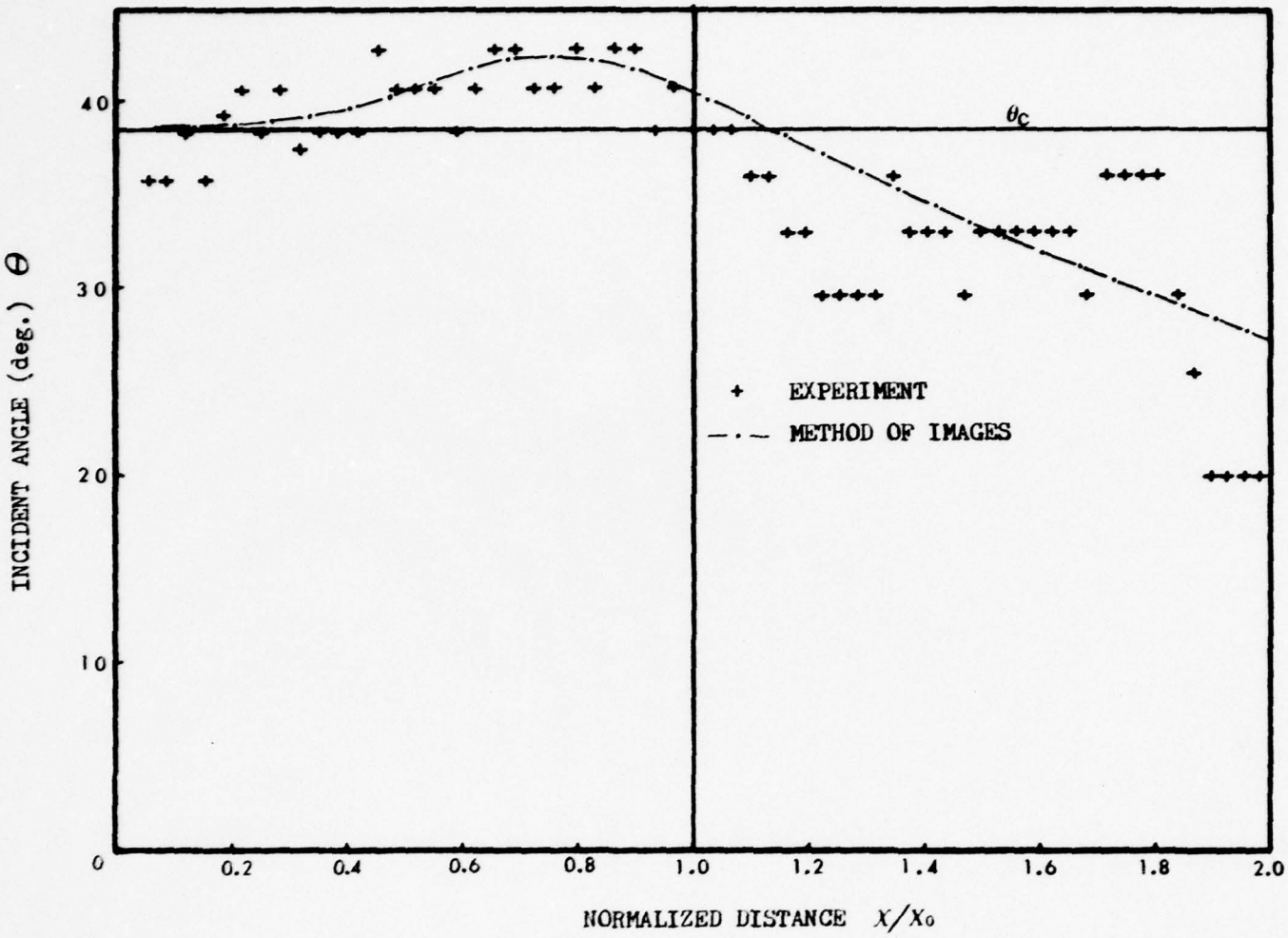


Fig.IV-8a Comparison of incident angle CASE 2
(Experiment VS. method of images)

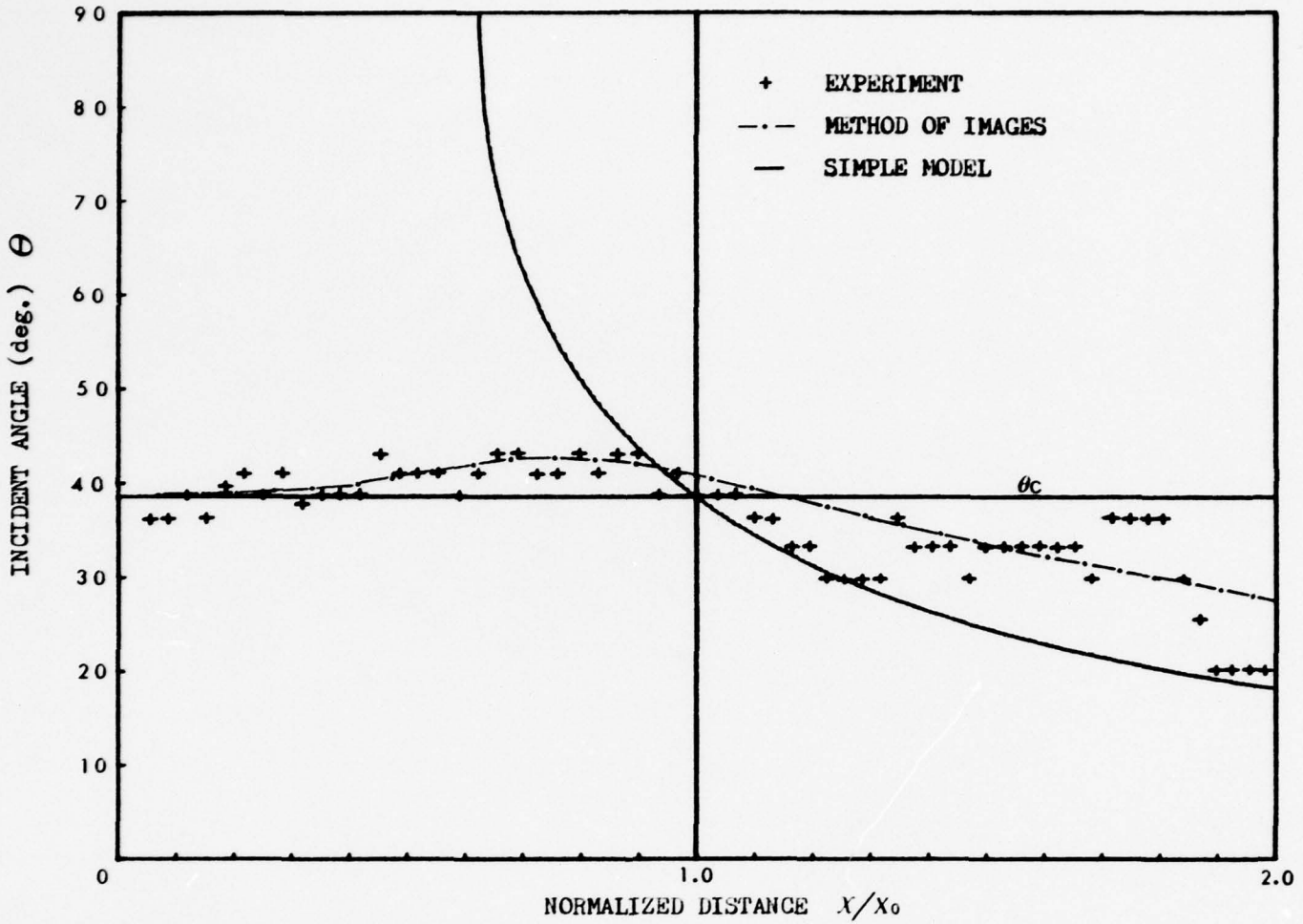


Fig. IV-8b Comparison of incident angle CASE 2
(Experiment VS. theories)

V. CONCLUSIONS

Two main conclusions should be emphasized.

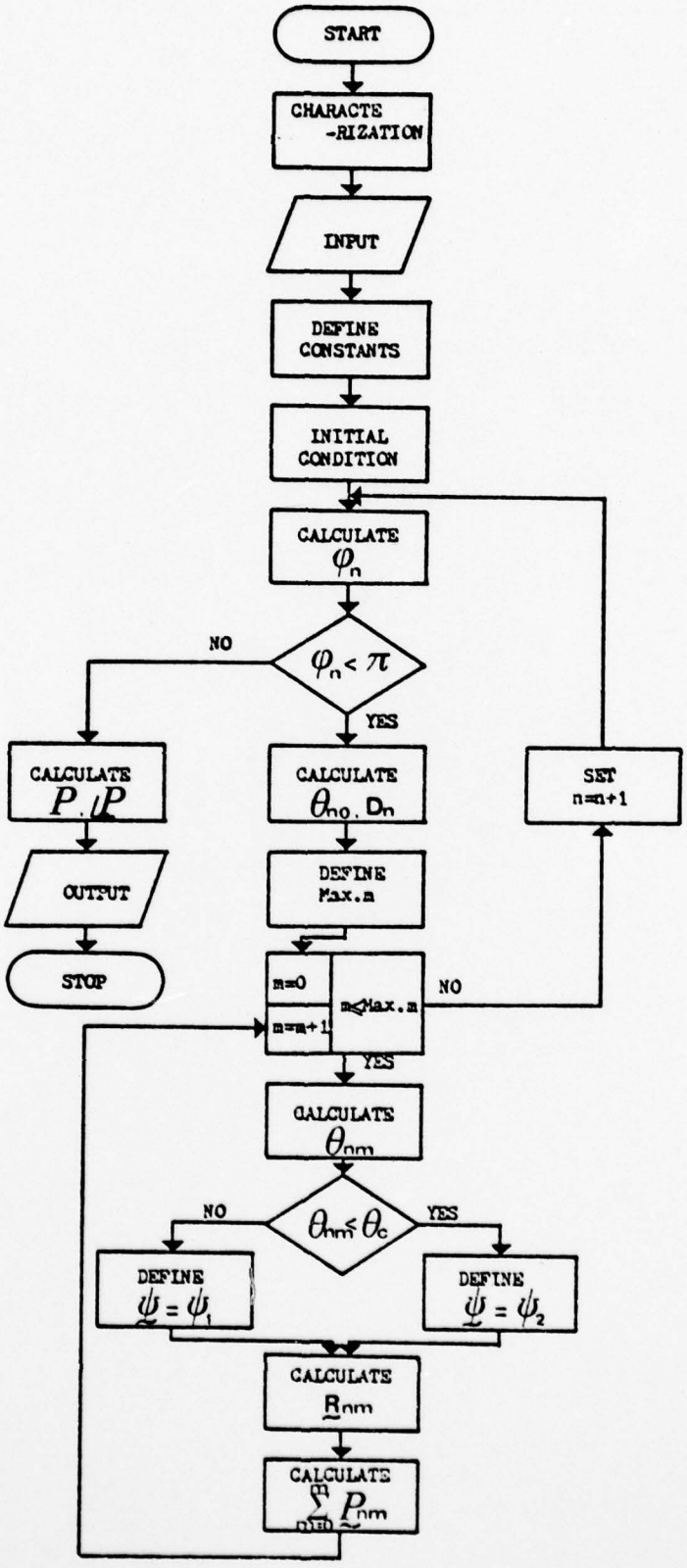
(1) After a careful examination of the simple model it is found to fail to describe adequately the pressure along the bottom and it is therefore not useful for future efforts in describing the pressure radiated into the bottom.

(2) On the other hand the method of images gives a good prediction of pressure amplitude and phase distributions along the interface and therefore offers us hope in attempting to predict the properties of the beam of sound in the bottom.

APPENDIX A

A computer program for the calculation of the pressure amplitude and phase distribution along the bottom by the method of images.

FLOW CHART OF THE SUBROUTINE "PRES"



THIS PAGE IS BEST QUALITY PRACTICABLE
FROM COPY FURNISHED TO DDC

```
C     WEDGE 0
C *** MAIN PROGRAM ***
C
C  ************************************************************************
C  * THIS PROGRAM EMPLOYS THE METHOD OF IMAGES TO OBTAIN THE PRESSURE     *
C  *AND PHASE DISTRIBUTION ALONG THE BOTTOM OF A WEDGE-SHAPED FLUID       *
C  *LAYER,OVERLYING A FAST BOTTOM.                                        *
C  *                                                                      *
C  *  ASSUMPTION                                                          *
C  *     PLANE WAVE REFLECTION COEFICIENTS.                               *
C  ************************************************************************
C
C  *  NOTATION
C     I/O    OUT=OUTPUT
C            IN =INPUT
C     CHARACTER
C            V  =VARIABLE
C            P  =PARAMETER
C            C  =CONSTANT
C
C            R  =REAL NUMBER
C            I  =INTEGER
C            Z  =COMPLEX NUMBER
C
C    ------------------------------------------------------------------------
C    SYMBOL            MEANING                                  I/O CHARACTER
C    ------------------------------------------------------------------------
C     PA       PRESSURE AMPLITUDE ON THE BOTTOM                 OUT   V,R
C     PH       PRESSURE PHASE ON THE BOTTOM                     OUT   V,R
C     C1       SOUND SPEED IN MEDIUM 1 (WEDGE)                  IN    C,R
C     C2       SOUND SPEED IN MEDIUM 2 (BOTTOM)                 IN    C,R
C     RO1      DENSITY OF MEDIUM 1                              IN    C,R
C     RO2      DENSITY OF MEDIUM 2                              IN    C,R
C     BETA     SLOPE ANGLE OF BOTTOM                            IN    C,R
C     X        SOURCE DISTANCE FROM THE APEX IN METERS          IN    C,R
C     XX       DISTANCE FROM THE APEX IN METERS                 OUT   V,R
C               AT WHICH PA AND PH ARE CALCULATED
C     F        DRIVING FREQUENCY                                IN    C,R
C     H        SOURCE DEPTH IN METERS                           IN    C,R
C     ANGLC    CRITICAL ANGLE                                         C,R
C     HO       LOWEST POSSIBLE MODE CUT OFF DEPTH IN METERS           C,R
C     XO       LOWEST POSSIBLE MODE CUT OFF DISTANCE FROM THE         C,R
C               APEX IN METERS
C     XN1      DISTANCE FROM APEX AT WHICH CALCULATION STARTS   IN    C,R
C               NORMALIZED BY DIVIDING BY XO
C     XN2      DISTANCE FROM APEX AT WHICH CALCULATION STOPS    IN    C,R
C               NORMALIZED BY DIVIDING BY XO
C     DISTX1   DISTANCE  XN1 IN METERS                                C,R
C     DISTX2   DISTANCE  XN2 IN METERS                                C,R
C     DX       RANGE OF CALCULATION IN METERS                         C,R
C     N        NUMBER OF POINTS FOR WHICH PA AND PH             IN    C,I
C               CALCULATED
C     PAI      3.1415.......                                          C,R
C     WN       WAVE NUMBER                                            C,R
C     C21      SOUND SPEED RATIO =C2/C1                               C,R
C     RC21     ACOUSTIC IMPEDANCE RATIO                               C,R
C     ANGLO    ANGLE FORMED BY SOURCE, APEX AND BOTTOM                C,R
C     DISTX    TEMPORARY FOR XX(I)/X                                  P,R
C     PAMP     TEMPORARY FOR PA                                       P,R
C     PHAS     TEMPORARY FOR PH                                       P,R
C    ------------------------------------------------------------------------
C
```

THIS PAGE IS BEST QUALITY PRACTICABLE
FROM COPY FURNISHED TO DDC

```
C ***************************************************************************
C
C     ((PROGRAM))
C
C DEFINE CHARACTERS OF VARIABLES,PARAMETERS AND CONSTANTS
C     IMPLICIT REAL*8(A-H,O-Z),INTEGER(I-N)
      DIMENSION PA(101),PH(101),XX(101)
      COMMON C21,RC21,BETA,WN,PAI,ANGLO,X,H,F
C
C READ IN DATA
C
      READ(5,100) C1,C2,R01,R02,BETA
      READ(5,500) XN1,XN2,X,H,F
      READ(5,600) N
C
C CALCULATE AND WRITE CONSTANTS
C
      WRITE (6,700) C1,C2,R01,R02,XN1,XN2,X,H,BETA,F
      ANGLC=DARCOS(C1/C2)
      HO=C1/(4.0D0*F*DSIN(ANGLC))
      XO=HO/DSIN(BETA)
      WRITE(6,400) HO,XO
C
C TRANSFER NORMALIZED DISTANCE TO ACTUAL DISTANCE
C
      DISTX1=XN1*XO
      DISTX2=XN2*XO
C
C CALCULATE RANGE DX
C
      DX=DISTX2-DISTX1
C
C CALCULATE CONSTANTS FOR SUBROUTINE
C
      PAI=4.0D0*DATAN(1.0D0)
      WN=2.0D0*PAI*F/C1
      C21=C2/C1
      RC21=C2*R02/(C1*R01)
      ANGLO=BETA-DARSIN(H/X)
      WRITE (6,200)
C
C CALCULATE PRESSURES WITH RESPECT TO DISTANCE XX.
C  WHERE XX IS CHANGED BY INCRIMENT
C
      L=N+1
      DO 10I=1,L
      XX(I)=DISTX1+DFLOAT(I-1)*DX/DFLOAT(N)
      DISTX=XX(I)/X
      CALL PRES (DISTX,PAMP,PHAS)
      PA(I)=PAMP
      PH(I)=PHAS
      WRITE (6,300) XX(I),PA(I),PH(I)
   10 CONTINUE
      WRITE (6,800)
C
C PLOT THE PRESSURE AMPLITUDE VS. DISTANCE XX
C  AND PRESSURE PHASE VS. DISTANCE XX
C
      WRITE (6,700) C1,C2,R01,R02,XN1,XN2,X,H,BETA,F
      CALL DPLTP (XX,PA,N,0)
      WRITE (6,800)
      WRITE (6,700) C1,C2,R01,R02,XN1,XN2,X,H,BETA,F
      CALL DPLTP (XX,PH,N,0)
C
```

THIS PAGE IS BEST QUALITY PRACTICABLE
FROM COPY FURNISHED TO DDC

```
C I/O FORMATS
C
  100 FORMAT (5F15.0)
  200 FORMAT (//22X,'DISTANCE',17X,'PRESSURE AMP.',12X,'PHASE ANGLE'//)
  300 FORMAT (  20X,D15.7,10X,D15.7,10X,D15.7)
  400 FORMAT (//20X,'LOWEST POSSIBLE MODE CUT OFF DEPTH',9X,D15.7
     C          /20X,'DISTANCE FROM APEX      ',20X,D15.7//)
  500 FORMAT (5F15.0)
  600 FORMAT (I3)
  700 FORMAT (//25X,'INPUT DATA',15X,'WEDGE0'//
     C           25X,'C1  =',D15.7,5X,'C2  =',D15.7/
     C           25X,'R01 =',D15.7,5X,'R02 =',D15.7/
     C           25X,'XN1 =',D15.7,5X,'XN2 =',D15.7/
     C           25X,'X   =',D15.7,5X,'H   =',D15.7/
     C           25X,'BETA=',D15.7,5X,'F   =',D15.7/)
  800 FORMAT (1H1)
      STOP
      END
C
```

THIS PAGE IS BEST QUALITY PRACTICABLE
FROM COPY FURNISHED TO DDC

```
C
C
C *** SUB PROGRAM ***
C
C  ************************************************************************
C  * SUBROUTINE 'PRES' CALCULATES THE PRESSURE AMPLITUDE AND PHASE AT A*
C  *POINT ON THE BOTTOM BY USING IMAGE THEORY.                          *
C  ************************************************************************
C
C   WHERE C21,RC21,BETA,WN,PAI,X,H AND F ARE INPUT CONSTANTS
C         FROM MAIN ROUTINE,
C         DISTX IS INPUT VARIABLE FROM MAIN ROUTINE, AND,
C         PAMP AND PHAS ARE OUTPUTS  TO MAIN ROUTINE.
C
C
C   *  NOTATION
C
C   ------------------------------------------------------------------------
C   SYMBOL          MEANING                                        I/O CHARACTER
C   ------------------------------------------------------------------------
C    PRES    PRESSURE CAUSED BY N TH PAIR OF IMAGES                  P,Z
C    P       SUM OF PRES.(IF ALL POSSIBLE PAIR OF IMAGES ARE         P,Z
C             ADDED P IS PAMP)
C    ANGLN   ANGLE FORMED BY IMAGE, APEX AND BOTTOM                  P,R
C    DD      PARAMETER FOR CONVENIENCE                               P,R
C    R       TOTAL REFLECTION LOSS OF (N')TH IMAGE                   P,Z
C    N       N TH IMAGE OR N TH PAIR OF IMAGES                       P,I
C    M       M TH BOTTOM BOUNCE                                      P,I
C    MM      MAXIMUM NUMBERS OF BOTTOM BOUNCES                       P,I
C    THETAO  ANGLE  FORMED BY THE N TH IMAGE,THE RECEIVING POINT     P,R
C             AND THE BOTTOM
C    DR      DISTANCE FROM N TH IMAGE TO THE RECEIVING POINT         P,R
C             NORMALIZED BY DIVIDING BY XO
C    THETAM  GRAZING ANGLE TO THE BOTTOM                             P,R
C             (INTERMEDIATE REFLECTION)
C    CHECK   IDENTIFIES IF GRAZING ANGLE EXCEEDS CRITICAL ANGLE      P,Z
C    PSAI    PARAMETER IN REFLECTION COEFFICIENT                     P,Z
C    REFL    RE·LECTION COEFFICIENT OF INTERMEDIATE BOUNCE           P,Z
C    REFLNO  REFLECTION COEFFICIENT OF THE LAST BOUNCE               P,R
C    DIRET   SOURCE DIRECTIVITY                                      P,Z
C    Z       PARAMETER FOR CONVENIENCE
C   ------------------------------------------------------------------------
C
C
```

AD-A067 561 NAVAL POSTGRADUATE SCHOOL MONTEREY CALIF F/G 20/4
PRESSURE ON THE INTERFACE BETWEEN A CONVERGING FLUID WEDGE AND --ETC(U)
DEC 78 M KAWAMURA, I IOANNOU

UNCLASSIFIED NL

2 OF 2
AD
A067561



END
DATE
FILMED
6-79
DDC

THIS PAGE IS BEST QUALITY PRACTICABLE
FROM COPY FURNISHED TO DDC

```
C ***************************************************************************
C
C      ((PROGRAM))
C
       SUBROUTINE PRES (DISTX,PAMP,PHAS)
C
C DEFINE CHARACTERS OF VARIABLE,PARAMETERS AND CONSTANTS
C
       IMPLICIT REAL*8(A-H,O-Z),INTEGER(I-N)
       COMPLEX*16 PSAI,REFL,REFLNO,R,Z,PRES,P
       COMMON C21,RC21,BETA,WN,PAI,ANGLO,X,H,F
C
C INITIALIZE COMPLEX PRESSURE P=0.0+J0.0
C
       P=DCMPLX(0.0D0,0.0D0)
C RESET COUNTER N=0
C
       N=0
    10 CONTINUE
C
C CALCULATE ANGLN AND DETERMINE IF ANGLE IS IN THE RANGE OR NOT
C  IF ANGLE.GT.PAI GO TO THE NEXT STEP
C
       ANGLN=2.0D0*INT((N+1.)/2.)*BETA+(-1)**N*ANGLO
       IF (ANGLN.GE.PAI) GO TO 50
C
C CALCULATE PARAMETER THETAO AND DR
C
       DD=DCOS(ANGLN)-DISTX
       THETAO=DATAN2(DSIN(ANGLN),DD)
       DR=DSQRT(1.0D0+DISTX**2-2.0D0*DISTX*DCOS(ANGLN))
C
C INITIALIZE THE TOTAL REFLECTION COEFFCIENT R=1.0+J0.0
C
       R=DCMPLX(1.0D0,0.0D0)
C
C DEFINE MM BY EACH PATH WHICH IS DETERMINED BY THE N TH IMAGE
C
       MM=IDINT(ANGLN/(2.0D0*BETA))
       L=MM+1
       DO 40 M=1,L
C
C CALCULATE PARAMETERS THETAM AND CHECK
C
       THETAM=THETAO-2.0D0*DFLOAT(M-1)*BETA
       CHECK=1.0D0-C21**2*DCOS(THETAM)**2
C
C IDENTIFY THE INCIDENT ANGLE WHICH IS LESS THAN THE CRITICAL
C  ANGLE OR NOT
C
       IF(CHECK.GT.0.0D0) GO TO 20
C
C CALCULATE PARAMETER PSAI FOR THE REFLECTION COEFFCIENT OF EACH
C  BOUNCE. THERE ARE TWO WAYS WHICH DEPEND ON THE IDENTIFICATION
C   OF A CHECK
C
       PSAI=DCMPLX(0.0D0,-DSQRT(-CHECK)/DSIN(THETAM))
       GO TO 30
    20 CONTINUE
       PSAI=DCMPLX(DSQRT(CHECK)/DSIN(THETAM),0.0D0)
    30 CONTINUE
C
C CALCULATE REFL
C
       REFL=(RC21-PSAI)/(RC21+PSAI)
```

THIS PAGE IS BEST QUALITY PRACTICABLE
FROM COPY FURNISHED TO DDC

```
C
C  IF THE BOUNCE IS THE LAST FROM THE SOURCE, THEN REFLNO=REFL
C
      IF(M.EQ.1) REFLNO=REFL
C
C  CALCULATE THE TOTAL REFLECTION COEFFCIENT R FOR EACH PATH
C
      R=R*REFL
   40 CONTINUE
C
C  CALCULATE PARAMETERS Z AND PRES
C   WHERE DIRET IS THE DIRECTIVITY OF THE SOURCE
C    DIRET IS USED ONLY WHEN THE SOURCE IS DIRECTIONAL
C     OTHER WISE DIRET=1.0
C
      Z=DCMPLX(0.0D0,-WN*X*DR)
      DIRET=DSIN(0.01D0*WN*DSIN(THETAM-ANGL0))/
     C           (0.01D0*WN*DSIN(THETAM-ANGL0))
      PRES=DIRET*CDEXP(Z)*(-1)**INT((N+1.)/2.)*
     C      (1.0D0+1.0D0/REFLNO)*R/DR
C
C  CALCULATE THE PRESSURE P WHICH IS A SUM OF PRES
C
      P=P+PRES
C
C  SET TO THE NEXT PAIR OF IMAGE
C
      N=N+1
      GO TO 10
   50 CONTINUE
C
C  CALCULATE PA AND PH, AND RETURN BACK TO THE MAIN ROUTINE
C
      PAMP=CDABS(P)
      PREAL=P
      P=P-PREAL
      PP=P*DCMPLX(0.0D0,1.0D0)
      PIMAG=DSIGN(CDABS(P),-PP)
      PHAS=DATAN2(PIMAG,PREAL)
      RETURN
      END
```

APPENDIX B

INCIDENT ANGLE FOR A DISTANCE SOURCE

General expression of an incident angle is given by Eq. (II 39-a)

$$\theta_{nm} = \theta_{no} - 2m\beta \qquad \text{(II 39-a)}$$

where the maximum number of bounces M is limited by

$$M = \text{INT}\left[\frac{\phi_n}{2\beta}\right] \qquad \text{(II-40)}$$

For a distance source

$$\theta_{mo} \simeq \phi_n \qquad \text{(II-48)}$$

A few incident angles θ_{nm} for a distance source are shown in Table B-1. From this table it is seen that the reflection coefficient for the 4^{th} image is

$$\underset{\sim}{\Gamma}(4) = \underset{\sim}{R}(\theta_{40})\underset{\sim}{R}(\theta_{41})\underset{\sim}{R}(\theta_{42}) = \underset{\sim}{\Gamma}(2)\underset{\sim}{R}(\theta_{40})$$

and by mathematical induction Eqs. II-50 can be deduced.

n \ m	0	1	2	3	. . . .
0	ϕ_o				
1	$2\beta-\phi_o$				
2	$2\beta+\phi_o$	ϕ_o			
3	$4\beta-\phi_o$	$2\beta-\phi_o$			
4	$4\beta+\phi_o$	$2\beta+\phi_o$	ϕ_o		
5	$6\beta-\phi_o$	$4\beta-\phi_o$	$2\beta-\phi_o$		
6	$6\beta+\phi_o$	$4\beta+\phi_o$	$2\beta+\phi_o$	ϕ_o	
7	$8\beta-\phi_o$	$6\beta-\phi_o$	$4\beta-\phi_o$	$2\beta-\phi_o$	
. . .					

Table B-1 θ_{nm}

BIBLIOGRAPHY

1. Edwards, J.N., Jr., A Preliminary Investigation of Acoustic Energy Transmission from a Tapered Fluid Layer into a Fast Bottom, M.S. Thesis, Naval Postgraduate School, Monterey, Dec. 1976.

2. Netzorg, G.B., Sound Transmission from a Tapered Fluid Layer into a Fast Bottom, M.S. Thesis, Naval Postgraduate School, Monterey, Dec. 1977.

3. Coppens, A.B., and Sanders, J.V., Notes in Acoustics material used in Underwater Acoustics Class, Naval Postgraduate School, Monterey, 1977.

4. Coppens, A.B., Sanders, J.V., Ioannou, G.I., Kawamura, M., Two Computer Programs for the Evaluation of the Acoustic Pressure Amplitude and Phase at the Bottom of a Wedge-Shaped, Fluid Layer Overlying a Fast, Fluid Half Space. Technical Report, Naval Postgraduate School 61-79-002, Dec. 1978.

5. Clay, C.S. and Medwin, H., Acoustical Oceanography Principles and Applications, John Wiley and Sons.

6. Sverdrup, Johnson, Fleming, The Oceans, Prentice-Hall, Inc.

7. Nariyuki, Nasu, "Occurrence of Continental Shelves," Takahiro Sato, "The Geological Structure of Continental Slope," Marine Science, V. 2, P. 17-22, 29-34.

INITIAL DISTRIBUTION LIST

		No. Copies
1.	Defense Documentation Center Cameron Station Alexandria, Virginia 22314	2
2.	Library, Code 0142 Naval Postgraduate School Monterey, California 93940	2
3.	Department Library Code 61 Department of Physics and Chemistry Naval Postgraduate School Monterey, California 93940	2
4.	Department Chairman Code 61 Department of Physics and Chemistry Naval Postgraduate School Monterey, California 93940	1
5.	Hellenic Navy Command Stratopedon Papagou Atehns, GREECE	3
6.	General Education and Training Division Maritime Staff Office Japan Maritime Self Defence Force 9-7-45 Akasaka, Minato-ku Tokyo, JAPAN	2
7.	Dr. E.P. Cooper, Code 013 Commander, Naval Ocean Systems Center San Diego, California 92152	2
8.	CDR. J.E. Minard, Code 462M Office of Naval Research Arlington, VA 22217	2
9.	Dr. A.B. Coppens, Code 61Cz Department of Physics and Chemistry Naval Postgraduate School Monterey, California 93940	1
10.	Dr. J.V. Sanders, Code 61Sd Department of Physics and Chemistry Naval Postgraduate School Monterey, California 93940	1

		No. Copies
11.	LCDR Ioannis Ioannou H.N. Plateia Barnaba 7 Pagration Athens, GREECE	2
12.	LT Masami Kawamura JMSDF 3400 Kamitsuruma, Sagamihara-shi Kanagawa-ken, JAPAN	2
13.	LT Dimitrios Mayiatis SMC # 1523 Naval Postgraduate School Monterey, California 93940	1
14.	LCDR J.H. Bremhorst Detachment Cubi Pt. Patrol Wing 1 FPO San Francisco 96654	1
15.	LT Zen-Wen Hwang 28 Lane 40 Park 2nd Rd. Yan-Cheng District Koohsiung, Taiwan, ROC	1
16.	Dr. H. Otsubo 5th Research Center Technical Research Development Institute, Defense Agency Nagase, Yokosuka, 239 JAPAN	1
17.	Dr. T. Kikuchi, Dr. T. Kishi Department of Applied Physics National Defense Academy 1-10-20 Hashirimizu, Yokosuka 239 JAPAN	2